Spring 2021

Identifying and Comparing Transcriptome Alterations in Saccharomyces cerevisiae Exposed to a Variety of Quantum Dots

Cullen Horstmann
Missouri State University

IDENTIFYING AND COMPARING TRANSCRIPTOME ALTERATIONS IN *SACCHAROMYCES CEREVISIAE* EXPOSED TO A VARIETY OF QUANTUM DOTS

A Master's Thesis

Presented to

The Graduate College of

Missouri State University

In Partial Fulfillment

Of the Requirements for the Degree

Master of Science, Biology

By

Cullen Michael Horstmann

May 2021

IDENTIFYING AND COMPARING TRANSCRIPTOME ALTERATIONS IN *SACCHAROMYCES CEREVISIAE* EXPOSED TO A VARIETY OF QUANTUM DOTS

Biology

Missouri State University, May 2021

Master of Science

Cullen Michael Horstmann

ABSTRACT

The primary focus of my research was to obtain global gene expression profiles of baker's yeast exposed to sub-lethal doses of nanoparticles, such as silver nanoparticles (AgNPs), yellow-emitting CdSe/ZnS quantum dots (QDs), green-emitting CdSe/ZnS QDs, and InP/ZnS QDs, to reveal novel insights on their unique mechanisms of toxicity. Despite their diverse applications, their long-lasting effects on the environment and human health are not well understood. To assess their toxicity, I administered experiments that exposed *Saccharomyces cerevisiae* to a variety of nanoparticles and measured cell viability, ROS levels, and changes in gene expression. Most notably, I used RNA-sequencing (RNA-seq) to identify gene identities of differentially expressed genes (DEGs) in nanoparticle-treated cultures. I found AgNPs altered genes implicated in rRNA processing, ribosome biogenesis, cell wall/cell membrane structure, and mitochondrial functions, yellow-emitting CdSe/ZnS QDs altered genes implicated in RNA processing, translation, oxidation-reduction, transmembrane-transport, and the ETC, green-emitting QDs altered genes implicated in translation, protein metabolic processes, transmembrane transport, cellular homeostasis, and cell wall organization, and InP/ZnS QDs altered genes associated with oxidation-reduction, transmembrane-transport, metal ion homeostasis, translation, and protein compound metabolic processes. Nevertheless, I concluded that all tested nanoparticles exerted some sort of cytotoxic effect by disrupting normal cellular functions of the budding yeast.

KEYWORDS: AgNPs, CdSe/ZnS, InP/ZnS, QDs, gene expression, RNA-seq, DEGs, *Saccharomyces cerevisiae*

IDENTIFYING AND COMPARING TRANSCRIPTOME ALTERATIONS IN *SACCHAROMYCES CEREVISIAE* EXPOSED TO A VARIETY OF QUANTUM DOTS

By

Cullen Michael Horstmann

A Master's Thesis
Submitted to the Graduate College
Of Missouri State University
In Partial Fulfillment of the Requirements
For the Degree of Master of Science, Biology

May 2021

Approved:

Kyoungtae Kim, Ph.D., Thesis Committee Chair

Laszlo Kovacs, Ph.D., Committee Member

Christopher Lupfer, Ph.D., Committee Member

Julie Masterson, Ph.D., Dean of the Graduate College

ACKNOWLEDGEMENTS

I would like to give thanks to Dr. Kyoungtae Kim for allowing me the opportunity to work in his lab. Without his patience and guidance, I would have never realized what I'm truly capable of. He provided my life with much needed structure and direction, keeping me grounded and focused, which is no simple feat. Thank you for taking me under your wing. Furthermore, I would like to thank Rishi Patel of Jordan Valley Innovation Center for his vital role, typically behind the scenes, in making my researching project possible. Additionally, I would like to give thanks to the many graduate students of Dr. Kim's, Lupfer's, and Kovacs' lab for their support over the last four years and for playing a pivotal role in my academic accomplishments. Lastly, I want to thank my family. No matter how difficult it might have been for them to listen to me go on about my research they always supported me, even if they're still not quite sure what I do.

I dedicate this thesis to my family.

TABLE OF CONTENTS

LIST OF TABLES

LIST OF FIGURES

CHAPTER 1: A REVIEW ON TRANSCRIPTOME PROFILE ALTERATIONS WITH CARBON NANOTUBES, QUANTUM DOTS, AND SILVER NANOPARTICLES

Introduction

Sequence based high-throughput research is quickly becoming the preferred choice in gene expression studies. These technologies are extremely sensitive and capable of whole-transcriptome sequencing and can determine the presence of and quantity levels of RNA. The most accurate technique, RNA-seq, has been around for more than a decade and can detect the slightest changes in gene expression with unprecedented accuracy [1]. It is quickly surpassing older technological sequencing methods, including microarray, in gene expression studies. RNA-seq has been shown to provide gene expression measurements with greater quantitative and qualitative information and with greater accuracy than the microarray method. Furthermore, RNA-seq technology coupled with bioinformatics tools has been shown to be the superior approach in studying global gene expression dynamics in practically all biological settings. Despite the numerous advantages of gene expression-based methods, these sequencing technologies still face statistical and computational challenges due to the limited availability of reliable software programs with large computational and storage capabilities.

In recent years, high-throughput sequencing has become more popular in studying the toxicity of chemical agents, including Engineered Nano Materials (ENMs), through observable changes in transcript levels. While steadily gaining popularity, these modern genomic approaches, used for studying the impacts of ENM-toxicity on living systems, remain infrequent in modern studies. ENMs are implemented in numerous commercial and industrial sectors due to their extremely small size ranges of 1-100 nm [2]. ENM-toxicity is an enormous area of research

that has adopted the microarray and, newer, RNA-seq methods. They have primarily been used to investigate the toxicity of ENMs through identifying similar changes in global gene expression among different cell types and organisms. Since their discovery, our understanding of nanotechnologies has broadened resulting in novel and innovative medical and commercial applications. ENMs have attracted attention from nearly every industry due to their promising potential applications in chemical, catalytic, electronic, optical, mechanical, magnetic, and medical fields. For instance, some of their applications are due to their capacity to diagnosis and treat a considerable number of human diseases [2]. Even so, there is still much we do not understand regarding their potential toxicity. If we want to continue to use these nanotechnologies responsibly, we must conduct more research to identify their unpredictable, and potentially negative, effects on our health and the environment.

ENMs have a lot of diversity, and there are many different classes, including single and multi-walled carbon nanotubes, gold and silver nanoparticles, fullerenes, dendrimers, metal oxides, quantum dots, and many more [3, 4]. There is even greater diversity in their physiochemical properties, which are believed to contribute to their toxicity, and which make it exceedingly difficult to characterize their mechanisms by which they induce toxicity. To make things even more challenging, it is possible that the physiochemical properties of ENMs change after interacting with bio-molecules [4]. Furthermore, findings on ENM toxicology can vary drastically among extremely similar ENMs with almost identical physiochemical properties. These setbacks present the field with enormously challenging limitations in creating regulatory methods of determining ENM toxicity. In this review, I attempt to examine the toxicity of three ENMs including carbon nanotubes (CNTs), quantum dots (QDs), and Ag nanoparticles (AgNPs)

by highlighting and cross-examining their effects on global gene expression profiles in multiple cellular and higher organism models.

Materials and Methods

AgNPs. 20 nm PELCO®NanoXact™ silver nanoparticle (AgNPs), suspended in a concentration of 20 μg/mL in 2 mM sodium citrate solution (pH 7.6), was obtained from Ted Pella, Inc (Redding, CA, USA). The average diameter of the spheroidal nanoparticles (NPs) was 20 ± 2.9 nm, measured by JOEL 1010 transmission electron microscope (for more chemical and physical information, visit: www.nanocomposix.com). This sample of NPs showed the absorption band at 393 nm (www.nanocomposix.com).

Yellow-Emitting CdSe/ZnS QDs. Yellow-emitting CdSe/ZnS QDs (catalog number CZW-Y) with an emission color of yellow and a carboxylic acid stabilizing ligand with <1% organic impurities (not including ligands), suspended in water (1000 μg/mL), were obtained from NN-Labs (Fayetteville, AR, USA). The ZnS shell around the CdSe-QD core protects and stabilizes the QD's unique optical properties while maintaining the same absorption (estimated 550–600 nm) and emission (570–585 nm) properties of the core. NN-Labs did not provide the size of their yellow CdSe/ZnS-QDs, and the size was not available on the NN-Labs website. Baig et al. and associates, via transmission electron microscopy (TEM), determined the sizes of CdSe/ZnS-QDs with emission colors of green, yellow, and red to be 3.0, 4.1, and 5.5 nm, respectively [5]. These results led us to assume the size of the yellow CdSe/ZnS-QDs to be approximately 4.1 nm.

Green-Emitting CdSe/ZnS and InP/ZnS QDs. Green CdSe/ZnS and InP/ZnS QDs with functionalized carboxylic acid ligands were suspended in water at a concentration of 1000

μg/mL. They were obtained from NN-Labs (Fayetteville, AR, USA). CdSe- and InP-QD cores were capped with ZnS-shells to stabilize their absorption and emission wavelengths. The core/shell nanocrystal structure demonstrates brighter fluorescence and increased control over the surface chemistry. The emission wavelength of green-emitting CdSe/ZnS QDs were found to be 530–550 nm [6] and InP/ZnS QDs 530 nm +/−15 nm (NNCrystal US Corporation, Fayetteville, AR, USA) (unpublished). The size of the 530 nm CdSe/ZnS QDs were found to be 6.1–9.5 nm [6] and the 530 nm InP/ZnS QDs were found to be 3.2–4.2 nm in diameter [7]. QD size was verified using a JEOL 7900F scanning electron microscope (SEM, JOEL, Peabody, USA) with a scanning transmission electron microscopy (STEM) detector to image individual QDs, and the results were in agreement with datasheet values provided by the NNCrystal US Corporation website (nn-labs.com, January 2021) [6, 7].

Growth Assay with Exposure to AgNPs, CdSe/ZnS, and InP/ZnS. Wild type *Saccharomyces cerevisiae* cells (S288C) were purchased from ATCC (American Type Culture Collection, Manassas, VA, USA) and cultured in synthetic defined glucose (SD-Glucose) media overnight in a shaking incubator (INFORS HT Minitron) at 30 °C. The optical density (OD) was recorded at 600 nm with a BioMate^{TM} 3S spectrophotometer (Thermo Scientific, Waltham, MA, USA). The cells were cultured for 16–18 h in the shaking incubator to a minimum concentration of 1×10^7 cells/mL. After confirming the OD was adequate, the cells were inoculated into a 2x SD-Glucose media stock to an OD of 0.1. The newly made stock of cells was plated on a 96-well culture plate following the plating of AgNPs at concentrations of 0.05, 0.1, 0.5, 1, 2, 5 and 10 μg/mL (Figure 1), yellow-emitting CdSe/ZnS QDs at concentrations of 0, 0.8, 1.6, 3.15, 6.25, 12.5, 25, 50, and 100 μg/mL (Chapter III), green-emitting CdSe/ZnS QDs at concentrations of 0, 10, 20, 50, and 100 μg/mL (Chapter IV), and InP/ZnS QDs at

concentrations of 0, 1, 10, 50, and 100 μg/mL (Chapter IV). Upon completion of plating QDs and cells, the 96-well plate was inserted into an ELx808^{TM} absorbance microplate reader (Biotek, Winooski, VT, USA) and grown, while shaken fast, for 24 h at 30 °C. Simultaneously, the plate reader recorded the OD every 30 minutes at a wavelength of 594 nm. Blank well ODs (media + nanoparticles without cells) were subtracted from nanoparticle-treated wells (with cells) and averaged to create growth curves that represented all eight test concentrations, and were then compared to the NTC growth curves. The log section of the growth curves was used to calculate doubling times for each treatment group. The growth curve assay was conducted in triplicate.

Metabolic Activity Assessment using FUN-1 Dye (Chapter II). FUN-1 cell stain dye, a viability probe for fungal cells, was purchased from Thermo Fisher Scientific. Yeast cells (S288C) were grown for 16–18 h to an OD of 1.0 in SD-Glu media. The following day second inoculation was made and once again grown for 16– 18 h to an OD of 1.0. The cells were then inoculated into SD-Glu media to an OD of 0.2 with an AgNP concentration of 0, 5 or 10 μg/mL and were grown for 5 h at 30◦C in a shaker incubator. The cells were spun and transferred to 0.2 μm filtered water containing 2% D-glucose and 10 mM Na-HEPES and stained using 1 μL of 10 mM FUN-1 stock solution (final concentration of 20 μM) for 30 min. Stained cells were then examined using an Olympus IX81 inverted fluorescent microscope equipped with an ORCA camera (Hamamatsu, Bridgewater, NJ) with the excitation/emission filter set at 480/620 nm.

Total RNA Extraction. Yeast cells (S288C) were grown in SD-Glu media to mid-log phase corresponding to an OD at 600 nm of 0.3–0.6. These cells were incubated at 30◦C with shaking at 220 rpm with either SD-Glu media only for the control or SD-Glu media containing 5 μg/mL of AgNPs for 5 h. These experiments were performed in triplicates. Total RNA was extracted with the protocol and materials from RiboPure Yeast RNA Extraction Kit (Thermo

Fisher Scientific) on three control, three AgNP-treated (Chapter II), three yellow-emitting CdSe/ZnS QD-treated (Chapter III), green-emitting CdSe/ZnS QDs (Chapter IV), and InP/ZnS QDs (Chapter IV). The RNA concentration was calculated by measuring the OD at 280 nm using NanoPhotometerR P330 (v1.0, Implen, Westlake Village, CA) or the Qubit 3.0 Fluorometer. Final concentrations of total RNA ranged from 960 to 1200 ng/μL.

mRNA Isolation and cDNA Synthesis (Chapters II and III). mRNA was isolated from the total RNA, using TruSeqR Stranded mRNA LT Sample Preparation Kit (Illumina, San Diego, CA) by following the Low Sample Protocol. The first strands of cDNA were synthesized from the purified mRNA, using SuperScript II Reverse Transcriptase from the kit, followed by synthesis of the second strand of cDNA. Each cDNA sample was ligated with a distinct adaptor for sequencing, and the ligated cDNA fragments on both ends were amplified for 15 cycles. The end products were suspended in 30 μL Resuspension Buffer with final concentrations ranging from 45 to 60 ng/μL. The enriched cDNA libraries were sequenced using an Illumina hiseq 2500 Sequencing system (Kansas Medical Genome Center). One hundred nucleotides from only one end of each sequence (single-end sequencing) were completed with the cDNA libraries originated from three control, three AgNP-treated, and yellow-emitting CdSe/ZnS cells.

mRNA Isolation and cDNA Synthesis (Chapter IV). Yeast cells (S288C) were grown in SD-Glu media to mid-log phase corresponding to an OD at 600 nm of 0.3–0.6. These cells were incubated at 30 °C and shaken at 220 rpm for 5 h. This experiment was performed in triplicate consisting of three control samples (containing only SD-Glucose media and cells), three samples treated with green-emitting CdSe/ZnS QDs (10 μg/mL), and three samples treated with InP/ZnS QDs (100 μg/mL). The RiboPure Yeast RNA Extraction Kit (Thermo Fisher Scientific) was used on all control and QD-treated samples. The RNA concentrations were

measured with a Qubit 3.0 Fluorometer (ThermoFisher, Waltham, MA, USA) and fell within the acceptable range of 10 ng to 1 μg for library amplification. The Universal Plus mRNA-Seq Kit (NuGEN, Reddwood City, CA, USA) was used to generate adaptor-ligated sequencing-ready cDNA libraries from treated and non-treated total RNA samples. cDNA libraries were sequenced using an Illumina HiSeq 2500 Sequencing system (Kansas Medical Genome Center, Kansas City, MO, USA). One hundred nucleotides from only one end of each sequence (double-end sequencing) were completed with the cDNA libraries originated from three control, three CdSe/ZnS QD treated, and three InP/ZnS QD treated cells.

Analysis of Sequencing Data. Data from cDNA sequencing were analyzed using Galaxy, a website platform for analyzing sequenced data (www.usegalaxy.org). The data obtained from the Kansas Medical Genome Center was uploaded to the Galaxy server, where sequences that were separated, when sent to us, were concatenated back together so the full reads could be analyzed. A quality check was carried out on each file of sequence data to check the quality of the reads and ensure good samples and that the data is interpreted correctly. The files were then re-formatted into Sanger, which is necessary for the steps to follow. To achieve high fidelity, the files were trimmed based on quality, and bases with a quality score below 20 were removed from the reads. For eliminating the bias of primers and to ensure the removal of adapters, 12 bases were trimmed from the 5′ end of the reads. The remaining reads were then filtered to remove any reads less than 80 base pairs. Next, reads were aligned to the wild type *Saccharomyces cerevisiae* reference genome (S288C) obtained from the Saccharomyces genome database (SGD) (YeastGenome.org) with Tophat in Galaxy. With Cufflink, the transcriptome was assembled using the reference annotation by comparing the reads to the reference genome. Lastly, using Cuffdiff, the aligned sequence expression rates were compared

between sample conditions, creating a list of differentially expressed genes (DEGs). When the final differential gene data was obtained, genes with a *q*-value greater than 0.05 were not included in the final list of genes analyzed. The remaining genes were grouped based on correlating gene ontology (GO) terms obtained from GOrilla.

Quantitative Reverse Transcription PCR (RT-qPCR). Total RNA samples isolated from three control and three experimental (AgNP or QD-treated) cell cultures were used to produce cDNA with the Verso cDNA conversion kit (Thermo Fisher Scientific). The resulting cDNA concentration was quantified with the Qubit 3.0 Fluorometer. A primer efficiency test was performed to validate DNA primers and cDNA samples for reverse transcription quantitative PCR (RT-qPCR) experiments. FAF1, SDA1, DAN1, TIR1, HXK1, SPS100, YDL012C, and ALG9 primers were chosen for this test. FAF1, SDA1, DAN1 and TIR1 genes were chosen because they were differentially expressed in AgNP- and yellow-emitting CdSe/ZnS-treated samples (Chapters II and III) and TIR1, HXK1, SPS100, and YDL012C were chosen because they were differentially expressed in green-emitting CdSe/ZnS-treated samples (Chapter IV), while the expression of ALG9, a housekeeping gene, was not affected by the presence of any nanomaterial. In this test, serially diluted cDNA (dilution factor of 5 or 2 depending on the nanomaterial) samples with or without a fixed amount of primers were subjected to PCR amplification using GoTaq qPCR kit (Promega, Madison, WI). The primer efficiency and R-squared values were calculated with MxProR software (Agilent, Santa Clara, CA) and my R-squared values for all primer sets were between 0.99 and 1.00, indicating good precision in the preparation of the dilution assay. Primer efficiency values for all primers ranged from 1.69 to 2.14. After testing efficiency, 60 ng of cDNA from three control and three experimental samples was used as a template for amplification of the cDNA for all genes by following the GoTaq

qPCR Master Mix protocol (Promega) for AgNP and yellow-emitting CdSe/ZnS-treated samples and using the PowerTrack SYBR Green Master Mix (ThermoFisher Scientific, Waltham, MA, USA) for green-emitting CdSe/ZnS and InP/ZnS-treated samples. For each target gene to be amplified, I prepared a non-treated control reaction mixture that contains all the same reagents including primers, GoTaq Master Mix or PowerTRack SYBR Green Master Mix, and water lacking any cDNA. After each well contained all reagents, primers, cDNA, and water, they were thoroughly mixed by pipetting up and down. Once mixed, the plate was capped and centrifuged for 1 min. Then, the 96-well plate was placed in the pre-heated MX3005p machine (Chapters II and III) or the QuantStudio 6 Pro instrument (Thermo Fisher Scientific, Waltham, MA, USA, USA) (Chapter IV) for PCR amplification. The pfaffl method was utilized to determine the relative fold change in gene expression of a target gene in comparison to ALG9, a housekeeping gene (Pfaffl 2001). The relative expression ratio of the target gene is calculated based on E (RT-PCR efficiencies) and CP (crossing point) deviation versus the control and then the expression was compared to that of ALG9.

Measurement of Reactive Oxygen Species. Reactive oxygen species (ROS) and superoxide levels were quantified with flow cytometry, and the experiment was performed twice in triplicate for each experiment (Chapters II-IV) testing 18 samples (per chapter). Each cell containing sample was diluted to have an OD of 0.1 in 100 μL of SD-Glu media and incubated in a shaking incubator for 6 h at 30◦C. At hour 6, 5 μg/mL of dihydrorhodamine 123 (DHR123) or dihydroethidium (DHE) was added, and all samples were incubated for an additional 2 h before being brought to 1 mL with 1X PBS buffer and quantified with flow cytometry (Attune NxT acoustic focusing cytometer, Life Technologies). Samples 1–9 tested for the presence of peroxynitrite ROS by utilizing the ROS indicator DHR123. Samples 10–18 tested for the

presence of superoxide by similarly utilizing the superoxide indicator DHE. Samples 1–3 and 10–12 had a concentration of 0 μg/mL of AgNPs or yellow-emitting CdSe/ZnS QDs or green-emitting CdSe/ZnS QDs and InP/ZnS QDs, samples 4–6 and 13–15 had a concentration of 5 μg/mL AgNPs (Chapter II&III) or 10 μg/mL of green-emitting CdSe/ZnS and InP/ZnS QDs (Chapter IV), and samples 7–9 and 16–18 had a concentration of 10 μg/mL AgNPs (Chapter II) or 20 μg/mL yellow-emitting CdSe/ZnS QDs (Chapter III), and 100 μg/mL green-emitting CdSe/ZnS or InP/ZnS QDs (Chapter IV). Once recorded with the cytometer, the data was gated and customized to account for the % fluorescence of each target indicator (DHR123 and DHE) in their respective sample.

Cell Wall Stability Assay (Chapter II). The cell wall integrity was tested with a cell-wall-degrading enzyme, Zymolase 100T, in triplicate. Each cell sample was diluted to an OD of 1.0 in a total volume of 200 μL in a 96-well plate. Each well also contained 0 or 10 μg/mL of Zymolase 100T and varying concentrations of AgNPs (0, 5 and 10 μg/mL). Once each sample was plated, the 96-well plate was inserted into the ELx808 plate reader (BioTek) and the OD at 595 nm was recorded every 10 min for 6 h.

Nanoparticles' Effects on Cells Lacking Cell Walls (Chapter III). The Zymolase assay was performed by culturing yeast cells in 3 mL of SD-Glucose overnight in a shaking incubator at 30 °C. The cell culture was then centrifuged at 2000× *g* for ten minutes, and the resulting cell pellet was re-suspended with 2X TE buffer to an OD of 1.0. The suspended cells were applied to a 96-well plate in a quadruplicate manner. To test the effects of green-emitting CdSe/ZnS QDs, the following samples were prepared: non-treated controls (cells with TE buffer), 10 μg/mL CdSe/ZnS-treated cells, and 20 μg/mL CdSe/ZnS-treated cells. To test the effects of AgNPs, samples prepared in a 96-well plate consisted of non-treated controls and 2.5

μg/mL and 5 μg/mL AgNP-treated cells. Cell walls were degraded by the introduction of Zymolase at a concentration of 0.5 μg/mL and incubated in an ELx808^{TM} absorbance microplate reader (Biotek, Winooski, VT) for four hours at 30 °C. During the incubation period, the optical density (594 nm) was measured in 30 min intervals, and each sample was independently tested without the use of Zymolase to serve as a control. The resulting changes in optical densities were recorded and averaged for each sample before plotting into a line graph.

Confocal Microscopy Analysis (Chapter IV). Wild type cells expressing Vps10-GFP were treated with CdSe/ZnS and InP/ZnS QDs, both QDs were treated at 10 μg/mL for six hours at 30 °C in a shaking incubator. After incubation with the QDs, 500 μL of each sample was transferred to a micro-centrifuge tube and centrifuged at 2000 rpm for 10 min. If a pellet was visible, remove 300 μL of media was removed, without disturbing the pellet. Next, the pellets were re-suspended by vortexing and transferred 2.8 μL of the concentrated sample onto a glass slide, where a coverslip was gently applied to the droplet, and visualized the cells with a confocal microscope. The green laser was used for confocal microscopy and the intensity was set to 200 to detect punctated Vps10-GFP with immunofluorescence images. I quantified the number of Vps10-GFP puncta in NTC, CdSe/ZnS- (10 μg/mL), and InP/ZnS-treated (10 μg/mL) samples.

Statistical Analysis. In the cell viability assay (Figure 2), 100 cells from non-treated, treated with 5 μg/mL and treated with 10 μg/mL samples were randomly selected, and levels of viability were determined. This viability assay was repeated in triplicate, and the mean number of viable cells in each of the three samples in each group was used to determine the final values depicted in Figure 2. A two-tailed equal variance Student's t-test was performed, and no statistical difference was seen between the three sample groups suggesting AgNPs up to 10 μg/mL have no effect on cell viability measured by Fun1 fluorescent dye.

RT-PCR was performed three times in triplicate for two target upregulated and downregulated genes found to be statistically significant from a list of differentially expressed genes created from the RNA-seq data. The resulting Ct values from RT-PCR were incorporated in the Pfaffl method to determine each gene's differential fold change. A similar Student's t-test was performed to determine P values.

ROS and superoxide levels were quantified with flow cytometry, and the experiment was performed twice in triplicate with each experiment testing 18 samples. The mean value for each group (Chapter II: 0, 5 and 10 μg/mL; Chapter III: 0, 5 μg/mL AgNP and 20 μg/mL yellow-emitting CdSe/ZnS QDs; Chapter IV: 100 μg/mL green-emitting CdSe/ZnS and InP/ZnS QDs) and corresponding standard deviation values were determined with a one-way ANOVA test.

Carbon Nanotubes

CNTs are an important and highly versatile class of ENMs that have a huge variety of uses ranging from high performance batteries and touchscreens to drug delivery systems [8]. They can be described as nanoscopic cylinders, resembling chicken wire, that typically stand shoulder to shoulder in a "nanotube forest" and is stronger and lighter than titanium. Their superior tensile strength and toughness come from the extremely strong bonds between carbon atoms that compose the nanotube structure. Their diverse capabilities have led to a fast-growing market for CNTs, yet research on their mechanisms of toxicity are debated and not complete. As a result, there has been an increase in CNT manufacturing, there is a strong possibility of increased CNT exposure on the environment. Unfortunately, their nano-size make them unpredictable and research on their biomechanics and toxicity in humans is limited. Until there is

a better understanding of the effects of CNTs on human health, their efficacy in medicine and safe use in manufactured products will remain unknown.

Previous studies have shown that exposure to CNTs can have toxic effects through the generation of oxidative stress or by inducing inflammation. Multi-walled carbon nanotubes (MWCNT) and single-walled carbon nanotubes (SWCNT) are two important classes of CNTs, and their underlying mechanisms of toxicity have been investigated using RNA-seq. To have a complete understanding of carbon nanotubes function in vivo, determining their structure is essential. Nano-carbons are built from sp2 hybridized carbon atoms, a strong molecular interaction which makes CNT more appealing in situations such as drug delivery [9]. The tubular structure of SWCNT depicted each carbon joined by three neighboring carbons essentially making a Sp2 hybridized structure [10]. The Sp2 structure of carbon nanotubes is greatly more effective than the Sp3 hybridized structure that can be found among SWCNT. The Sp3 structure can cause deformations by bending or twisting of the nanotube on the wall [10]. These structure deformations can raise some concerns as well as the size of carbon nanotubes. SWCNTs can have a diameter as small as .4 nm and MWCNT can range from 5-100 nm [9]. Smaller CNTs can lead to an increased surface area and a greater potential opportunity for interaction and uptake by living cells [11]. Most studies are in agreement that the smaller size of SWCNT show a greater cytotoxic effect compared to MWCNT.

There is a study that was conducted in 2019 to investigate the changes in protein and gene expression when *Escherichia coli* (*E. coli*) are exposed to SWCNTs: 10 and 100 μg/ml pristine SWCNTs, and hydroxyl and carboxylic functionalized SWCNTs. Le et al., found that there are more damages or death of *E. coli* cells in higher concentration of SWCNTs [12]. When *E coli.* were exposed at low concentration (10 μg/ml) of SWCNTs, *E. coli* produced phage

shock pathway and altered protein regulations. At the high concentration (100 μg/ml) of SWCNTs, several proteins were shut down [12]. Moreover, PspA gene expression (responded to the membrane stressor) in cells exposed to 100 μg/ml SWCNTs was lower than that in the control group because of increased cell damage or death [12]. Another study was conducted by Yadav et al., in 2015 to investigate the toxic effect of MWCNTs on up flow anaerobic sludge blanket (UASB) microbial activity. In their study, they found MWCNT has effects on microbial viability: when the microbial cells were exposed to 1 and 100 mg/L of MWCNT, the reduction of colony forming units (CFU) was 29% and 58%, respectively [13]. Additionally, they found MWCNT-mediated damage to microbial cells [13]. Due to these findings, Le et al. and Yadav et al. revealed SWCNTs and MWCNTs induced negative cytotoxic effects on E. coli.

In 2014, there was a study investigated the effects of SWCNTs on bacterial growth and had similar results. In this study, Zheng et al., found that when the outside and inside of *P. denitrificans* were exposed to 10 and 50 mg/L of carboxyl-modified SWCNTs in 8-20 hours, there was a kind of inhibiting effects on bacterial growth rates and densities. However, non-modified SWCNTs was no significant effects on bacterial growth rates and densities during the 24-hour exposure of 10 and 50 mg/L [14]. This result is due to carboxyl-modified SWCNT that are transcriptional activators of genes encoding nucleotide reductases. These reductases respond to DNA damage and reduce gene expression and energy production associated with glucose metabolism. Furthermore, carboxyl-modified SWCNT leads to significant downregulation of nitrate reductases, reducing their activity [14]. These results highlight the influence physiochemical properties have on toxicity. Each CNT (modified and non-modified SWCNTs), though extremely similar in structure and composition, had very different effects on growth.

Gene expression studies on bacteria, specifically *Salmonella typhimurium*, can help clarify the mechanisms of CNT toxicity and if this treatment could be a possible anti-bacterial agent. *Salmonella typhimurium*, a gram-negative food borne pathogen, was exposed to SWCNTs in order to study the genes association with bacterial metabolism, structural integrity, and antibacterial components of nanoparticles, using electron microscopy and molecular studies such as qRT-PCR. Two silver coated carbon nanotubes (SWCNT-Aag and pSWCNT-Aag) are predicted to have antibacterial activity mediated through generation of ROS from the bacterial cells [15]. Interestingly, bacteria treated with plain SWCNT-Ag showed upregulation of *ychP* gene (associated with invasion) and downregulation of *ompF* gene (outer membrane protein). The bacteria treated with pSWCNT-Ag downregulated *ompF, safC* (outer membrane protein), and *ychP* genes, but only upregulated *cigR* gene (inner membrane protein) [15]. The expression of *ompF, cigR, and ychP* genes are all associated with membrane integrity and consistently downregulated in both SWCNT-Ag and pSWCNT-Ag [15].
Interestingly, *ychP* and *safC* genes are exclusively downregulated in pSWCNT-Ag. In summary, pSWCNT-Ag are non-toxic to human cells compared to SWCNTS-Ag. Experiments show that pSWCNT-Ag proves to be a potential safe alternative antimicrobial agent to treat food borne pathogens.

Woodmen et at emphasizes the effects of CNT on Saccharomyces cerevisiae [14]. This model organism has fast cell division which is preferred for cell culture and treatment.
Also, being eukaryotic is adequate when comparing to more advanced organisms. RNA-seq dependent transcriptional analysis constructed gene expression of CNT treated cells. Genes related with membrane transport and stress response were differentially expressed in CNT treated cells [14]. To conclude, CNT serves as environmental toxic factors to eukaryotic cells.

In 2012, Guo et al., investigated multi-walled carbon nanotube-induced gene signature in the mouse lungs and the association between these genes and human lung cancer risk and prognosis. Mice in this experiment were divided into vehicle control group and multi-walled carbon nanotubes (MWCNT) groups: Mice either received DM (vehicle control), 10, 20, 40 or 80 μg MWCNT [16]. Then, RNA was extracted and 24 genes were selected by using microarray and linear modeling. These 24 genes have significant changes in at least two time points. Their changes were more than 1.5 times at all doses. At day 56 after exposing to MWCNT, 330 genes were differentially expressed, and 38 of them were related to cancer [16]. A closely related study conducted with mouse lung revealed similar effects: a subset of mouse lung cancer biomarkers is affected after exposing to MWCNT. In this study, mice were divided into different groups: mice received either DM (vehicle control), 10, 20, 40 or 80 μg MWCNT [17]. Pancurari et al. found that 7 of a total 63 lung cancer prognostic and major signaling biomarker genes had different expression levels compared to the control group at 7 days after exposing to MWCNT, and 11 genes had different expression levels compared to the control group at 56 days after exposing to MWCNT by using qRT-PCR. At 56 days after exposing to MWCNT, the gene expression level of 3 overlapping genes was decreased compared to their expression level at 7 days [17]. Also, among the 11-gene associated canonical pathways, the molecular mechanisms of cancer pathway ranked the most significant at 56 days after exposure [17].

Moreover, there is another study conducted with mouse lung in 2014. Fujita et al., investigated time dependent changes in gene expression associated with the pulmonary toxicity of single-wall carbon nanotube (SWCNT). SWCNTs suspensions were administered one time in each rat (0.2 mg or 0.4 mg). After dissection, researchers found that the appearance of SWCNT aggregates decreased in a time-dependent manner [18]. In addition, at 90 days

after SWCNT exposure, the persistence of macrophages laden with SWCNT aggregates were observed in the alveolar walls and alveoli [18]. At 180 days, they observed macrophage-containing granuloma around the sites of SWCNT aggregates. Additionally, many genes involved in inflammatory response were significantly up-regulated on days 7, 90, and 180 and the number of up-regulated genes gradually decreased 180 days after instillation, but increased again at 365 days [18].

Due to their excellent physical and chemical properties, carbon nanotubes have shown potential application prospects in the fields of biology and medicine. From the long-term development of nanotechnology, the safe application and potential toxicological evaluation of carbon nanotubes are very important. With the deepening of research, it has been found that carbon nanotubes have a wide range of applications in the field of biomedicine. However, due to their small size and they can be deposited in the main organs of the human body, the possible biological effects and safety in human cells have gradually become the focus of attention. A previous study in 2014 investigated the correlation and concordance of MWCNT-induced gene expression in vitro monoculture and co-culture of human small airway epithelial cells (SAEC) and human microvascular endothelial cells (HMVEC) with gene expression in vivo mouse lung exposed to MWCNT. Snyder-Talkington et al., compared MWCNT-induced mRNA gene expression from human small airway epithelial cells (SAEC) and microvascular endothelial cells (HMVEC) in monoculture and co-culture [19]. When human lung epithelial and microvascular endothelial cells were co-cultured and treated with MWCNT, there were more concordant genes (both up- or downregulated in vivo and in vitro) than those of monoculture, particularly disease-related concordant genes [16, 19]. Since the gene expression of co-culture model better correlated to the in vivo gene expression, MWCNT could also be the potential biomarker for

human lung diseases. A similar study was conducted in 2019 to explore the data of mRNA in the mice and SAEC and HMVEC exposed to MWCNT. Snyder-Talkington et al. found that 4 concordant mRNAs (MYBPC2, PSD4, TMPRSS6, and S100A5) between mouse lung tissues and SAEC exposing to MWCNT were upregulated and 40 concordant mRNAs were downregulated [12]. Also, 4 concordant mRNAs (HIST1H3F, HIST1H2AL, MID1, and NUDT8) between mouse lung tissues and HMVEC exposing to MWCNT were upregulated and 20 concordant mRNAs were downregulated [12]. Importantly, concordant mRNAs-- SLC7A1 and SLC22A5 were downregulated in all mice and human tissue, blood and cell analyses, which could cause human primary hypertension, cardiovascular diseases, encephalopathy, cardiomyopathy, cardiomegaly, metabolic derangement, hypoglycemia, and muscle weakness [12]. This reveals that MWCNTs have similar effects in mouse and human models.

Treatment of CNT on human cells was conducted in a 2017 study. RT-PCR was used to quantify the mRNA level of *ddit3(chop)* and *xbp-1s,* two gene biomarkers for ER stress. A recent study found that ER stress caused possible dysfunction of endothelial cells via the ER stress pathway when exposed to CNT [20]. Human umbilical vein endothelial cells (HUVECs) were treated with 32 mg/mL of XFM22 (shorter MWCNT) and XFM19 (longer MWCNT) in a 6-well plate [20]. Using specific primers for each gene, mRNA was quantified. Exposure of XFM22 to the HUVECs decreased the expression of *ddit3* in mRNA; whereas, when HUVECs were treated with XFM19 the cells expressed significant increase in *ddit3.* The expression of *xbp-1s* gene remained constant when treated with XFM22 but XFM19 downregulated the expression of *xbp-1s* [20]. *Ddit3* is a transcription factor that regulates inflammatory cytokines like IL-6. XFM19, the longer MWCNT, increased *ddit3* expression, meaning that XFM19 treated HUVEC cells may be able to produce more IL-6. It is important to note that this study illustrates modest ER-

stressed compared to studies conducted in the past. Overall, the treatment of XFM22 and XFM19 in HUVEC cells conveyed less ER stress than initially expected. The influence of MWCNT on gene expression associated with ER stress in in HUVECs was also investigated in 2018. Chang et al. found the expression of genes associated with ER was induced by high concentrations of MWCNTs in HUVECs cultured in the upper chambers, such as HSPA5, DDIT3 and XBP-1s [13]. In summation, they provided evidence of CNTs negatively affecting HUVECs via ER damage.

In 2010, Patlolla et al., tested potential effects of MWCNT on normal human dermal fibroblast (NHDF) cells based on three doses: 40, 200, and 400 μg/mL [21]. After exposure to different concentrations of MWCNT, cell viability was significantly reduced, especially at the highest dose. The cytotoxicity appeared to be dose dependent and increased as the dose concentration increased [21]. Additionally, they tested genotoxicity and apoptosis for NHDF cells and found a direct correlation between the concentration of MWCNT and the levels of tail DNA, which is a parameter in evaluating cell DNA damage. Notably, the percentage of apoptosis increased with the increasing doses of MWCNT [21]. In another study, Siegrist et al., also tested the genotoxicity effects of MWCNTs on the cultured primary and immortalized human airway epithelial cells, and their results showed there was an increase in spindle disruption, abnormal mitotic spindles, and aneuploid chromosome number with the increased doses of MWCNTs. Thus, they revealed MWCNTs to cause dose-dependent genetic damage [22]. Furthermore, in 2019, Snyder et al., employed qPCR to measure the potential effects of MWCNTs on mitochondrial gene expression in human bronchial epithelial cells (BECs) after exposing to up to 3 μg/ml of MWCNTs. As the result, the mitochondrial gene expression in

some BECs was significantly upregulated [9, 23]. All data demonstrated the levels of DNA and mitochondrial damages in human cell lines were increased by MWCNT.

In conclusion, the potential effects of CNTs on gene expressions was studied to promote the application of nanotechnology and the development of nanoparticles. Although they are a very popular nanoparticle for biomedical applications, several studies have also demonstrated that CNTs can be harmful by affecting gene expression and protein pathways. Those studies demonstrated the exposure of bacteria, fungi, animal and human tissues to CNTs led to up-regulation of gene expression for oxidative stress, inflammation, and cancers. These articles provided empirical evidence and support for an accurate assessment of the potential risks in bacteria, animal, and human models that will help us to better understand their long-term effects on our health and the environment. The effect of CNTs on gene expression may serve as a potential biomarker for human medical and occupational monitoring in future studies. Due to the lack of research on gene expression, the production and use of CNTs in biomedical technologies such as disease diagnosis and drug delivery are still at risk. Hopefully, they can be used responsibly after more investigations have been conducted on their unique properties and affects on gene expressions.

Quantum Dots

Quantum dots are a new class of ENMs, with a diameter of 2-10 nm [11, 12, 14], that possess unique physical and chemical properties that include high stability, narrow emission ranges, and high quantum yield [13]. Therefore, QDs are broadly used in biosensors, molecular imaging, multicolored labeling, drug carrier cosmetics, therapeutic targeting, photodynamic therapy, and real-time tracking [13, 14]. Most QDs are considered non-toxic and as a result are

of enormous interest in chemical, catalytic, electronic, optical, mechanical, magnetic, and medical fields and are becoming more common in many diverse commercial and industrial sectors, including but not limited to, textiles, medical products, cosmetics, paints, and plastics [2]. Similar to CNTs, QDs are a potential smart drug delivery vehicle in new and innovative cancer treatments [15]. Their photo-stability, tunable emission, and broad excitation range make them a more effective fluorescent tag than organic dyes in biological applications (protein labels, real-time trackers, and FRET sensors) [16, 17]. Previously, there have been conflicting results regarding QD cytotoxicity due to their diverse physiochemical properties (size, charge, composition, concentration, outer coating bioactivity, and stability) believed to be determining factors of toxicity [12, 18, 19]. Thus, the high possible combinations of properties result in a wide possibility of cytotoxic effects. Cytotoxicity has been investigated extensively; the scope of this section is to provide the most relevant and current findings on the transcriptomic effects of QDs on the cellular and organismal level.

Given the exceedingly broad potential applications of QDs, it is vital to resolve their toxic effects in prokaryotic and eukaryotic organisms. To date, very few global transcriptomic analyses of the effects of QD exposure on bacterial toxicity have been reported on. A study on the response of *E. coli* to CdTe-GSH QDs revealed that the same QD displayed differential toxicity based on size. Red QDs were found to be more toxic than green QDs when treated to *E. coli* at MICs of 125 and 2000 μg/mL, respectively. To determine the bacteria's global response to QDs of both sizes, microarray analysis was used to measure changes in gene expression. 95 genes were altered in response to red QDs while only 42 genes were changed in response to green QDs. Moreover, there were 7 genes differentially regulated by both QDs that gene ontology (GO) analysis reported to be implicated in processes related to transport, biosynthesis,

and metabolism. Furthermore, red QDs upregulated genes related to glycolysis and the TCA cycle slightly and transport by nearly 4-fold compared to green QD exposure [14]. Additionally, a transcriptomic response of *Pseudomonas stutzeri* exposed to cationic polythylenimine (PEI) coated CdSe/CdZnS QDs was observed. Changes in 7 genes, mostly implicated in denitrification (narG, napB, nirH, and norB) and the upregulation of superoxide dismutase (sodB), suggests the production of ROS as a response to QD exposure [20]. Correspondingly, Yang et al. found *P. aeruginosa* PAO1 exposed to CdSe QDs altered the expression of genes implicated in response to heavy metals and oxidative stress [21].

With RNA-seq, Horstmann et al. investigated the effects of CdSe/ZnS QDs on the yeast *Saccharomyces cerevisiae* and found exposure to the QDs had resulted in thousands of DEGs most notably involved in rRNA transcription, ribosomal subunit assembly, ribosomal subunit transport, tRNA maturation, and translation machinery assembly [22]. Hosiner et al. (2014) used microarray to investigate the effects of several metal ions ($CdCl_2$) on *Saccharomyces cerevisiae* and found antioxidant genes and redox homeostasis genes to be upregulated, such as GRX2 and TRR1, TRR2, and TRX3, respectively [23]. Interestingly, in 2016 researchers exploited a mutant *S. cerevisiae* strain to identify the genetic basis of CdS QD resistance. They found that in response to CdS QD exposure, several metabolic processes were altered, including abiotic stress response, mitochondrial organization, transport, and DNA repair [24]. The same research team later conducted a transcriptomic analysis and found mitochondrion organization as the primary functional category affected genes fell under. Additionally, they observed diminished oxygen consumption, cytochrome content, and mitochondrial membrane potential [25].

A recent study on soybean tissue investigated the effects of CdS QDs on transport proteins and biological pathways. Majumdar et al. (2019) identified 1690 genes that were

common between each CdS-QD treatment and GO term analysis suggests the affected proteins in CdS-exposed soybean roots are localized in the cell wall, extracellular region, membrane-bound organelles, and function as integral components of the membrane [26]. CdS-QD-treated soybean root tissue has been found to significantly alter protein levels involved in transmembrane transport of metal ions or protons, chitin binding, carbohydrate metabolism, and responding to oxidative stress [26]. Interestingly, short-term CdS-QD exposure (14 days) on soybean roots were found to upregulate cytosolic proteins involved in metabolic pathways including glycolysis, the TCA cycle, fatty acid β-oxidation, amino acid biosynthesis, and secondary metabolite biosynthesis. Upregulated cytosolic proteins responsible for converting proteins into useable substrates involved in the TCA cycle were unique to CdS-QD exposure. Additionally, downregulated proteins involved in glycogen metabolism (such as uridine-triphosphate- (UTP) glucose-1-phosphate uridylyltransferase involved in uridine diphosphate-glucose (UDP-glucose) regeneration from glucose-1-phosphate) were identified suggesting that CdS-QD exposure alters soybean metabolic pathways to favor glycolysis [26]. Similarly, in 2013, Simon et al. utilized RNA-seq to investigate the effects of CdTe/CdS QDs on green algae and identified, through GO analysis, DEGs involved in oxidative stress, redox potential, protein folding, and chaperone activity processes [27].

A 2010 study investigated the geno-toxic effects of green CdSe (455 nm), blue Cd1-xZnxS/ZnS (550 nm), and red CdSe/ZnS (625 nm) QDs on human embryonic kidney fibroblast cells (HEK293) by whole-genome microarray. HEK293 cells were treated with 200 nM, 60 nM, and 10 nM of red, blue, and green QDs, respectively. Interestingly, more genes were upregulated in green and blue QD treated cells and red QD treated samples downregulated more genes. GO-term analysis of DEGs showed that response to wounding, cell stress, apoptosis, and defense

response functions were enriched in all three of the QDs tested. The expression of metallothionein superfamily genes were induced when treated with red and green QDs, however, these genes were not affected in blue QD treated samples. Metallothioneins (MTX2a, MTX1h, MTX1g, MTX1f) are metal binding proteins that play a role in detoxification and protect against ROS and are also upregulated when exposed to Cd^{2+} ions [28].

Zhang et al., 2006 investigated PEG-silane-CdSe/ZnS QDs on human skin fibroblasts (HSF-42) with a genome-wide expression array analysis at concentrations of 8 and 80 nM. Approximately 50 genes had significantly altered expression levels greater than 2-fold and were found to be involved in carbohydrate binding, intracellular vesicle formation, and cellular response to stress. Interestingly, PEG-silane-QDs were found to downregulate genes involved in modulating the M-phase progression of mitosis, spindle formation, and cytokinesis. However, PEG-silane-QDs do not induce immune and inflammatory responses or heavy metal related toxicity, unlike exposure to CNTs. This study provided evidence that if CdSe/ZnS QDs are appropriately coated they will have very little impact on HSF-42 cells and PEG-coated QDs do not pose a major threat and reduce the toxicity of CdSe/ZnS QDs [29].

Unlike previous gene expression studies that mainly focus on fibroblast cell lines, a new 2020 study investigated the effects of Cd QDs on the growth of human cervical cancer cells (HeLa). Hens et al., 2020 implemented the RNA-seq method to analyze transcriptomic changes in HeLa cells when exposed to QDs. They identified many significantly up- and down-regulated genes and conveniently grouped them based on their functions using GO-terms. When exposed to QDs, they observed upregulated cellular functions in HeLa cells such as anti-apoptotic, anti-proliferative, and anti-tumorigenic functions. Additionally, they identified downregulated functions including pro-proliferation, mitochondrial respiratory chain, detoxification, and

receptor-mediated endocytosis. Based on new insights from their transcriptomic analysis, they provide evidence that CdSe/ZnS QDs could be effective as an alternative anticancer drug [6]. A similar study was conducted by Davenport et al., 2021 used InP/ZnS QDs on HeLa cells. Their RNA-seq and gene expression analysis revealed many genes involved in developmental processes including differentiation, tissue and nervous system development, and morphogenesis to be upregulated. They also found major processes such as metabolic and biosynthetic processes to be significantly downregulated. Both up- and down- regulated processes suggested expression of pro-apoptotic gene processes and control over cell motility [7]. They, like Hens et al., 2020 suggested the QD treatment be considered for anticancer drug development [7]. Additionally, carboxylated CdSe/ZnS QDs upregulated genes implicated in DNA repair, responding to stress, ATP functions, and RNA activities and downregulates genes involved in cellular division in alveolar epithelial cells [30].

In summation, Cd based QDs, despite their different spectral characteristics and composition, display toxic effects. Dua et al. and coworkers found with microarray analysis, QD exposure induces the expression of genes involved in oxidative stress, apoptosis, and inflammation that result in decreased cellular viability. Furthermore, they stated QD-mediated toxicity is highly dependent on the core material (CdSe) and the coating (ZnS) partially reduces the toxic effects [28]. Their results suggest that the use of unmodified QDs in biomedical applications should be used carefully and with much consideration. Contrarily, Zhang et al. showed by adding a polymer coat, such as a PEG-silica-coat, it allows for their safe use in vivo. They provided evidence with a comprehensive analysis of genome-wide expression alterations that PEG-silica-coated CdSe/ZnS QDs have minimal impacts on cellular health. These results contradict many popular beliefs that CdSe-based QDs are toxic due to Cd^{2+} leakage. These

potentially safer polymer coated QDs could be a large step toward their safe and widespread use in biomedical studies and applications [29]. These initial findings provide a solid foundation on QD toxicity necessary in identifying patterns in altered gene expression levels that will ultimately help build a network of global transcriptomic data on lower and higher organisms exposed to QDs. Future studies should focus on QDs long-term fate in living organisms, including their breakdown, to help better fully understand their toxicity. Understanding their effects in biological systems is crucial if we want to responsibly continue to use or incorporate them in industrial or commercial settings in the future.

Ag Nanoparticles

Silver has been studied and used for thousands of years in the medical and engineering fields because of its antimicrobial properties against bacteria, viruses, and fungi [31, 32]. In recent decades, the use of silver has been studied on a micro level in the form of nanoparticles. Silver nanoparticles (AgNP) range from 1-100 nm in size and have gained popularity for their optical, thermal, and electrical properties [33, 34]. With increasing levels of antibiotic resistance, AgNP have been hypothesized as a solution for improving current antibiotic treatment options for diseases like tuberculosis [35]. More specifically, AgNP have been used to innovate water disinfection, medical diagnostics, pharmaceutical development, anti-cancer therapies, and agriculture/live stock treatment [35-37]. While silver is found in many daily activities, AgNP production and application have potentially toxic effects. AgNP exposure in humans has been linked to disrupting function of mitochondria, sperm cells, and cytokine expression [38]. Studies on AgNP toxicity are widespread in focus; this thesis is specifically interested in the effect of

AgNP on gene function and transcriptome alterations across species. The scope of this section will summarize current findings on AgNPs effect on the transcriptome of different organisms.

As mentioned, AgNPs are known for having antimicrobial/bacterial activity and have been widely studied against various bacterial strains. It has been hypothesized that AgNP could decrease antibacterial activity to be an alternative to antibiotics in treating bacterial infections. To test this hypothesis, Ashmore et. al. studied AgNPs against *E. coli* using qRT-PCR. Supporting the proposed hypothesis, their findings show AgNPs to significantly downregulate genes associated with TCA cycle (aceF, gadB) and amino acid metabolism (argC, metL, gadB), pointing to effective antibacterial properties of AgNPs. The downregulated genes positively correlate with the proposed hypothesis, however there was upregulation in genes relevant to bacterial virulence (fliC, msbB) and DNA repair mechanisms (mfD) as well [38]. Similarly, antimicrobial effects of AgNP have been studied against *Staphylococcus aureus* and *Staphylococcus epidermidis* that produce biofilms and cause biomaterial-related infections in surgically inserted devices [39]. Through qRT-PCR methods, genes implicated in biofilm formation (icaA and icaR in S. epidermidis, fnbA and fnbB in S. aureus) were significantly downregulated with the presence of AgNP; these results conclude AgNP to inhibit transcription of biofilm related genes and to be inhibitory towards *S. aureus* and *S. epidermidis* bacteria [39]. An important regulator of *S. aureus* growth is found in small regulatory RNAs (sRNA) that require Hfq protein to mediate sRNA and their target mRNA [40]. Targeting activity of Hfq with AgNPs for antibacterial treatment was studied by Tian et. al. in which they specifically investigated sRNA-TEG49 expression (a key mediator of Hfq) [41]. Once again qRT-PCR was used along with high-throughput RNA sequencing and northern blot analysis. AgNP exposure to *S. aureus* resulted in loss-of-function of Hfq and subsequent inhibition of sRNA-TEG49. These

results suggest regulation of Hfq function with AgNP to be important to the NPs antibacterial mechanisms [41]. Collectively, applications of AgNPs against different bacteria support claims that they are effective in altering gene function to control bacterial growth.

Many different fungal species are involved in pathogenesis affecting mammalian life and need effective prevention and treatment methods. Along with their antibacterial properties, AgNPs have been investigated for potential antifungal properties as well. Some fungi have been investigated for their production of aflatoxins (AF), such as *Aspergillus flavus* and *Aspergillus parasiticus*. Aflatoxin B_1 (AFB_1) has been identified in these fungi and classified as a group 1 carcinogen to mammals; the use of AgNPs as treatment to inhibit AFB_1 production is proposed by Deabes et al. [42]. It was previously reported that there are three main genes responsible for aflatoxin biosynthesis: *aksA*, *ver-1*, and *omt-A* [43]. Within their study, Deabes et. al. measured expression levels of these three genes, along with the *AFB_1* gene itself, in *A. flavus* ATCC28542 using qRT-PCR. Their findings showed inhibited *AFB_1* and *omt-A* expression, leading them to conclude AgNPs to be effective in preventing AF production by *A. flavus* [42].

In some fungi, synthesis of structural molecules aid in their pathogenicity- as seen in *Bipolaris sorokiniana* and melanin production [44]. Specifically related to melanin production, expression of genes *viz*, *PKS1*, and *SCD1* were observed using qRT-PCR. Downregulation of genes *PKS1* and *SCD1* were observed in *B. sorokiniana* exposed to AgNPs, concluding the treatment to reduce melanin synthesis [44]. These results suggest AgNP to be viable in antifungal treatment, but the authors note further investigation is needed to understand the correlation between pathogenicity and melanin production in *B. sorokiniana*.

In addition to pathogenic fungi, other related species are commonly used as model organisms for studying biological processes. *Szhizosaccharomyces pombe* (fission yeast) is

commonly used to study cell morphogenesis and division; after constructing a genome-wide deletion library of fission yeast, Lee et. al. used the organism to identify target genes for tolerance against AgNP-induced cytotoxicity [45]. Target screening and q-PCR were used to identify 7 nonessential genes related to sulfur metabolism (*gcs1, gcs2, hmt2,* and *rdl2*) and MAPK kinase signaling (*mcs4, wis4* and SPCC1827.07*c*), all of which were previously linked to metal resistance and stress response. Three essential genes (*met9, sfh1,* and *peg1*) related to carbon metabolism were linked to AgNP-induced cytotoxicity for the first time [45]. The findings of this study are important to understanding genetic defenses against AgNP cytotoxicity within fission yeast.

Other fungal species, such as *Folsomia candida* and *Saccharomyces cerevisiae*, are often studied because they culture easily and grow quickly. Both *F. candida* and *S. cerevisiae* were studied by Sillapawattana et. al. to understand molecular toxicity of AgNPs and propose their relevance as eukaryotic model organisms in ecotoxicological testing. Target genes *GST* and *MT* were measured using qRT-PCR; *F. candida* observed upregulation of target genes when exposed to AgNPs, demonstrating the organism's ability to respond to a changing environment and use employed gene expression to examine chemical effects in toxicogenomic studies [46]. Observing the yeast genome showed code for only one cytosolic and one mitochondrial enzyme. This exemplifies the handling of yeast for chemogenetic screening to understand AgNP toxicity in yeast [46].

AgNP toxicity in S. cerevisiae was also investigated by Horstmann et. al. After observing decreased viability following AgNP treatment, RNAseq was used to identify genetic alterations to the yeast. Specifically, upregulated gene processes are suggested to disrupt healthy ribosome function and successive rRNA/tRNA synthesis [47]. The study also analyzes downregulated

processes that point to a defect in cell wall organization [47]. Conclusively, AgNP toxicity in yeast appeared to be heavily influenced by gene expression alterations.

Expanding from bacterial and fungal treatments, AgNPs have been proposed for medical therapies and technologies as well. To understand the positive and negative results of using AgNPs in humans, scientists have turned to various human cell lines and mice models for answers. Within these efforts, it is important to focus on gene expression changes to determine how the NPs interact with the cell. Using RNA-seq, Gurenathan et. al. observed changes to gene expression of in vitro NIH3T3 mouse embryonic fibroblasts. Alteration of processes involving epigenetics, such as nucleosome assembly and DNA methylation were found when treated with AgNPs. The study also found increased levels of apoptosis, which the authors suggest is influenced by a repression of genes related to cell survival [48]. In a similar model, mice neural cells were observed with AgNPs to relate gene expression changes to the development of neurological disorders like Alzheimer's disease. RT-PCR and western blot revealed increased gene expression related to the Amyloid beta peptide responsible for causing Alzheimer's (Genes *GSS*, *CYCL13*, and *MARCO*) [49]. The conclusions from this RT-PCR analysis suggests AgNP exposure accelerates the formation of plaque associated with Alzheimer's disease and emphasizes a need to monitor our daily interaction with Ag.

The toxicity of AgNPs is prevalent, however its properties have potential to be productive as well. The use of AgNPs as an anti-cancer treatment shows potential for applying toxic properties to cancer cells to destroy them. This was observed in combination with another cancer treatment, campotothecin (CPT) in cervical cancer cells (HeLa) by Yuan et. al. The combined treatments increased expression of proapoptotic genes like *p53*, *p21*, *Cyt C*, *Bid*, *Bax*, and *Bak*; modification of signaling molecule expression related to cell survival, viability, and cytotoxicity

were also observed [50]. NGS has also been used to show negative effect of AgNP treatment on human lung cells; evidence of DNA damage raises concern for human exposure *in vitro* [51]. It is suggested that the combination of these therapies, at low enough doses, could be successful at inducing apoptosis in cancer cells without causing unwanted cytotoxic effects [50].

The study of AgNPs in human tissue is crucial to discovering the strengths/limitations of their application to human cancer. Opposing their anti-cancer potential, recent evidence shows AgNPs to alter genetic expression to increase susceptibility to carcinogens [52]. Our understanding of the long-term *in vitro* effects on carcinogenicity can be improved by future studies of these nanoparticles [51]. The future use of genomic studies will be valuable for advancing the applications of AgNPs in the oncology field.

In conclusion, the use of AgNPs has greatly impacted antibacterial, anticancer, and antifungal treatment methods. This review only touches the surface of data that has been reported, but shows evidence concluding AgNPs to be effective in the alteration of gene expression among species. While its properties are promising, careful consideration is still needed in reference to their toxicity within mammalian cells. Going forward, more research is needed to understand what levels of AgNPs are safe for human consumption and ways to harness their toxicity so that they can continue to be an effective treatment against pathogenesis.

Future Trends

High-throughput sequencing technology has allowed researchers to observe the slightest changes in transcript levels and has given us much insight on the effects of ENMs on many different cell types and organisms. However, these modern genomic approaches like RNA-seq and DNA Microarray are not a perfect science. Simply because the number of mRNA is

increased or decreased in the presence of an ENM does not necessarily mean there are more proteins being translated. Future trends in this field need to include proteomic studies to verify changes in transcript levels found with gene expression studies. Through coupling gene expression studies with proteomic studies, we can gain a clearer understanding of the molecular changes, especially changes in protein levels, ENMs have on the cellular or organismal level.

CHAPTER 2: TRANSCRIPTOME PROFILE WITH 20 NM SILVER NANOPARTICLES IN YEAST

Introduction

Engineered nanomaterials (ENMs) are valuable and unique due to their small size, large surface-area-to-volume ratio, aggregation, chemical composition, solubility and shape [53]. They are currently used in over 1000 commercially avail- able products, ranging from sunscreens to water-resistant sur- faces [54]. ENMs have been predicted to play a part in future-targeted disease treatment, nanorobotics and next-generation electronics. Although the application of ENMs is increasing almost daily, our understanding of their toxicity is lagging behind the technology, thus encumbering safe and rapid deployment of these materials. In order to responsibly use these technologies, understanding how ENMs interact with the environment is a necessity. Their size allows them to interact at a molecular level, making them potentially useful in many applications; however, it also makes them potentially dangerous.

Nearly every class of ENMs has been found to have some negative biological effects; the question however is whether or not these effects pose a significant health or environmental risk [55, 56]. In order to determine whether a particular ENM is toxic or not, one must consider the specific properties of the materials being investigated, such as size, shape, etc. Studies have shown that even between batches of nanomaterials, toxicity may vary. Many studies in academia and industry have attempted to develop methods of understanding the toxicity of ENMs. Gold nanoparticles (GNPs) have gained considerable attention for potential application in cancer treatment such as photothermal therapy [57], and it was found that GNPs of different sizes are not inherently toxic to human cells including keratinocytes and leukemia [58, 59]. However, 2

nm GNPs functionalized with both cationic and an- ionic surface groups were toxic [60]. Another metal nanomaterial that has been widely used in a range of biomedical applications, including diagnosis, treatment, drug delivery and medical device coating, is silver nanoparticles (AgNPs) [61]. While it is well known that AgNPs exhibit antibacterial [62], antifungal, antiviral [63] and anti-inflammatory properties [64], there exists a report demonstrating that AgNPs at 100 μg/mL with different sizes in HaCat cells are not toxic [65]. Although the mechanism underlying their toxicity in different cells and organisms is not yet fully understood, the general consensus is that AgNPs cause cell membrane disruption [66-68], as well as oxidative stress [69, 70].

An emerging ideal tool to assess how an organism responds to a spectrum of ENMs is RNA-seq analysis that involves quantification of the expression of its genome. This high-throughput genomic/transcriptomic technology has been implemented for investigating the effects of AgNPs in aquatic organisms, soil invertebrates, green algae and bacteria [27, 63, 71, 72] and revealed that AgNPs cause differential expression of transcripts encoding components of the cell wall. Consistently, recent cell biological analyses with *Candida albicans*, a pathogenic fungus, have shown that AgNPs disrupt the membrane [62], induce apoptosis [73] and cause ultrastructural changes [74]. However, little is known about transcriptomic profiles of fungal cells treated with AgNPs. Therefore, the present study has used the budding yeast, *Saccharomyces cerevisiae,* to assess effects of AgNPs on the transcriptional activities of individual genes, offering a comprehensive picture of cellular function in the presence of AgNPs. The rationale for the use of *S. cerevisiae* was that it is one of the simplest eukaryotic organisms, but carries genes and their corresponding proteins that function in a spectrum of biological processes taking place in our cells. Another purpose of this study is to provide a standard operating procedure for assessing the effects of nanomaterials on fungal organisms be- fore they

are put into the environment. I reveal that a sub-lethal amount (5 μg/mL) of 20 nm spherical AgNPs in yeast culture leads to a significant change in transcriptome pro le when compared with non-treated cell culture, supporting the notion that AgNPs are environmental stress factors.

Results

AgNPs Negatively Affect Yeast Growth. To investigate the effects of spherical AgNPs (~20 nm in diameter) on the yeast growth, unicellular budding yeast cells were incubated for 24 h at 30◦C at varying concentrations of AgNPs (0–10 μg/mL) (Figure 1A). I observed that the mean growth rate for three non-treated controls was similar to those of AgNP-treated compared groups when the tested AgNP concentrations were below 5 μg/mL (Fig. 1A). However, a treatment with more than or equal to 5 μg/mL of AgNPs led to a significant growth rate reduction compared with non-treated controls. The mean maximum ODs at 600 nm reached by cells exposed to 10 and 5 μg/mL of AgNPs were 0.57 ± 0.2 and 1.61 ± 0.03, respectively, compared to the average maximum OD at 600 nm (1.73 ± 0.01) reached by non-treated control experiments (Fig. 1B). The average amount of time during the growth cycle spent in lag phase for each concentration below 5 μg/mL was very similar to the time spent in lag phase for the controls (10.6 ± 0.3 h) (Fig. 1C). However, the average times spent in lag phase by cells grown in 5 μg/mL (13.2 ± 0.80 h) and 10 μg/mL (19.9 ± 0.54 h) of AgNPs were significantly longer than that of the control (10.6 ± 0.3 h) (Fig. 1C). The mean doubling times of control cells (1.28 ± 0.13 h) was the shortest among all experiments, and the corresponding doubling time for each AgNP-treated culture increased in a dose-dependent manner. In particular, the doubling times of the cells exposed to AgNP concentrations of 5 and 10 μg/mL were 1.8 ± 0.24 and 2.7 ± 0.15 h, respectively (Fig. 1D). Taken together, these results suggest that exposure to AgNPs at

concentrations higher than 5 μg/mL inhibits the efficient growth of exposed yeast cells. Ivask et al (2014) previously demonstrated that AgNO3 is more toxic than AgNPs when they are similar in size [75]. Therefore, I tested the effect of AgNO3 on yeast cell growth and found that the cell culture with 0.05 μg/mL of AgNO3 showed a slower rate of yeast growth than the non-treated control culture. The culture with 0.1 μg/mL did not support yeast growth, suggesting that 0.1 μg/mLAgNO3 is minimum inhibitory concentration. My experiment with AgNO3 indicates that free silver ions affect more negatively on yeast proliferation.

Measurement of FUN-1 Dye Transport to the Vacuole. FUN-1 dye staining assay is often used as a live/dead assay for yeast. The dye enters the cytoplasm where it emits green fluorescence. As transported to the vacuolar lumen, it selfassembles into fluorescent red cylindrical intravascuolar structures (CIVS) [8]. In an attempt to understand what may cause growth defects in the presence of AgNPs, yeast cells were incubated with FUN-1 dye (20 μM, final concentration) with or without AgNPs. Yeast cells emitting green fluorescence in the cytoplasm with visible CIVS in the vacuole are considered active cells due to the process in which they transport the dye to the vacuole (Figure 2A, left), whereas cells emitting green fluorescence in the cytoplasm with no visible CIVS are considered metabolically inactive or presumed to be dead (Figure 2A, right). From all yeast cells exposed to 0, 5 and 10 μg/mL of AgNPs for 5 h, I found no significant difference in the percentage of cells showing the metabolic activity of FUN1 dye transfer to form CIVS between the exposure concentrations and the control (Figure 2B and C). Regardless of the presence or absence of AgNPs, at any concentration, over 90% of the cells were found to have no defect in transporting FUN-1 dye to the vacuole, indicating no effect of AgNP treatment on the trafficking of FUN-1 dye to the vacuole.

cDNA Sequencing Reveals Up- and Downregulated Genes with AgNPs. In lieu of harnessing 1000 different metabolic assays to identify changes occurring in the cell treated with AgNPs, I wanted to determine differential gene expression that may have occurred in response to 5 μg/mL of AgNP exposure by examining the transcriptional profiles of S. cerevisiae. I utilized RNA-Seq (sequencing of cDNA) to determine the expression profiles of both the control and AgNP-treated cells. Cells were grown and tested in triplicates, and I then performed a total RNA extraction, isolated mRNA and converted it into cDNA for sequencing (Figure 3A). After trimming and processing through Galaxy, a total of 42,808,285 accepted reads were obtained from three control and three AgNP-treated samples. Of these clean reads, an average of 92.0 and 93.5% of the total reads mapped to the reference genome (S288C) in the absence and presence of AgNPs, respectively, indicating that the sequenced reads accurately reflect the transcriptional expression of S. cerevisiae. I identified 7126 genes (including non-coding cDNA), of which expression levels of 1845 genes in AgNP-treated samples were found to be statistically different from those of non-treated control samples (q-values < 0.05) (Table 1). Of these, 1077 genes were upregulated and 768 genes were downregulated. My GO-term analysis with SGD revealed that 60% of all statistically upregulated genes (651 out of 1077) are implicated in nitrogen compound metabolism, and that genes functioning in gene expression comprise up to 49.6% (Figure 3A). Many upregulated genes are found to be implicated in ribosome biogenesis (26.4%), RNA processing (24.8%), translation (20%) or translational initiation (2.5%). Among 285 upregulated genes in the ribosome biogenesis category (Figure 3A), 268 genes are found to be functioning for rRNA processing. Genes involved in single organism metabolic process comprise up to 25.3% of all statistically downregulated genes (195 out of 768) (Figure 3B).

To understand how cellular mRNA level changes upon the treatment of AgNPs, I selected 144 most upregulated and 144 most downregulated genes, a total of 288 genes. Consistent with the data shown in Figure 3A, the vast majority of highly upregulated genes are implicated in the following, but not limited to, cellular processes: rRNA processing, ribosome biogenesis, nuclear export, rRNA transcription, response to chemicals, protein targeting, chromatin organization, DNA replication, cellular response to DNA damage stimulus, DNA repair and response to oxidative stress (Figure 4A and Table 2). In the 'rRNA processing' category, DBP2 and FAF1 genes are 7.9-fold and 7.2- fold upregulated. However, the most significantly upregulated gene is CTR1, a copper transporter that mediates nearly all copper uptake under low copper conditions.

My GO-term analysis with 144 most downregulated genes displayed that 38 out of 144 genes are unknown in their function (Figure 4B and Table 3). More than a dozen genes (15 out of 144) are identified to be involved in lipid metabolic processes, including genes implicated in ergosterol synthesis (ERG11, ERG25, ERG28, ERG3, ERG5, and ERG6). Among 12 downregulated transmembrane transporters, 2 genes, AAC3 and MPC3, are implicated in transporting ADP/ATP at the inner membrane of mitochondria and in transporting pyruvate to mitochondria, respectively. More genes whose functions are implicated in mitochondria-mediated cellular respiration are highly downregulated. These include AAC3, ACO1 (required for TCA cycle), CIT3 (citrate synthase) and ISF1 (affecting mitochondrial function). I identified 11 genes that play a role in responding to chemicals. In particular, 4 genes (GRX6, TSA2, VHR1 and ZTA1) out of these 11 downregulated genes are involved in an oxidative stress response, while 2 genes (CIN5 and NRG2) play a role in regulating the osmotic stress response. Among 10 genes involved in cell wall organization or biogenesis, 4 genes (GIP1, GSC2, OSW2 and

SPO73) function for spore cell wall formation, whereas the rest (TIP1, TIR1, TIR2, TIR3, TIR4 and DAN1) are cell wall mannoproteins. In particular, DAN1 that codes for a cell wall mannoprotein displayed 174-fold downregulation with AgNPs.

Validation of RNA-Seq Data by RT-qPCR. To validate the gene fold-change data obtained through a RNAseq method, a real-time RT-qPCR test was used. Two upregulated genes (FAF1 and SDA1) functioning in rRNA processing/ribosome biogenesis and two downregulated genes (DAN1 and TIR1) coding for cell wall mannoproteins were chosen as well as ALG9, a housekeeping gene whose expression does not change with AgNP treatment based on my RNA-seq data. The genes FAF1 and SDA1 exhibited 2.88 ± 0.44-fold and 3.12 ± 0.53- fold upregulation in gene expression with treatment of 5 μg/mL AgNPs, whereas DAN1 and TIR1 expression levels decrease more than 270-fold and 12-fold, respectively (Figure 5A&B). Together, the results of gene fold change measurement with RT-qPCR are consistent with our RNA-seq assay.

Determination of ROS in Cells Incubated with AgNPs. Several genes implicated in mitochondrial functions are downregulated (Figure 4B and Table 3), and therefore, I wanted to test levels of ROS originated from the mitochondria. To measure the total level of ROS from the mitochondria I used DHR123, which enters the cell and is oxidized by ROS to form R123 and to emit green fluorescence [76]. It was found that total levels of mitochondria-driven ROS in response to up to 10 μg/mL of AgNPs was not changed when compared to the ROS level of non-treated groups or 5 μg/mL AgNP-treated groups (Figure 6A–D). Given that the concentration of superoxide in cells with stress rises, I then determined levels of superoxide by using DHE, a superoxide indicator emitting red fluorescence [77]. Interestingly, the data showed that levels of superoxide in the presence of both 5 and 10 μg/mL of AgNP were decreased (Figure 6E–H). It is

not clear why superoxide levels in cells with AgNPs decreases, but Jones et al. (2011) recently proposed that cellular superoxide can be quenched in the presence of Ag ions derived from AgNPs. Therefore, I concluded that the decrease of superoxide in AgNP-treated cells may be due to ionized Ag reacting with superoxide in the cell [78].

Investigation of Cell Wall Integrity in Cells Incubated with AgNPs. I found several genes involved in cell wall organization and genes that code for cell wall structural proteins, such as manno-proteins, to be downregulated (Figure 4). I wanted to test the integrity of the cell wall in yeast treated with varying concentrations of AgNPs. To investigate the stability of the cell wall, I used an enzyme, Zymolase 100T, that creates spheroplasts and degrades the cell wall. It was found that the rates of cell wall degradation in samples treated with Zymolase 100T were much higher in samples treated with 10 μg/mL AgNPs than 5 μg/mL AgNPs and the same relationship was observed between 5 μg/mL AgNPs and samples not treated with AgNPs (Figure 7). Therefore, I concluded that the rates of cell wall degradation of AgNP-treated cells are higher than non-treated cells and the cell walls of AgNP-treated cells are less stable than their untreated counterparts.

Discussion

There are increasing concerns for AgNPs' potential environmental risks due to the fact that AgNPs are widely used in many commercial products. However, the temporal resolution of their effects on cellular and molecular dynamics is poorly understood. I elucidated the molecular mechanisms of cytotoxicity caused by AgNPs in the budding yeast, *S. cerevisiae*, by comprehensively investigating global mRNA expression patterns, and to my knowledge the

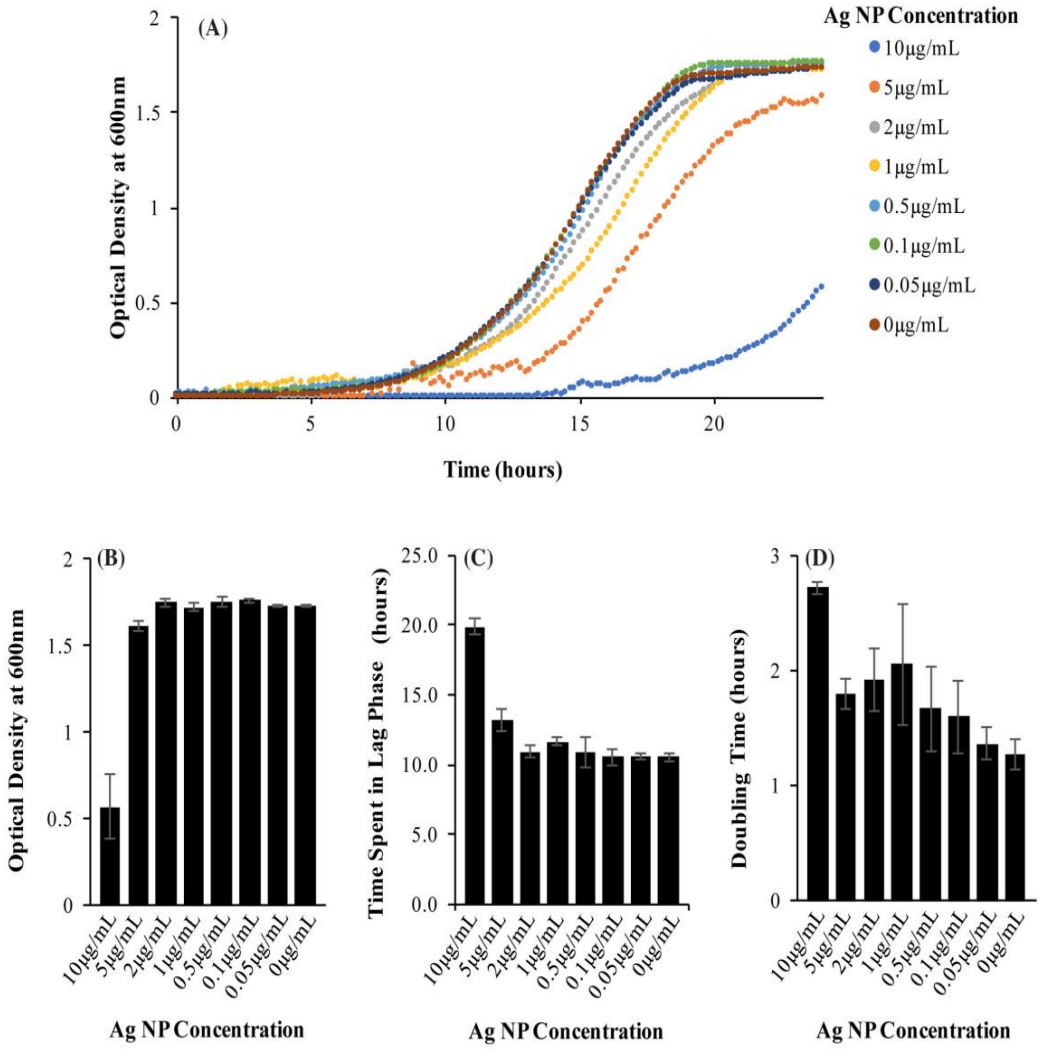

Figure 1. Effects of silver nanoparticles on the viability of yeast. **(A)** Growth curves of wild-type (S288C) cells grown in SD-Glu media containing different concentrations (0–10 µg/mL) of silver nanoparticles. The graph was produced by measuring the optical density (OD) at 600 nm of the solution once every 10 min for 24 h. Each plate contained four replicate experiments. Two plates were tested. Each point on the curve is an average of eight experiments. **(B)** The maximum OD at 600 nm of each test concentration of silver nanoparticles, with the background subtracted. Control wells containing only media and silver are subtracted from each test well resulting in an optical density reading indicative of cell concentration. **(C)** Average amount of time spent in lag phase of cell cycle for each sample. **(D)** Doubling time of each concentration of silver nanoparticles was found using the natural log of growth curves from **(A)** to determine the growth rate, which was then used to calculate the doubling time. Each bar represents an average doubling time of eight experiments.

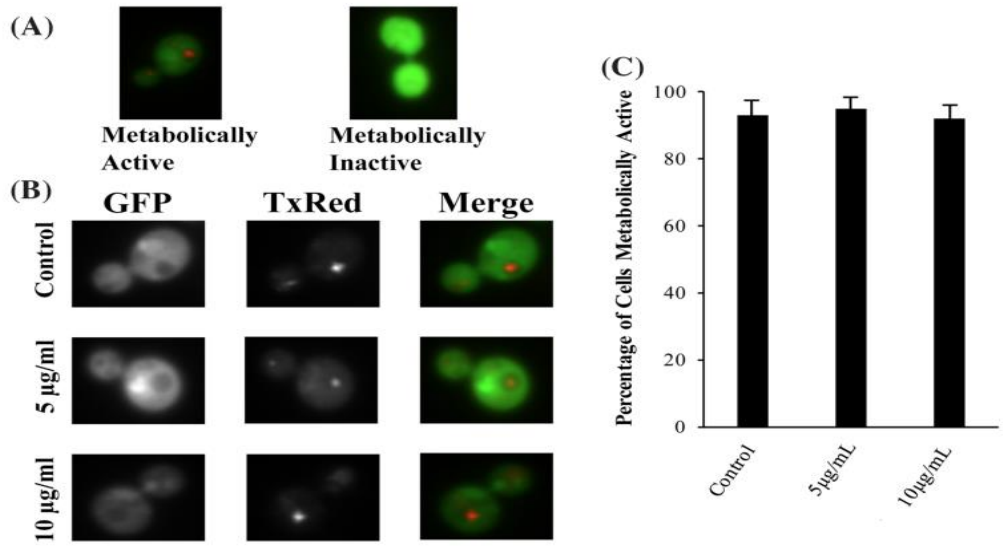

Figure 2. FUN-1 stain to determine metabolic activity of AgNP-treated yeast cells. **(A)** Example of a metabolically active yeast cell stained with FUN-1 (left). Example of a metabolically inactive and presumably dead yeast cells treated with FUN-1 dye (right). **(B)** Control cells with no AgNP treatment, cells treated with 5 µg/mL AgNPs and cells treated with 10 µg/mL AgNPs after being incubated for 30 min with FUN-1. **(C)** Quantification of percentage of cells considered metabolically active based on their successful transport of FUN-1 dye to the vacuole.

Table 1. Number of DEGs when exposed to 5 µg/mL AgNPs

Total number of genes found (including noncoding genes)	Not differentially expressed	Number of DEGs ($q < 0.05$)	Number of DEGs (fold change ≥ 2.82)
7126	5281	1845	196
Percent of total	74.11%	25.89%	2.75%

present study is the first RNA-seq report that indicates that a sub-lethal amount of AgNPs negatively affects many cellular processes occurring in the budding yeast. Though the current study does not illustrate differentially expressed genes, a recent study revealed a significant overlap (13–21%) of differentially expressed genes among AgNO3- and AgNP-treated Arabidopsis thaliana [79], indicating that this gene alteration in AgNP-treated groups was, at least in part, originated from Ag ions released by AgNPs. In the future, it is of great interest to

identify differentially expressed genes shared (or distinctive) upon exposure to AgNPs and Ag ions.

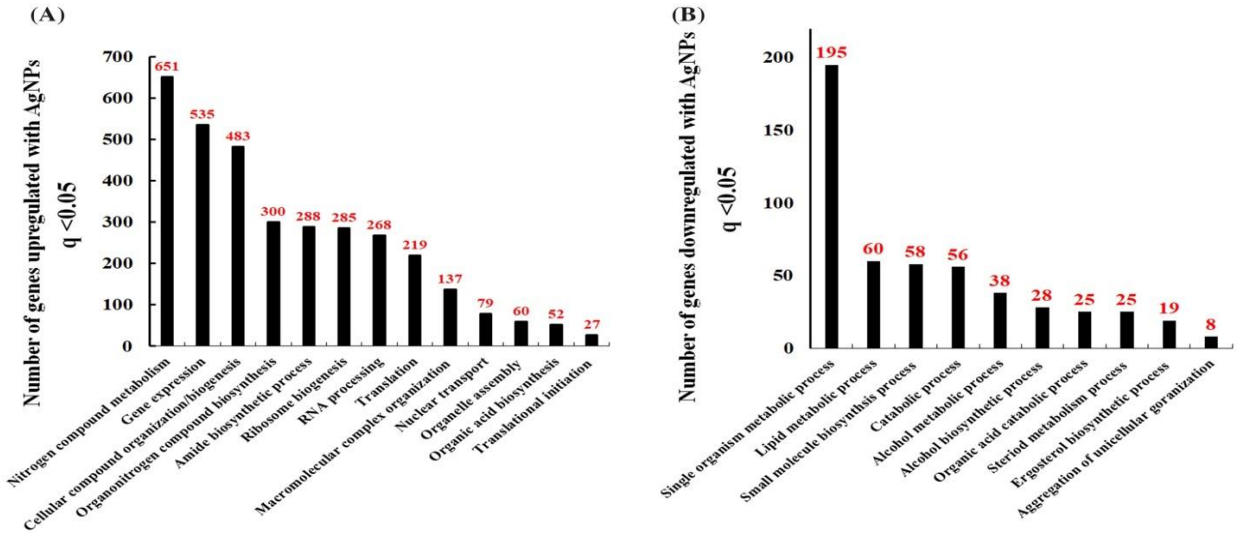

Figure 3. Differentially expressed genes with AgNPs. Differentially expressed genes with a q-value lesser than 0.05 were analyzed to find Gene Ontology terms (GO-terms) that correspond with each individual gene's biological process. Out of 7126 total genes, 1845 were found to be statistically significant. **(A)** The quantitation of upregulated genes associated with its specific GO term(s). Of the 1845 statistically significant genes, 1077 are found to be upregulated. **(B)** The quantification of downregulated genes associated with specific GO-terms. The other 768 statistically significant genes were found to be downregulated.

Upregulated mRNAs and their Potential Impacts on the Cell Integrity. I found more than 80 genes out of 144 most upregulated genes upon 5 μg/mL treatment of AgNPs are identified to function for rRNA processing/ribosome biogenesis. Many translated products of these 80 genes locate at the nucleolus, associated with rRNA processing/ribosome biogenesis (Figure 6A). For instance, genes coding for Enp2, Faf1 and its binding partner Krr1 [80] are highly elevated in their expression with AgNP treatment. All of these proteins are synthesized in the cytoplasm and then travel to the nucleolus to help with 18S rRNA processing, a component of the small ribosomal subunit [80]. According to a previously published paper from Dr. Baserga lab, Krr1 is a component of the small subunit (SSU) processome, a 2.2-MDa ribonucleoprotein

complex involved in the processing, assembly and maturation of the SSU of the ribosome in Eukaryotes [81]. Upon looking closely at the 'rRNA processing' and 'ribosome small subunit biogenesis' rows in Table 2, I found 22 more upregulated genes that code for the known and putative protein components of the yeast SSU processome: Nop1, Nop56, Nop58,

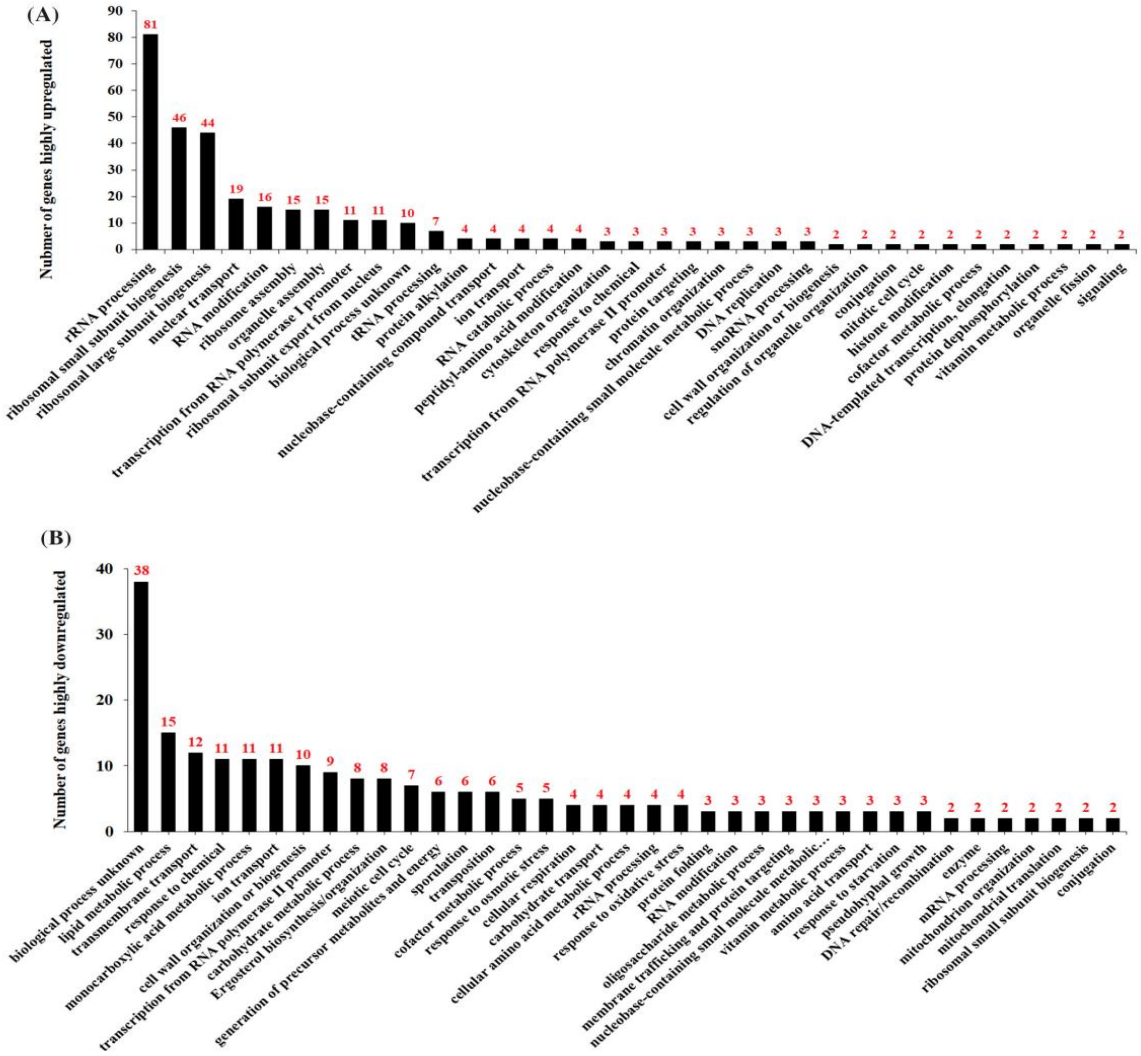

Figure 4. GO-term analysis of genes whose expression levels are significantly altered. A total of 144 most upregulated and downregulated genes with q-values less than 0.05 were analyzed and matched with corresponding GO-terms to better illustrate the biological processes most affected. **(A)** The quantification of the 144 most upregulated genes associated to their specific GO-term(s). **(B)** The quantification of the 144 most downregulated genes associated to their specific GO-term(s).

Imp4, Utp10, Utp13, Utp21, Rrp36, Utp11, Utp14, Noc4, Utp20, Utp23, Utp24, Bms1, Dbp8, Dhr2, Rc1, Rok1, Rrp3, Rrp5, Enp1. The upregulated gene list (Table 2) also contains 39 genes that code for assembly factors that function in maturation of 60S ribosomal subunit (or large subunit [LSU] of ribosome) in S. cerevisiae [82], including Rrp5, Nop4, Urb1, Nop8, Mak21, Noc2, Dbp3, Mak5, Ssf1, Mak16, Brx1, Rpf1, Ytm1, Erb1, Nop7, Drs1, Nop15, Nsa1, Rlp7, Has1, Nop2, Rpf2, Rrs1, Rlp24, Nog1, Spb1, Nsa2, Nug1, Rix7, Rix1, Mdn1, Rsa1, Sda1, Rei1, Yvh1, Mrt4, Puf6, Arx1 and Nmd3. Consistent with these upregulations of factors for SSU and LSU of ribosome, a number of genes that code for RNA polymerase 1 holoenzyme were upregulated upon AgNP treatment (See 'transcription from RNA polymerase 1 promoter' category of Table 2). Tying together, my observation is that sub lethal amounts of AgNPs in the budding yeast stimulate ribosome biogenesis at the nucleolus (Figure 8A). A fundamental question in relation to this observation is the potential cause of these upregulations. Previous results from Escherichia coli–AgNP interaction studies can provide hints for interpreting the RNA-seq data. It has been shown that AgNPs release Ag+ ions, which bind to thiol groups (SH) of the protein [83, 84]. Furthermore, AgNPs were found to interact with ribosomes in a manner similar to the binding mode suggested above, leading to denaturation or inactivation of ribosome proteins and thereby resulting in inhibition of translation and protein synthesis [84-86]. By interpolating the negative consequence of Ag+ binding to ribosomes into our RNA-seq results, one can put forth the idea that Ag+ affects yeast ribosome functions negatively via temporal or stable interactions with ribosomal components. In response to the signal of the presence of com promised or inefficient ribosomes, the cell might stimulate de novo formation of healthy ribosomes, for which the corresponding activities of SSU and LSU processosomes, rRNA synthesis, tRNA synthesis (see Table 3 for upregulated genes implicated in tRNA processing)

and ribosome export to the cytoplasm (Table 3) should be upregulated (see the model in Figure 8A).

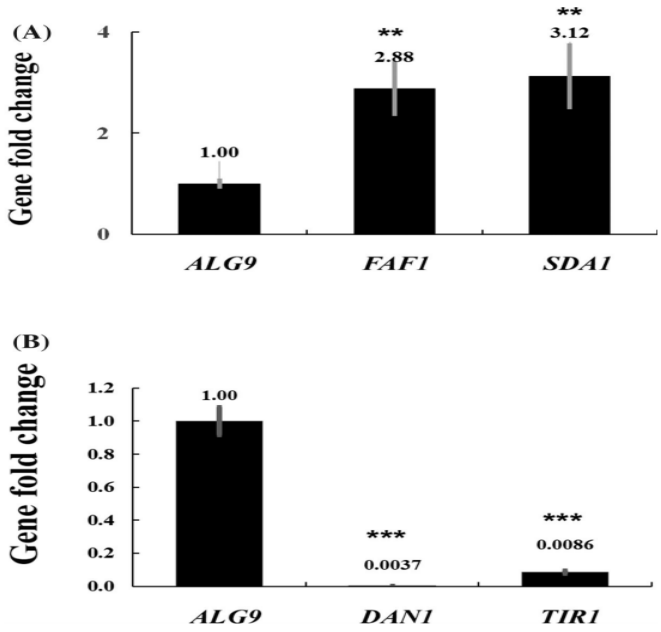

Figure 5. Assessment of gene expression fold-change with RT-qPCR. Fold-change values of two up and downregulated genes, which were identified by the RNA-seq experiments, were compared to a housekeeping gene (ALG9) that was not be differentially expressed when treated with AgNPs. Fold-change values were calculated with data obtained from RT-qPCR and the Pfaffl equation. The fold changes found with RT-qPCR were done to validate RNA-seq data. **(A)** The calculated fold changes of the upregulated genes FAF1 and SDA1. **(B)** The calculated fold changes of the downregulated genes DAN1 and TIR1. Student's t-test results are indicated either ** ($P < 0.01$) or *** ($P < 0.001$).

Downregulated mRNAs and their Potential Impacts on the Cell Integrity. It has been well known that AgNPs display their antimicrobial potential through impairing biological membranes. Ag+ ions released from the surface of AgNPs can bind to proteins carrying SO4 −, causing irreversible structural alteration, which in turn disrupts cell membrane integrity [87, 88]. In agreement to this concept, a recent SEM (scanning electron microscopy) study with Candida albicans revealed that yeasts with AgNPs 0.0089 ppm treatment for 1 day displayed a rough cell

surface, indicating outer cell wall damage [89]. Their TEM (transmission electron microscopy) data further displayed that the yeast cell wall treated with AgNPs was swollen thicker (nearly 2-

Table 2. GO term analysis with 144 most upregulated genes.

Gene Ontology term	No. of genes	Corresponding genes
rRNA processing	81	BMS1, BMT5, BMT6, CGR1, DBP2, DBP3, DBP8, DBP9, DHR2, DIM1, DRS1, EBP2, ECM16, EFG1, ENP1, ENP2, ERB1, FAF1, FAL1, HAS1, HCA4, IMP4, KRI1, KRR1, MAK16, MAK5, MDN1, MRD1, MRT4, MTR4, NAN1, NIP7, NOC3, NOC4, NOG1, NOP1, NOP12, NOP14, NOP2, NOP4, NOP56, NOP58, NOP7, NOP8, NSA2, NSR1, NUG1, PRP43, PWP1, PWP2, RCL1, REX4, RIX1, RLP7, RNT1, ROK1, RPF1, RPF2, RRP12, RRP3, RRP36, RRP5, RRP8, RRS1, SAS10, SPB1, SSF1, TSR1, TSR4, URB1, UTP10, UTP11, UTP13, UTP14, UTP20, UTP21, UTP23, UTP4, UTP5, UTP6, UTP8
Ribosomal small subunit biogenesis	46	BMS1, DBP8, DHR2, DIM1, ECM16, EFG1, ENP1, ENP2, FAF1, FAL1, HAS1, IMP4, KRE33, KRI1, KRR1, LTV1, MRD1, NAN1, NOC4, NOP14, NOP58, NOP7, NSR1, PRP43, PWP2, RCL1, ROK1, RRP12, RRP3, RRP36, RRP5, RRS1, SAS10, TSR1, TSR4, UTP10, UTP11, UTP13, UTP14, UTP20, UTP21, UTP23, UTP4, UTP5, UTP6, UTP8
Ribosomal large subunit biogenesis	44	BRX1, DBP3, DBP9, DRS1, ERB1, HAS1, MAK16, MAK21, MAK5, MDN1, MRT4, NIP7, NOC2, NOG1, NOP12, NOP15, NOP2, NOP4, NOP7, NOP8, NSA1, NSA2, NUG1, PRP43, PUF6, REI1, REX4, RIX1, RIX7, RLP24, RLP7, RPF1, RPF2, RRP5, RRP8, RRS1, RSA4, SDA1, SPB1, SSF1, SYO1, URB1, YTM1, YVH1
Nuclear transport	19	ARX1, ENP1, KAP123, LTV1, MTR4, NMD3, NOG1, NOG2, NUG1, REI1, RIX1, RIX7, RPF1, RRS1, RTP1, SDA1, SRP40, SYO1, UTP8

Table 2 Continued. GO term analysis with 144 most upregulated genes.

RNA modification	16	BMT5, BMT6, DIM1, DUS3, ELP3, GAR1, GCD10, NOP1, NOP2, NOP56, PPM2, RRP8, SPB1, TRM1, TRM11, TRM2
Ribosome assembly	15	BRX1, DRS1, MAK21, MDN1, MRD1, MRT4, NSR1, REX4, RIX1, RPF1, RPF2, RRP5, RSA4, SSF1, YVH1
Organelle assembly	15	BRX1, DRS1, MAK21, MDN1, MRD1, MRT4, NSR1, REX4, RIX1, RPF1, RPF2, RRP5, RSA4, SSF1, YVH1
Transcription from RNA polymerase I promoter	11	NAN1, RPA135, RPA190, RPA34, RPA43, RPA49, RRN11, UTP10, UTP4, UTP5, UTP8
Ribosomal subunit export from nucleus	11	ARX1, LTV1, NMD3, NOG1, NOG2, NUG1, RIX1, RIX7, RPF1, RRS1, SDA1
Biological process unknown	10	CMS1, GFD2, IMD4, NOP13, NRP1, RRT14, YBL028C, YCR016W, YDL050C, YPR123C
Signaling	2	EFG1, YVH1
Cytokinesis	1	NOP15
mRNA processing	1	PRP43
Cellular response to DNA damage stimulus	1	TRM2
Vacuole organization	1	YVH1
Regulation of cell cycle	1	SDA1

Table 2 Continued. GO term analysis with 144 most upregulated genes.

RNA splicing	1	PRP43
Regulation of DNA metabolic process	1	RIX1
DNA-templated transcription, initiation	1	RRN11
Sporulation	1	YVH1
DNA-templated transcription, termination	1	RNT1
DNA repair	1	TRM2
Transmembrane transport	1	AGP1
Regulation of protein modification process	1	FPR4
Proteolysis involved in cellular protein catabolic process	1	ACL4
Pseudohyphal growth	1	KAP123
Lipid metabolic process	1	URA7
Cytoplasmic translation	1	RBG1
Response to oxidative stress	1	LTV1

Table 2 Continued. GO term analysis with 144 most upregulated genes.

Cell budding	1	REI1
Meiotic cell cycle	1	YVH1
Amino acid transport	1	AGP1
Response to osmotic stress	1	LTV1
Regulation of translation	1	PUF6
Response to starvation	1	RBG1

fold increase in thickness) and was partially disruptive, consistent with the presence of holes and pits on the cell wall of yeast treated with AgNPs [67]. Importantly, the RNA-seq results in conjunction with GO term analysis provide a more comprehensive view of defects in cell wall organization caused by AgNPs. First, it appears that AgNPs affect proper turnover rate of cell wall components including mannoprotein and glycans. I postulate this idea because the thickening of yeast cell wall upon treatment of AgNPs [89] might be due to either a unsteady organization of the cell wall or an accumulation of cell wall proteins. The idea of destabilization of the cell wall has been proven true [67], while the possibility of the accumulation of cell wall mannoproteins and glucans in the presence of AgNPs has yet to be tested. Based on my RNA-seq data, the following seven genes implicated in cell wall organization are highly

downregulated: TIR1–4, DAN1, GSC2 and RNT1. These four TIR and DAN1 genes code for cell wall mannoproteins, while the gene product of GSC2 is a catalytic subunit of β-1,3-glucan synthase required for cell wall glucan synthesis and remodeling in S. cerevisiae [90]. RNT1 gene is involved in cell wall stress response and in regulating degradation of cell wall integrity [91]. The significant reduction of these mRNA levels indicates the possibility that the cell senses an abnormally thick cell wall caused by AgNPs. Even though the thicker wall does not necessarily mean an increase in the number of manno-proteins and glucans, we cannot exclude the possibility that the abnormality is, in part, due to an accumulation of these cell wall components. In this scenario, genes for these cell wall components can be downregulated since the regulatory factors for cell wall integrity would act against the expression of cell wall components (Figure 8B, model B).

In light of the finding of the downregulation of six ergosterol synthesis genes (Table 3), including ERG11, 25, 28, 3, 5 and 6, one can conjecture that the integrity of the plasma membrane is compromised in the presence of AgNPs. Consistent with this idea, genes for membrane sugar transporters such as HXT13, HXT17 and HXT2 are differentially expressed (Table 3 and Figure 8B, model B). Furthermore, multiple genes implicated in carbohydrate metabolism in the cytoplasm (Figure 6, model B) were downregulated. The possibility is that both destabilization of the plasma membrane and decreased levels of sugar transporters in AgNP-treated samples limit the amount of sugar to be metabolized in the cytosol (Figure 8B, model B). In addition to the metabolic defects, genes associated with pyruvate transport (MPC3), TCA cycle (ACO1, CIT2, CIT3) and NADH regeneration (ALD4 and GUT2) were downregulated with AgNPs (Table 3, and Figure 8B). Therefore, my observation is not only

Table 3. Go term analysis with 144 most downregulated genes.

Gene Ontology term	No. of genes	Corresponding genes
Biological process unknown	38	CMC4, ECM13, FMP23, HBN1, ICY1, LEE1, MMO1, PBI1, RTS3, SNR190, TDA4, TOS8, TBR012C, YBR056W-A, YBR201C-A, TDR182W-A, YDR535C, YER121W, YER188W, YFL051C, YGR035C, YGR066C, YGR107W, YHL045W, YHR033W, YHR210C, YJL213W, YJL215C, YLR053C, YLR108C, YLR152C, YLR342W-A, YML083C, YML131W, YMR196W, YOR032W-A, YOR387C, YOR392W
Lipid metabolic process	15	ATF2, CIT3, CYB5, ECI1, EEB1, ERG11, ERG25, ERG28, ERG3, ERG5, ERG6, PDH1, POT1, UPC2, YEH1
Transmembrane transport	12	AAC3, ADY2, BAP2, ENA1, HXT13, JEN1, MPC3, PRM6, SCR1, STL1, SUL1, ZRT1
Transmembrane transport	12	AAC3, ADY2, BAP2, ENA1, HXT13, JEN1, MPC3, PRM6, SCR1, STL1, SUL1, ZRT1
Response to chemical	11	ATF2, CIN5, GRX6, MF(ALPHA)2, NRG2, PRR2, TSA2, UPC2, VHR1, ZNF1, ZTA1
Monocarboxylic acid metabolic process	11	ALD4, ALD6, CIT2, CIT3, DLD3, ECI1, EEB1, FMS1, MLS1, PDH1, POT1
Ion transport	11	ADY2, ALP1, ATO2, BAP2, DIP5, ENA1, JEN1, MPC3, PRM6, SUL1, ZRT1
Cell wall organization or biogenesis	10	GIP1, GSC2, OSW2, SPO73, TIP1, TIR1, TIR2, TIR3, TIR4, DAN1

Table 3 Continued. Go term analysis with 144 most downregulated genes.

Transcription from RNA polymerase II promoter	9	CIN5, NRG2, PHD1, PRR2, ROX1, UPC2, VHR1, YAP6, ZNF1
Ergosterol biosynthesis/organization	8	HES1, ERG11, ERG25, ERG28, ERG3, ERG5, ERG6, UPC2
Carbohydrate metabolic process	8	CIT2, GSC2, GUT2, IMA1, MAL32, MLS1, PYC1, SUC2
Meiotic cell cycle	7	GIP1, GSC2, MPC54, MSH5, OSW2, SPO20, SPO73
Transcription from RNA polymerase II promoter	9	CIN5, NRG2, PHD1, PRR2, ROX1, UPC2, VHR1, YAP6, ZNF1
Ergosterol biosynthesis/organization	8	HES1, ERG11, ERG25, ERG28, ERG3, ERG5, ERG6, UPC2
Carbohydrate metabolic process	8	CIT2, GSC2, GUT2, IMA1, MAL32, MLS1, PYC1, SUC2
Meiotic cell cycle	7	GIP1, GSC2, MPC54, MSH5, OSW2, SPO20, SPO73
Generation of precursor metabolites and energy	6	AAC3, ACO1, ATF2, CIT3, ISF1, RGI2
Sporulation	6	GIP1, GSC2, MPC54, OSW2, SPO20, SPO73
Transposition	6	YBL005W-B, YBL100W-B, YBR012W-B, YDR261W-B, YMR045C, YNL284C-B
Cofactor metabolic process	5	ALD4, ALD6, FMS1, GUT2, HEM13

Table 3 Continued. Go term analysis with 144 most downregulated genes.

Response to osmotic stress	5	ALD6, CIN5, ENA1, NRG2, ROX1
Cellular respiration	4	AAC3, ACO1, CIT3, ISF1
Carbohydrate transport	4	HXT13, HXT17, HXT2, STL1
Cellular amino acid metabolic process	4	BAT2, CAR2, CIT2, PUT1
rRNA processing	4	SNR10, SNR17A, SNR34, SNR37
Response to oxidative stress	4	GRX6, TSA2, VHR1, ZTA1
Vitamin metabolic process	3	FMS1, SNZ1, THI4
RNA modification	3	SNR10, SNR34, SNR37
Oligosaccharide metabolic process	3	IMA1, MAL32, SUC2
Membrane trafficking and protein targeting	3	COS4, SCR1, SPL2
Amino acid transport	3	ALP1, BAP2, DIP5
Response to starvation	3	ENA1, UPC2, VHR1
Pseudohyphal growth	3	NRG2, PHD1, MIT1

Table 3 Continued. Go term analysis with 144 most downregulated genes.

Protein folding	2	EUG1, HSP26
Nucleobase-containing small molecule metabolic process	2	ALD4, ALD6, GUT2
DNA repair/recombination	2	IRC4, MSH5
mRNA processing	2	AI1, SNR19
Mitochondrion organization	2	ACO1, THI4
Mitochondrial translation	2	15S˙RRNA, 21S RRNA
Ribosomal small subunit biogenesis	2	SNR10, SNR17A
Conjugation	2	MF(ALPHA)2, PRR2
Enzyme	2	ERR3, MAN2
Cellular response to DNA damage stimulus	1	IRC4
Translational elongation	1	ANB1
Protein dephosphorylation	1	GIP1
Protein phosphorylation	1	PRR2
Invasive growth in response to glucose limitation	1	NRG2

Table 3 Continued. Go term analysis with 144 most downregulated genes.

Signaling	1	MF(ALPHA)2

consistent with previous findings that demonstrated that nano-silver particles cause direct mitochondrial damage, disturb the function of respiratory chain, increase ROS production and induce apoptosis [92-94], but also provide new mechanistic insights into mitochondrial dysfunction mediated by AgNPs.

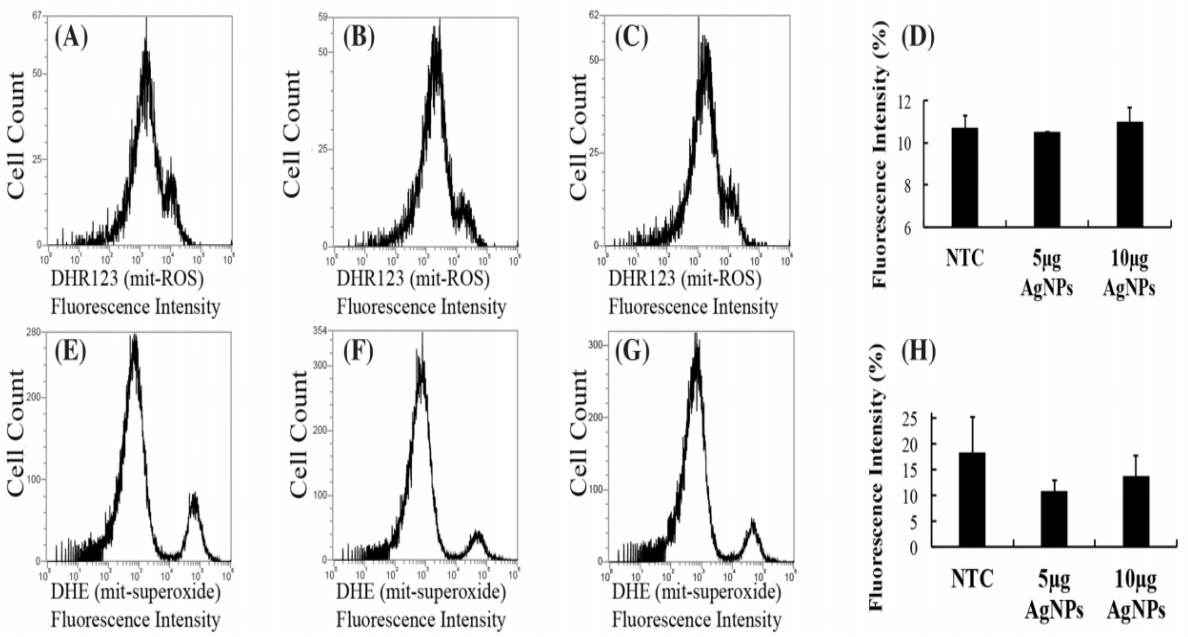

Figure 6. Assessment of ROS and superoxide levels in flow cytometry experiments. Two mitochondrial ROS indicators, DHR123 and DHE, were utilized in the quantification of ROS and superoxide in yeast cells treated with varying concentrations of 20 nm AgNPs for 8 h. DHR123 and DHE were added at concentrations of 5 µg/mL for the last 2 h of incubation. Each treatment concentration (0, 5 and 10 µg/mL of AgNPs) was tested in triplicate. A two-tailed equal variance Student's t-test was performed, and no statistical difference was observed between the three groups. **(A–C)** Representative DHR123 fluorescent intensity charts of cells treated with DHR123 and grown in the presence of no AgNPs **(A)**, 5 µg/mL AgNPs **(B)** or 10 µg/mL AgNPs. **(D)** Quantification of DHR123 levels. The total % fluorescence means from each replicate in the ROS detection assay. **(E-G)** Representative DHE fluorescent intensity charts of cells treated with DHE and grown in the presence of no AgNPs **(E)**, 5 µg/mL AgNPs **(F)** or 10 µg/mL AgNPs **(G)**. **(H)** The total % fluorescence means from each replicate in the superoxide detection assay.

Additionally, a recent study with S. cerevisiae where 9 nm AgNPs were used showed that 5 or 10 µg/mL of AgNPs caused a drastic inhibition of cellular respiration taking place in mitochondria [95], augmenting the notion that mitochondrial functions are downregulated. Consistently, the present study shows downregulation of AAC3, a ADP/ATP translocator gene functioning for exchanging ADP generated by the F1F0-ATPase for ATP (Table 3, not shown in Figure 8B) [96, 97]. It is highly likely that low levels ADP in the mitochondrial matrix due to downregulation of AAC3 by AGNPs limit the substrate concentration for the ATP synthase, which may limit the amount of ATP production. Yet to maintain cell viability, the limited amount of ATP must be

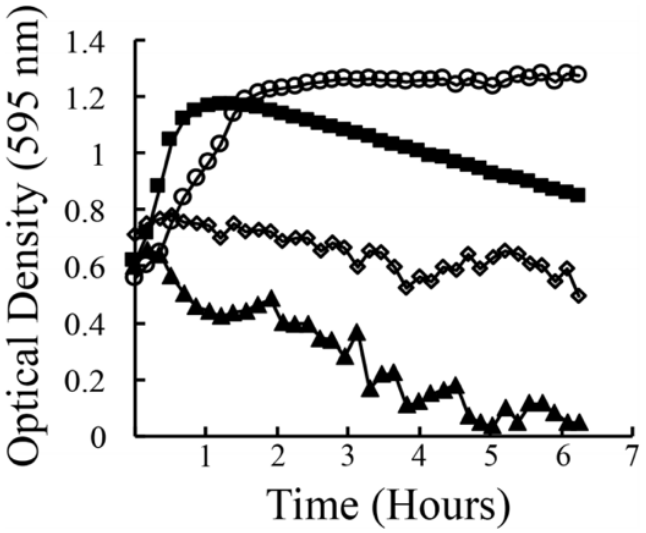

Figure 7. Assessment of cell wall stability with Zymolase 100T enzyme. The rate of yeast cell wall degradation was observed in samples treated with 0, 5 and 10 µg/mL AgNPs, and each sample was tested in triplicate. When treated with Zymolase 100T, the OD's of each sample was recorded every 10 min for 6 h. The rate of cell wall degradation mediated by Zymolase 100T indicates the integrity of cell walls when incubated with varying concentrations of AgNPs. The empty circles represent the mean of the samples treated with no Zymolase 100T. The solid black squares represent the mean of the samples treated with 0 µg/mL AgNPs and 10 µg/mL Zymolase 100T. The empty diamonds represent the mean of the samples treated with 5 µg/mL AgNPs and 10 µg/mL Zymolase 100T. The solid black triangles represent the mean of the samples treated with 10 µg/mL AgNPs and 10 µg/mL Zymolase 100T.

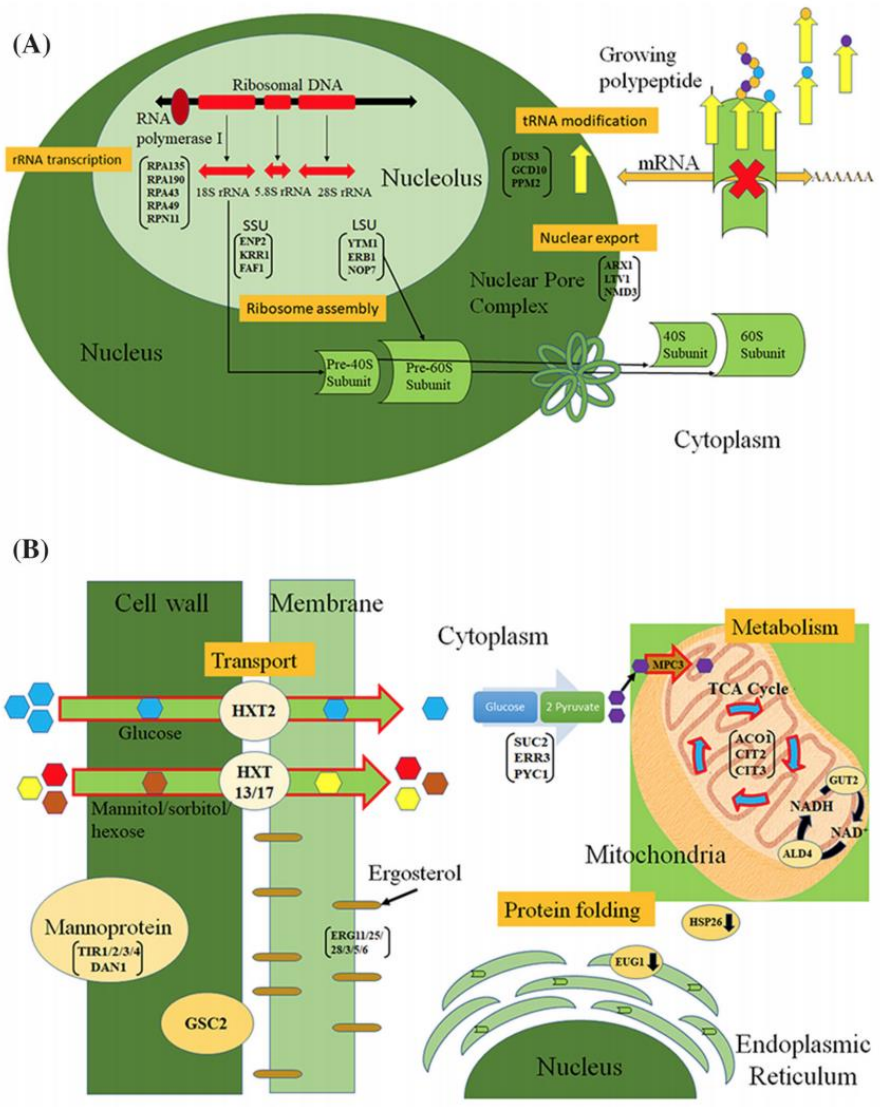

Figure 8. Schematic model of changes of cellular processes with spherical 20 nm AgNPs in yeast cells. **(A)** AgNPs appear to affect the integrity of ribosome, which might end up elevating expression levels of genes implicated in rRNA processing and the biogenesis of small large subunit ribosomes as well as nuclear export of ribosomes. **(B)** Several classes of cellular activities appear to be downregulated by the presence of AgNPs, including cell wall/membrane integrity, sugar import, metabolism in the cytosol, cellular respiration in mitochondria and protein folding.

Conclusion

In the present study, I assessed potential toxicity of AgNPs and provided evidence that yeast cells exposed to these NPs displayed minor defect in growth rates. Accordingly, the

presence of 5 μg/mL AgNPs in the culture media led to significant transcriptome changes in yeast, manifested by the differential expression of several hundred genes implicated in diverse cellular processes. Given many genes that play roles in ribosome biogenesis, cell wall/membrane integrity and mitochondrial functions are significantly altered with the treatment of AgNPs, my conclusion is that even sublethal amounts of AgNPs could serve as a potential environmental stress factor to living cells.

CHAPTER 3: TRANSCRIPTOME PROFILE ALTERATION WITH CADMIUM SELENIDE/ZINC SULFIDE QUANTUM DOTS IN *SACCHAROMYCES CEREVISIAE*

Introduction

Quantum Dots (QDs) are extremely small colloidal semiconductor nanoparticles (NPs) typically 1–10 nanometers in diameter. They are a diverse group of nanomaterials (NMs) that are classified based on physical properties, such as their size, charge, shape, and the chemical composition of their core and shell [11]. These materials (typically Cd-QDs) are an attractive topic in research due to their unusual optical characteristics, mainly, their photo-stability, narrow-tunable emissions, and broad excitation ranges [16, 18]. They have become widely incorporated in electronics, agriculture, and textile production, but they are mostly sought out for their biomedical applications (cellular and protein labels, real-time trackers, fluorescence resonance energy transfer (FRET) sensors, etc.) and used as a smart drug delivery system (SDDS) for treating cancer [11, 15-17, 19, 98, 99]. They make excellent fluorescent probes because their optical properties are size-dependent and are easily manipulated. In addition, they resist photo-bleaching and produce a greater brightness than conventional organic dyes [16, 17]. QDs make a prime candidate for use as nanocarriers in SDDSs because, unlike other nanocarriers, they can simultaneously visualize tumors in addition to delivering a drug to its target [15]. Although QDs are diverse and utilized in numerous applications, there is an increasing concern on their leakage and long-term effects on the environment and human health [11, 19].

Previously published works on QDs present conflicting results regarding cytotoxicity, but most articles that investigate their effects, *in vitro* and *in vivo*, seem to agree that their

physiochemical properties, such as size, charge, composition, and concentration, are responsible for their toxicity [18, 100]. Herein lies the challenge of studying QD toxicity. Their high possible combinations of physiochemical properties result in a broader spectrum of toxic effects. It's been reported that small 2.2 nm CdTe-QDs localize in the nuclear compartment, and the same QDs at 5.2 nm localize in the cytosol [100]. Negatively charged zwitterionic QDs with functionalized surfaces reduce mitochondrial activity by up to 25%, and cellular impedance is reported due to receptor-independent entry through the membrane [17]. However, positively charged CdSe/ZnS-QDs have been found to be less toxic [16]. CdTe-QDs exhibit a dose-dependent cytotoxic effect on cell viability, membrane integrity, metabolic activity, mitochondria integrity, and chromatin quality in an array of cells (HeLa, MCF-7, and NIH/3T3) [101]. The potential number of interactions between QDs and biological components are high, leaving essential questions regarding their toxicity unknown [16].

Previous studies have revealed that long-term exposure of 20 nM CdSe/ZnS-QDs, coated with polyethylene glycol (PEG), amines, or carboxylates, to the eye results in decreased cell viability [102]. Another study found that injecting 0.5 nM CdSe or CdSe/ZnS-QDs into the hippocampal area in rats impairs synaptic activity. This was thought to be induced by increasing calcium levels and Cd^{2+} ions that lead to defects in neuro-secretion [103, 104]. In addition, they have been found to accumulate in the liver and kidneys in rats and could release Cd^{2+} ions in the body of the individual being exposed [105]. On the cellular level, CdSe/ZnS-QDs can enter the cell through the plasma membrane and have been found to inhibit viability in macrophage [106, 107], human keratinocyte HaCaT [108], and human dermal fibroblast cell lines exposed to 15 nm QDs at concentrations of 30–60 nM [109]. Previous studies have found that the degradation of Cd-based QDs releases harmful Cd^{2+} ions that indirectly increase ROS levels (typically H_2O_2,

$\cdot O_2^-$, and ·OH), capable of damaging proteins and membrane lipids, inhibiting DNA repair, disrupting cellular signaling, and causing apoptosis [110-113]. In addition, the precipitation of QD aggregates on the surface of the cell may impair the integrity of the cell wall [111]. In yeast, CdTe-QDs have been shown to exhibit cytotoxicity at concentrations as low as 80.81 and 17.07 nmol/L for green and orange emitting QDs, respectively [114]. Xiaole Han et al. revealed that QDs as small as 4.1 to 5.8 nm could be internalized in *Saccharomyces cerevisiae* and induce cytotoxicity through cell wall breakage and cytoplasm blebbing. Nevertheless, the details on what molecular mechanisms contribute to Cd-based QD toxicity are still poorly understood. To this end, my RNA-seq revealed more in-depth information on the processes and mechanisms that might be responsible for Cd-QD-induced toxicity.

Research papers investigating QD toxicity typically look at mechanisms, such as cell viability and induction of reactive oxygen species [16]. Gene expression assays are not common in studies on Cd-QD-induced toxicity. Using high-throughput quantitative reverse transcript polymerase chain reaction (qRT-PCR) assays, recent studies reported differentially expressed genes affected by CdSe/ZnS-QD toxicity, including genes involved in cellular stress and toxicity, DNA damage and repair, mitochondrial function, proliferation, and ovarian function in vivo [16, 115, 116]. RNA-seq has become the standard for assessing entire genomes and identifying differentially expressed genes (DEGs), and Simon et al. (2013) utilized this process to investigate the effects on transcriptomic profiles of green algae exposed to CdTe/CdS-QDs. They reported via a gene ontology (GO) analysis that DEGs were involved in oxidative-stress, redox potential, protein folding, and chaperone activity pathways in the Cd-treated cells [27]. Hosiner et al. (2014) conducted a microarray experiment on *Saccharomyces cerevisiae* that was exposed to several different metal salts to observe the effects of different metal ions on yeast's

transcriptional profile [23]. Their study revealed anti-oxidative genes (*GRX2*) and redox homeostasis genes (*TRR1*, *TRR2*, and *TRX2*) to be upregulated in response to $CdCl_2$ exposure, due to potential release of Cd^{2+} ions [23]. Interestingly, cadmium is not redox-active, which means it cannot generate ROS directly, yet, Cd-induced ROS is a commonly observed response [117]. They pointed out that metals, such as As^{3+}, Cd^{2+}, and Hg^{2+}, had an affinity toward thiol groups (-SH), which play disparate roles in the function of enzymes, transcription factors, and membrane proteins [23]. A more recent study conducted in 2016 employed RNA-seq to assess differences in gene expression when exposed to 320 μM $CdSO_4$ in *Saccharomyces cerevisiae* [117]. They sorted DEGs into functional classes and found upregulated DEGs belonged to classes, such as transcription factors involved in GSH metabolism, proteins of cellular response to oxidative stress and regulation, enzymes of carbohydrate metabolism, proteins with antioxidant properties, mitochondrion related proteins, peroxisome, and other regulator/transcription factors, while downregulated DEGs belonged to a class of normal expression genes under anaerobic condition (*DAN1*, *AAC3*, *ANB1*, and *YER188W*) and heme biosynthesis key genes (*HEM3* and *HEM13*). In addition, their study revealed that $CdSO_4$ decreased the mitochondrial membrane potential by over 52% and significantly increased ROS levels [113]. However, little is still understood on the transcriptional profiles of *Saccharomyces cerevisiae* when treated with a non-ionizing, Cd-based QD (CdSe/ZnS) that possesses a ZnS shell meant to prevent any harmful Cd^{2+} from leaking out of the CdSe core.

Though CdSe/ZnS-QDs have been used in many ways and conjugated or coated with various molecules and exposed to a variety of organisms, their impact on cellular environments and gene expression is not well understood and raises concerns about their potential toxicity, despite their “safe” core/shell structure. Chibli et al. found other “safer” core/shell QDs, such as

InP/ZnS-QDs, generating ROS despite their ZnS shell [118]. Their study attributed the generation of ROS in NIH3T3 fibroblasts, KB cells, B16 murine melanoma cells, and MDA-MB-231 breast adenocarcinoma cells to the poor coordination strength between the InP core and ZnS shell, resulting in an unstable core/shell relationship that left the InP core exposed in some areas [118]. With the addition of a second ZnS shell around InP/ZnS-QDs, exposed sections of the core were contained, and a decrease in ROS generation was observed [118]. It was noted that a CdSe core and ZnS shell had a better coordination strength, resulting in a stable core/shell structure with minimum CdSe core exposure [118]. Due to these interesting results, it is unlikely that CdSe/ZnS-QDs require a second ZnS shell for their safe use. In addition, the CdSe/ZnS-QDs were synthesized with a carboxylic acid stabilizing ligand that is capped on the surface on the ZnS shell. Capping ligands are often used to prevent QDs from aggregating, and some may play a major role in the uptake of QDs into cells and where they are localized. Kunstman and associates (2018) bio-conjugated CdTeS/ZnS-QDs with a galactose ligand and successfully achieved fluorescent imaging of yeast cells [119]. They revealed that CdTeS/ZnS-QDs capped with galactose ligands accumulated in the membrane of yeast cells, while CdTeS/ZnS-QDs with unmodified surfaces failed to accumulate in the membrane or enter the yeast cells, suggesting that specific associations between the ligands and cell surface may play a role in the entry of Cd-QDs into yeast cells [119]. Due to CdSe/ZnS-QDs seemingly more stable structure than other core/shell QDs, their effects on cell physiology have remained elusive and require further explanation. The present study utilized deep sequencing technologies like RNA-seq to assess to what extent CdSe/ZnS-QDs affect the transcriptome profile of *Saccharomyces cerevisiae* with great precision.

Results

CdSe/ZnS-QDs Negatively Affect Yeast Growth. To investigate the effects of CdSe/ZnS-QDs on yeast growth, I utilized AgNPs as a positive control, as they have been shown to cause growth defects in yeast cells by Horstmann and coworkers [47]. As expected, the treatments of AgNPs obtained results consistent with the findings of Horstmann and coworkers, where the concentrations of 5 µg/mL and 10 µg/mL of AgNPs showed significant growth rate reduction when compared to non-treated controls (Figure 9A,B). In contrast, CdSe/ZnS-QDs did not show any effects on yeast growth when compared to the non-treated controls, even when treated with 100 µg/mL of CdSe/ZnS (Figure 9A,B). In order to more clearly define the differences of cell growth in the steady-state, I analyzed the last optical density value (endpoint $OD_{600\ nm}$ at 24 h) for both the AgNPs and CdSe/ZnS-QD-treated cells. In the CdSe/ZnS, there was no significant difference in endpoint OD values compared to the non-treated control according to the ANOVA test (Figure 9C,D). Similarly, the endpoint OD of AgNPs showed no significant difference from the non-treated control, via an ANOVA test (Figure 9C,D). However, when performing a student *t*-test on ODs exposed to both AgNP and CdSe/ZnS-QDs, the results revealed the endpoint ODs were statistically different from those of the non-treated control in cells treated with 5 µg/mL AgNPs (20 nm) and 6.25 µg/mL CdSe/ZnS-QDs (estimated 4.1 nm). During the exponential growth period, I analyzed the difference in doubling times between the non-treated controls and the treated cells. For the CdSe/ZnS-treated cells, the student *t*-test revealed that the average time spent in exponential growth was not significantly different from the non-treated control. As for the AgNP-treated cells, the average doubling time was significantly different from the non-treated control for most of the concentrations, according to the student *t*-test. Before the cells grew exponentially, the cells treated with either AgNPs or

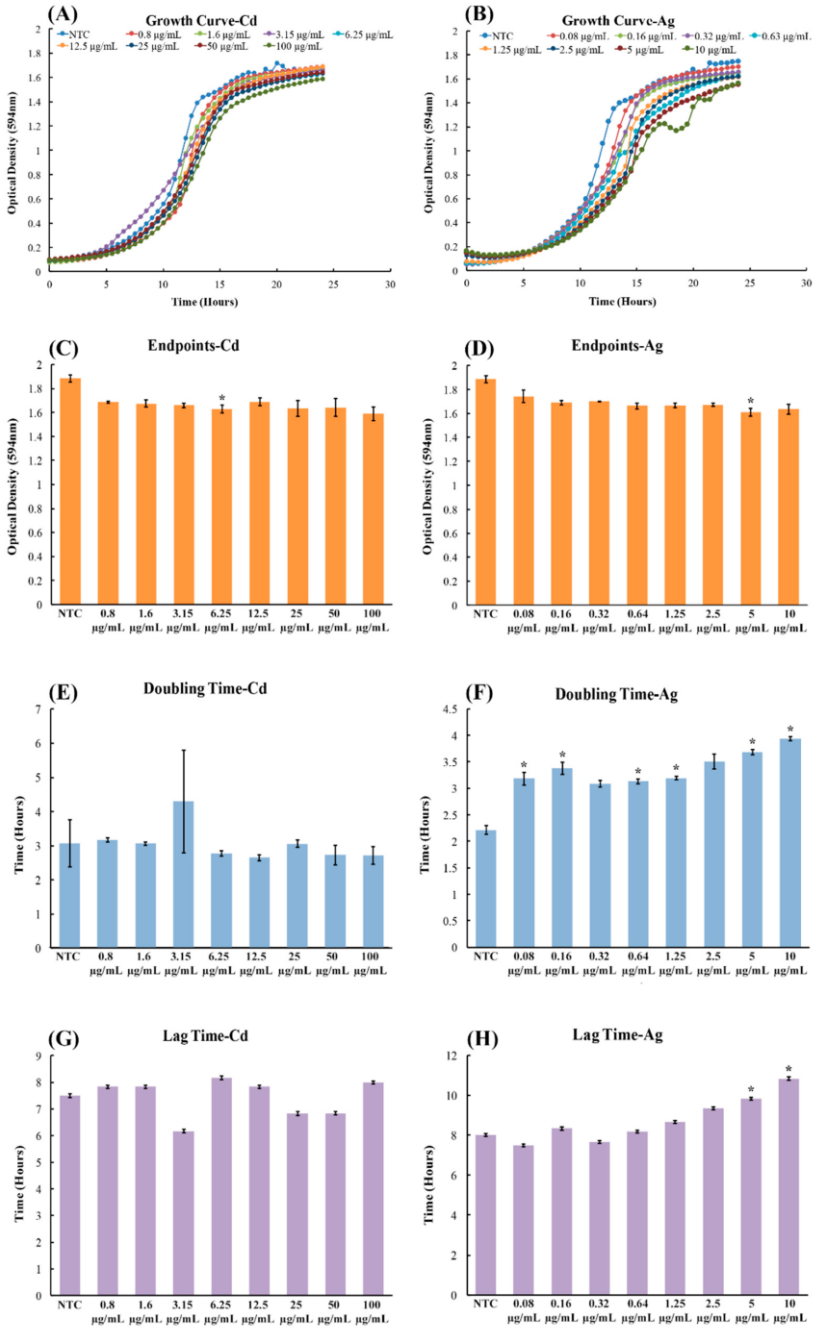

Figure 9. Growth assay to determine growth rates of CdSe/ZnS and AgNP-treated yeast cells. **(A,B)** Quantification of cell optical densities over a 24 h period, where the cells were treated with CdSe/ZnS and AgNPs, respectively, at 30 °C while shaking. **(C,D)** Measurement of cell optical densities at 24 h of treatment with CdSe/ZnS and AgNPs, respectively. The bar represents the average ODs (600 nm) of each concentration at the 24 h mark. Significant statistical differences are indicated by *p*-values less than 0.05. **(E,F)**. Doubling time takes place during the phase of exponential growth for the cells treated with CdSe/ZnS and AgNPs, respectively, and was measured as the amount of time it takes for cells to double their ODs. *p*-values of less than 0.05 indicate statistical differences with an asterisk. **(G,H)**. The mean lag time before the exponential growth phase. AgNP, silver nanoparticle; OD, optical density.

CdSe/ZnS-QDs showed, based on the student *t*-test, no significant difference from the non-treated controls. Taken together, based on the results obtained from the endpoint ODs, doubling times, and lag times, CdSe/ZnS did not have any negative growth effects on yeast cell growth, whereas the AgNPs showed adverse effects on yeast cell growth.

cDNA Sequencing Reveals Up- and Downregulated Genes with CdSe/ZnS-QDs. Instead of relying on the limited simple methods of proliferation, organelle integrity, or metabolic assays to gain insight on how CdSe/ZnS QDs interact with fungal cells, I decided to look into differential gene expression profiles to examine a broader range of cellular processes being affected. I determined the transcriptomic response in *S. cerevisiae* exposed to 10 μg/mL CdSe/ZnS-QDs by performing an RNA-seq that produced gene expression profiles for both the control and CdSe/ZnS-treated cells. Briefly, the control and CdSe/ZnS exposed cells were subjected to a total RNA extraction. Then, the mRNA was isolated from the total RNA, followed by a cDNA conversion step. Both control and QD-treated samples were tested in triplicate, and the newly synthesized cDNA libraries were sequenced with a next-gen DNA sequencer (Illumina®, San Diego, CA, USA) that produced sequenced datasets for each replicate. Each cDNA dataset had to be uploaded to a computational data analysis platform (usegalaxy.org) for processing, and all control and CdSe/ZnS-treated replicates were concatenated, leaving the first dataset composed of the three control samples and the second of the QD-treated samples. Every cDNA fragment underwent a quality check (FastQC) and quality trimming (FASTQ Quality Trimmer) before being mapped to the reference genome (S288C). An average of 19,619,921 accepted reads was gathered from the control groups and 19,205,868 from the CdSe/ZnS-treated groups. Of these quality reads, an average of 91.7% and 93.6% of the total reads mapped to the reference genome, and an average of 9.9% and 10% of the mapped reads had multiple

alignments in control and CdSe/ZnS-treated groups, respectively. The high percent of mapped reads indicated that the cDNA sequence data accurately corresponded to the transcriptional expression in *S. cerevisiae,* and the multiple sequence alignments indicated the successful alignment of the fragmented sequence data to their homologous segments on the reference genome. The gene identities were also accurately identified.

A total of 7127 genes, including non-coding cDNA, were identified, and of those, 4478 genes were found to have significant changes in transcript expression ($q < 0.05$) when compared to the non-treated controls. From the pool of genes with q-values below 0.05, 2267 genes were found to be upregulated, and 2211 genes downregulated. From each pool of up and downregulated genes found to be significantly different, those differentially expressed by a fold of 1.5 or greater were selected (2839 genes). From the gene pool of DEGs with a fold-change of 1.5 and up, I obtained GO terms with GOrilla and found 47.6% (742 of 1560 genes) of upregulated genes involved in cellular nitrogen compound metabolic processes (Figure 10A). Several upregulated genes were implicated in non-coding RNA (ncRNA) processing (18.7%), rRNA processing (14.6%), translation (13.2%), ribonucleoprotein complex biogenesis (13.2%), and cell cycle process (11.6%) (Figure 2A). For the above GO terms, 291 and 228 upregulated genes were involved in ncRNA and rRNA processes, respectively (Figure 10A). Additionally, 206, 206, and 181 genes were implicated in translation, ribonucleoprotein complex biogenesis, and cell cycle processes, respectively (Figure 10A). Enrichment values for GO terms found with genes with a fold-change of 1.5 or greater fell between 1.0 and 2.0, meaning each GO-term was approximately as meaningful as any other GO term shown. To gain a clearer understanding of the changes in the cellular transcriptome after treating with CdSe/ZnS-QDs, I selected the 150 most upregulated and 150 most downregulated genes, i.e., 300 genes total, and obtained GO-

term data consistent with my data represented. I also created a heatmap of these 300 genes to visually depict their highly up- and downregulated expression levels compared to the non-treated controls. I found 102/150 (68%) of these upregulated genes to be involved in cellular component organization or biogenesis, such as ribosomal subunit biogenesis and its assembly to form functional ribosomes. Several of the other highly upregulated genes were involved in ribosomal RNA metabolic processes (63.33%), cleavage involved in rRNA processing (18%), maturation of LSU (large subunit of ribosome, 12.66%) and SSU rRNA (small subunit of ribosome, 18.66%), ncRNA transcription (6%), macromolecule methylation (6%), and genes involved in cell cycle DNA replication (2.66%). Of the 21 GO-terms, five GO-terms described the maturation of rRNA, four GO-terms were involved in pre-ribosome biogenesis or assembly, four GO-terms involved in transcription of rRNA by RNA polymerase I, and three GO-terms involved in the transport and export of RNA and ribosomal subunits.

GO-term analysis on the downregulated genes with a fold difference of at least 1.5 indicated that metabolic processes were negatively affected (Figure 10B). Most downregulated genes were implicated in small molecule metabolic (16.5%) and oxidation-reduction processes (13.0%) (Figure 10B). Several more downregulated genes were involved in carbohydrate metabolic processing (8.0%), responding to chemicals (7.5%), proteolysis (7.5%), ion transmembrane transport (5.7%), import into the cell (3.9%), and the electron transport chain (2.6%) (Figure 10B). For the downregulated GO-terms, 211 and 166 genes were implicated in small molecule metabolic and oxidation-reduction processes, respectively (Figure 10B). In addition, 102, 96, 96, 73, 50, and 33 genes were involved in carbohydrate metabolism, response to chemicals, proteolysis, ion transmembrane transport, import into cell, and the electron transport chain, respectively (Figure 10B). Enrichment values for GO-terms found with genes

A

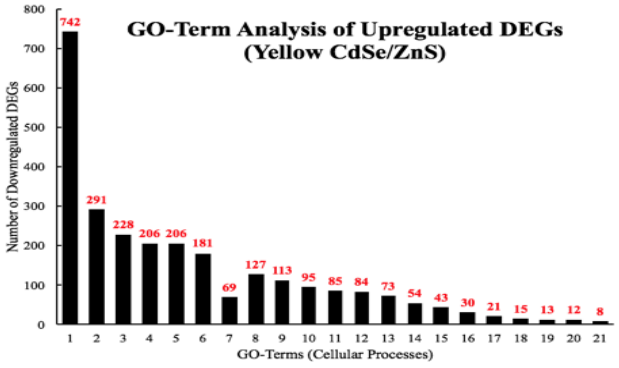

Key	GO-terms
1	cellular nitrogen compound metabolic process
2	ncRNA processing
3	rRNA processing
4	Translation
5	ribonucleoprotein complex biogenesis
6	cell cycle process
7	heterocycle biosynthetic process
8	tRNA metabolic process
9	cellular amino acid metabolic process
10	chromosome organization
11	carboxylic acid biosynthetic process
12	RNA transport
13	cell division
14	post transcriptional regulation of gene expression
15	DNA replication
16	snoRNA processing
17	aromatic amino acid family metabolic process
18	snRNA processing
19	purine ribonucleoside metabolic process
20	pyrimidine nucleoside monophosphate biosynthetic process
21	nuclear-transcribed mRNA catabolic process

B

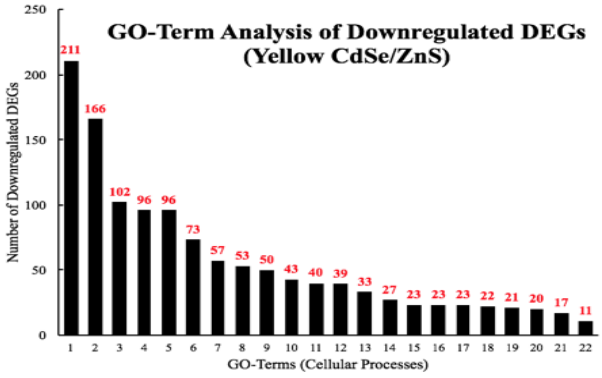

Key	GO-term
1	small molecule metabolic process
2	oxidation-reduction process
3	carbohydrate metabolic process
4	response to chemical
5	proteolysis
6	ion transmembrane transport
7	cation transmembrane transport
8	process utilizing autophagic mechanism
9	import into cell
10	purine ribonucleotide metabolic process
11	endocytosis
12	response to oxidative stress
13	electron transport chain
14	ATP metabolic process
15	endosome transport (multivesicular sorting pathway)
16	glucan metabolic process
17	lipid catabolic process
18	mitochondrial respiratory chain complex assembly
19	ATP biosynthetic process
20	detoxification
21	respiratory chain complex IV assembly
22	glucose transmembrane transport

Figure 10. Differentially expressed genes with CdSe/ZnS QDs. GO-terms corresponding to each differentially expressed gene's biological process. Out of 4478 genes with a *q*-value below 0.05, 2839 genes with a fold change greater than or equal to 1.5 were incorporated. **(A)** The quantification of upregulated genes associated with their specific GO terms. Of the 2839 statistically different genes, 1560 were found to be upregulated. **(B)** The quantification of downregulated genes associated with their specific GO terms. Of the 2839 genes, 1279 were found to be downregulated.

with a fold-change of 1.5 or greater fell between 1.0 and 2.0, meaning each GO-term was approximately as meaningful as any other GO-term shown. From the list of 150 most downregulated genes, I found 26 GO-terms on their cellular processes compared to only 21 GO-terms pertaining to the pool of 150 most upregulated genes. The downregulated GO-terms were found to affect genes involved in various metabolic processes and were more diverse in the cellular processes they effect compared to the upregulated GO-terms that are predominantly involved in ribosomal biogenesis (Figure 10A,B). The GO-term with the most highly downregulated genes from the list of 150 was the oxidation-reduction process with 31/150 (20.66%) genes involved. Other highly downregulated genes and their GO-terms given, based on their cellular processes, were included but not limited to the Generation of precursor metabolites and energy (18%), carbohydrate metabolic processes (16%), cellular response to chemical stimulus (9.33%), alcohol metabolic process (5.33%), antibiotic metabolic process (6%), response to drug (4%), and response to salt stress (3.33%). Of the 21 GO terms involved in highly downregulated gene pool, 14 were directly involved in metabolism, four GO terms acted as a response to stimuli, such as chemical stimulus, oxidative stress, drug, and salt stress, and three GO terms were found to be directly involved in oxidation processes. I found many GO terms involved in similar processes and several that share many of the same genes and several that do not. For instance, of the four GO terms that represented genes that were involved in responding to stimulus (cellular response to chemical stimulus, response to oxidative stress, response to drug, and response to salt stress), the gene *CTT1* was involved in each except in the GO term response to chemical stimulus. Interestingly, *NCE103* was found to be involved in the GO terms response to chemical stimulus and oxidative stress, but not in the GO terms response to drug or salt stress. Similarly, *CIN5* was involved in the GO terms response to drug and salt

stress but not in the GO terms response to chemical stimulus and oxidative stress. Some GO terms that represent metabolic processes contained the exact same genes, such as the GO terms ethanol metabolic process (four genes involved: *PDC6*, *ALD4*, *ALD6*, and *NDE2*) and alcohol metabolic process (eight genes involved: *DSF1*, *PDC6*, *ALD4*, *GUT2*, *YNR073C*, *YAT2*, *ALD6*, and *NDE2*). Likewise, there were GO terms that represent metabolic processes that had no genes in common, such as the GO terms polysaccharide metabolic process (10 genes involved: *YMR084W, GSY1*, *GLC3*, *GIP2*, *GPH1*, *PGM2*, *GAC1*, *GDB1*, *UGP1*, and *SUC2*) and antibiotic metabolic process (nine genes involved: *CTT1, TSA2, PDC6, ALD4*, *ACH1*, *ALD6*, *NDE2*, *SDH1*, and *SHH4*).

Validation of RNA-Seq Data by RT-qPCR. I validated my differentially expressed gene data and expression profiles generated from the RNA-seq experiment by conducting a real-time RT-qPCR test. I selected two upregulated genes (*FAF1* and *SDA1*) that play a role in rRNA processing/ribosomal biogenesis, two downregulated genes (*DAN1* and *TIR1*) that form structural mannoproteins that help maintain cell wall integrity, and a housekeeping gene (*ALG9*) whose expression is unchanged in the presence of CdSe/ZnS QDs, based on the RNA-seq fold-change data with a *q*-value less than 0.05. *FAF1* and *SDA1* were found to have 7.32 ± 0.52-fold and 8.06 ± 2.15-fold upregulation in expression, and *DAN1* and *TIR1* were found to have 5.3-fold and 3.3-fold downregulation in expression, respectively, when treated with 10 μg/mL CdSe/ZnS-QDs (Figure 11A,B). The resulting fold-changes for *FAF1*, *SDA1*, *DAN1*, and *TIR1* were measured with RT-qPCR and graphed along with each gene fold-change found with RNA-seq. A linear regression line was drawn to represent the correlation between the fold-changes found with each method, and the RT-qPCR fold-changes were found to be consistent with my RNA-seq expression data (Figure 11C).

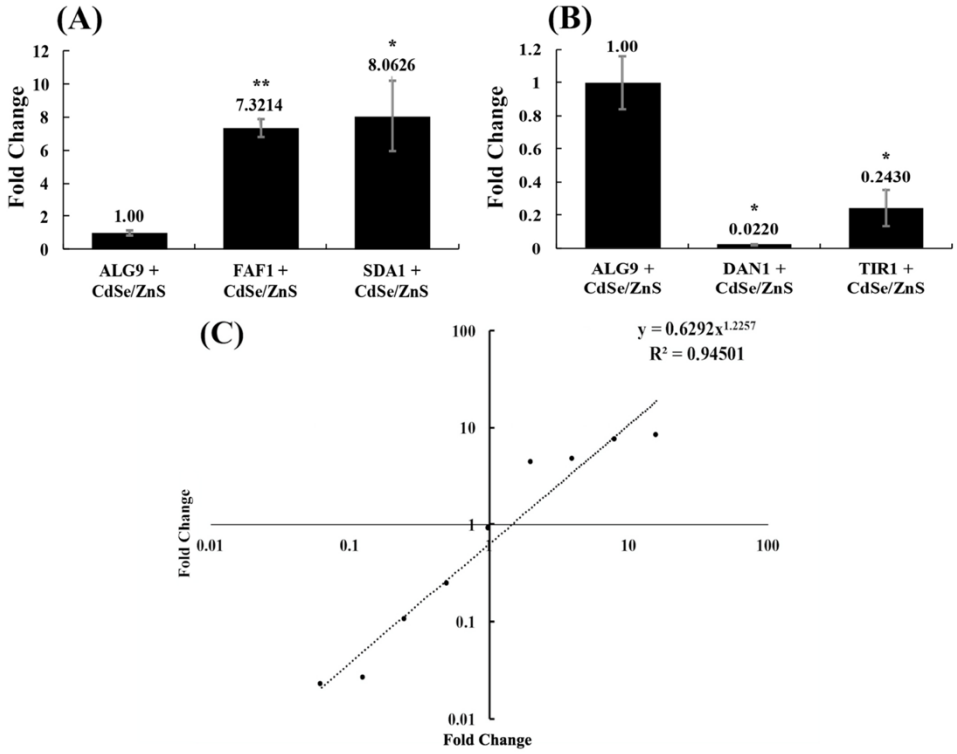

Figure 11. Fold-change values acquired through RT-qPCR. Two up and downregulated genes chosen from the RNA-seq experiments were compared to a housekeeping gene (*ALG9*) found to not be differentially expressed when exposed to CdSe/ZnS-QDs. The fold changes of the two up and downregulated genes were calculated from the RT-qPCR data by utilizing the Pfaffl equation. Fold changes were found with RT-qPCR to validate fold-changes obtained with the RNA-seq. **(A)** The fold changes of the upregulated genes (*FAF1* and *SDA1*) obtained with RT-qPCR. **(B)** The fold-changes of the downregulated genes (*DAN1* and *TIR1*) obtained with RT-qPCR. A student's *t*-test results are represented with * ($p < 0.05$), ** ($p < 0.01$). **(C)** The fold change correlation represented by a trend line that shows the power regression line with the equation and R^2 value of 0.94501. The x and y-axes are in 2- base logarithmic scale, and fold-changes that are <1 and >1 correspond to down and upregulation, respectively.

ROS in Response to CdSe/ZnS. It is known that cells respond to environmental factors, including nanoparticles, by producing reactive oxygen species that affect the physiology of the cells. To assess the amounts of superoxides produced by the cell when treated with CdSe/ZnS (20 µg/mL) or AgNPs (5 µg/mL), I measured the fluorescent intensities of dihydroethidium (DHE) at 600 nm using a flow cytometer. The rationale for measuring the DHE at 600 nm was to

detect the amount of red fluorescence emitted by the oxidation of DHE that is caused by superoxide. The no-cell controls, including only PBS, AgNPs, or CdSe/ZnS-QDs, displayed a little background noise, which was manifested from their low cell counts, along with missing DHE fluorescent intensity peaks (Figure 12A–C). However, the non-treated cell control sample revealed a peak of cells that have oxidized DHE, along with a bigger peak that represents cells carrying non-oxidized DHE. I found that the fluorescent intensities of the oxidized DHE in the AgNP- and CdSe/ZnS-treated cells were not statistically different from that of the non-treated cell control (Figure 12D–G). This suggests that both AgNPs and CdSe/ZnS-QDs have no significant effect on the production of superoxide in the cells.

The Vulnerability of Cell Wall Integrity in Yeast Cells. Yeast cells maintain a cell wall, which allows the cell to stay well protected from many threats across the board. However, when treated with Zymolase, the cell wall breaks down and leaves the cell with only its plasma membrane, making the cells more sensitive to environmental factors. It is known that nanomaterials are coated with a diverse number of materials, such as sodium citrate coatings on AgNPs and zinc sulfide coatings on CdSe, to minimize their toxicities. Based on the observations made in the previous section (Figure 9), where CdSe/ZnS did not show any significant effects on yeast cell viability, I was interested in observing what effects AgNPs and CdSe/ZnS would have on sensitized yeast cells without cell walls. The no-cell control (Figure 13A) showed that the AgNPs and CdSe/ZnS-QDs induced no change in the optical densities, ensuring that any decrease in optical density during the cell cultures treated with the nanomaterials might be due to cell death with adverse effects by the nanomaterials. The cells compromised by Zymolase showed a modest decrease in cell density over time in the presence of CdSe/ZnS-QDs (20 μg/mL) when compared to the non-treated control, whereas the cells that were not treated with

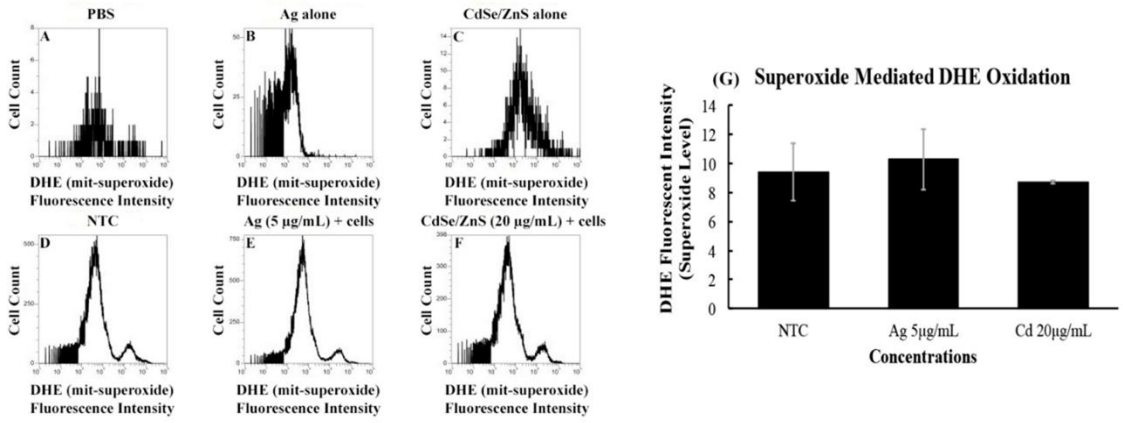

Figure 12. Quantitation of the levels of superoxide produced by cells treated with AgNP- or CdSe/ZnS-treated samples. The cells were cultured for six hours with the nanomaterials, then cultured for 2 h with DHE (dihydroethidium) prior to the measurement of the amount of oxidized DHE, which indicates the levels of superoxide produced. **(A)** Non-treated cell control with only PBS and DHE; minimal background noise was detected. **(B)** Non-treated cell control with only AgNPs and DHE in PBS; a slight increase in background noise compared to PBS and DHE alone. **(C)** Non-treated cell control with only CdSe/ZnS and DHE in PBS (the highest background shows a fluorescent intensity detected at 10^3). **(D)** Non-treated control with cells with DHE in PBS. The major peak indicates the number of cells carrying non-oxidized DHE, while the small peak at fluorescent intensity $10^{4.5}$ represents the number of cells carrying DHE oxidized by the superoxide produced. **(E)** The effects of AgNPs (5 µg/mL) on the production of superoxide, utilizing a similar method to Figure 4D. **(F)** The effects of CdSe/ZnS (20 µg/mL) on the production of superoxide in cells is indicated by the second peak, as explained in Figure 4. **(G)** Comparison of the percentage of cells that carry oxidized DHE in the non-treated control, AgNPs (5 µg/mL)-treated cells, and CdSe/ZnS (20 µg/mL)-treated cells. Each bar in the graph represents the average of three data sets, and this graph is one representation of three repeated experiments.

Zymolase showed no significant changes in cell density over time (Figure 13B). Similarly, the AgNPs caused cell density decrease in the presence of Zymolase, at higher concentrations than 5 µg/mL (Figure 13C). The rate of density decrease was more pronounced in the presence of AgNPs than CdSe/ZnS-QDs, and therefore I re-plotted the cell density curves of Zymolase-treated cells from both Figure 13B,C. As a result, I observed that the CdSe/ZnS-treated cells (20 µg/mL) with Zymolase displayed less vulnerability to a decrease in cell density than AgNP-treated cells (5 µg/mL) with Zymolase. This suggests that the cell wall plays a major role in preventing cell death caused by nanomaterials. In this sense, the AgNP-mediated growth defects,

shown in Figure 9, appeared to be due to growth delay rather than cell death in the presence of AgNPs. Further, without the presence of the cell wall, both AgNP and CdSe/ZnS-treated cells showed sensitivity to cell death, although in varying degrees.

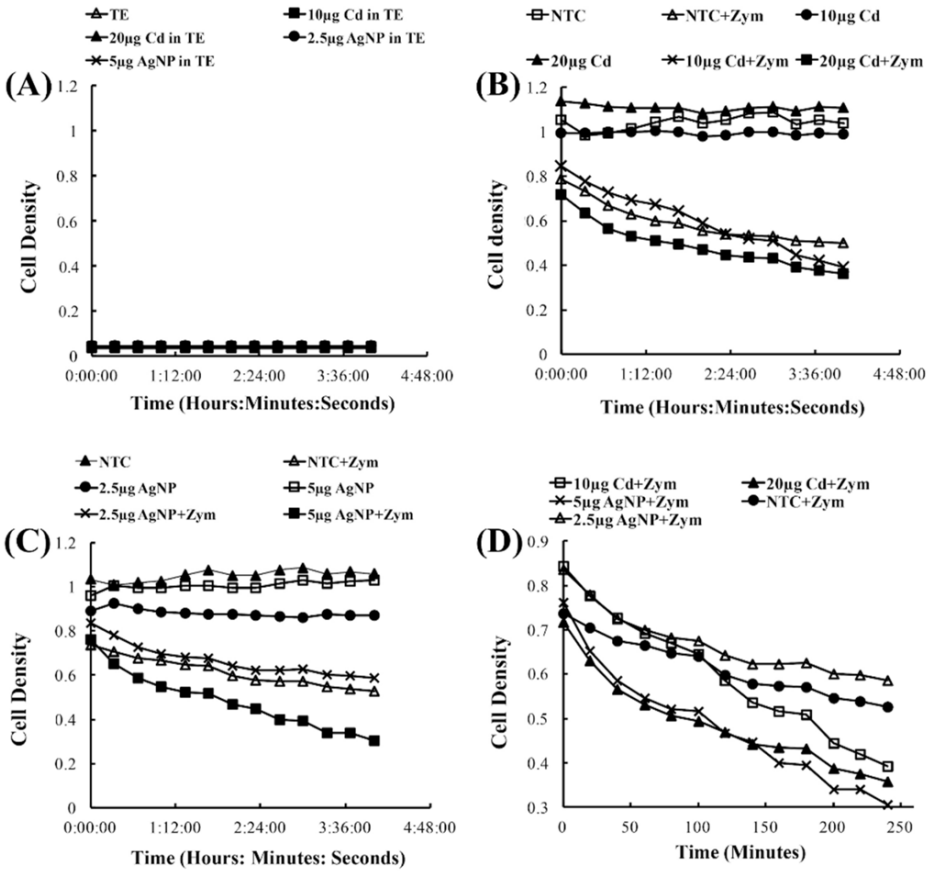

Figure 13. Cell wall viability assay to determine the effects of AgNPs or CdSe/ZnS-QDs on yeast cells lacking cell walls via Zymolase treatment. **(A)** The optical densities of the nanomaterials in TE buffer without yeast cells were measured at a wavelength of 594 nm for four hours while shaking at 30 °C. **(B)** The cell density of yeast cells when treated with differing concentrations of CdSe/ZnS (10 and 20 µg/mL), with or without Zymolase (non-Zymolase-treated cells did not show a significant change in optical density over time). **(C)** Cell density measurements of yeast cells when treated with different concentrations of AgNPs (2.5 and 5 µg/mL), with or without Zymolase. **(D)** Rearrangement of optical densities from Zymolase-treated cells in Figure 5B,C. The non-treated control with Zymolase (filled circle) was compared with 2.5 (empty triangle) and 5 (X symbol) µg/mL AgNP-treated cells, and 10 (empty square) and 20 (filled triangle) µg/mL CdSe/ZnS-treated cells.

Discussion

In August of 2017, the Environmental Protection Agency (EPA) enacted an "Information Gathering Rule", which requires companies that manufacture or process nanomaterials, regarded as chemical substances, currently in commerce to inform them of the nanomaterials specific chemical identity, production volume, methods of manufacture, processing, use, exposure and release information, and available health and safety data. According to epa.gov, they are attempting to facilitate innovation while ensuring the safety of the nanoscale substances but also states that the information collected on the nanomaterial is not intended to conclude that nanomaterials will cause harmful effects to human health or the environment. The EPA claims that the information gathered is to be used in determining if any further action needs to be taken. In addition, the U.S. Food and Drug Administration (FDA) has established guidelines on assessing the safety, effectiveness, and quality of products containing nanomaterials, and the FDA does not make categorical judgments on the safety or dangers of nanomaterials (epa.gov). My discussion covers comparisons of old and recent articles, and I hope the data collected will help expedite the EPA's decision to take further action. The current investigation contributed to the field of nanomaterial toxicity to gain a better understanding of how CdSe/ZnS-QDs and AgNPs affect living organisms differently and on how nanomaterials of different compositions and shell/core structures interact with cellular environments. To my knowledge, this is the first RNA-seq report on an estimated 4.1 nm CdSe/ZnS-QDs in the budding yeast, *Saccharomyces cerevisiae*, providing a list of differentially expressed genes. Furthermore, I offered a comprehensive model of CdSe/ZnS-QD impacts on cell physiology, which was compared to the previously proposed model that postulates AgNP-mediated changes occurring in yeast.

The Role of the Carboxylic Acid Ligand. The CdSe/ZnS-QDs were synthesized with a carboxylic acid stabilizing ligand that is capped on the surface on the ZnS shell. The un-dissociated form of a carboxylic acid is lipid-soluble and capable of crossing the membrane by diffusion and can be taken up by specific transport proteins [120]. Once inside the cell, the pH change causes carboxylic acids to dissociate into anions and accumulate because they can no longer diffuse out of the cell. A build-up of protons can increase the acidity of the cytoplasm and change the normal regulation of several metabolic pathways [120]. In addition, a build-up of protons can also generate free radicals that cause oxidative stress. I did not find any increase in ROS, but the accumulation of the QDs in the cell might be altering metabolic gene regulation by decreasing the cellular pH. The budding yeast possesses active transport systems that allow carboxylic acid-containing molecules, such as acetate, pyruvate, and lactate, to cross the plasma membrane [120]. These alternate metabolic pathways are typically turned on in the absence of glucose in a process called the diauxic shift [120]. During the diauxic shift, this study found 700 genes increased in their expression, and 1000 genes decreased in their expression [120]. Interestingly, when comparing yeast cells grown in glucose with cells grown in acetate, genes involved in activating translation machinery, rRNA maturation, and mitochondrial biogenesis were upregulated [120], similar to the results I found during gene expression analysis. These findings could suggest that many of the upregulated genes found in the presence of the CdSe/ZnS-QDs could result from the carboxylic acid stabilizing ligands capped on to the surface of the QDs.

Why CdSe/ZnS is Less Toxic Than AgNPs. Of the two nanomaterials, CdSe/ZnS-QDs and AgNPs, the latter was found to have a profound negative effect on cellular proliferation, while no effect was observed in CdSe/ZnS-treated cells (Figure 9). Geisler-Lee et al. (2013)

recently demonstrated that approximately more than 10% of AgNPs released Ag^+ ions in 24 h of exposure in plants [121]. Therefore, I conjectured that the growth defect observed in cells treated with 20 nm AgNPs was due to, in part, potential leakage of Ag^+ ions out of the citrate coat. However, the ZnS shell might efficiently prevent the short-term release of Cd^{2+} ions from escaping the core of a Cd-based QD, which led to no growth defects. This assumption can be supported by a previous study that found CdSe/ZnS-QDs, conjugated with COOH, are significantly degraded in cells after two days of exposure. Furthermore, Cd^{2+}-mediated toxicity only occurs when cellular Cd^{2+} concentrations exceed a certain threshold, and in highly proliferating cells, in which cell division exceeds the rate of free Cd^{2+} release [16]. Yeast is known to have a 90-min doubling time, and it is likely that its rate of proliferation may exceed the rate of Cd^{2+} release, which could explain the lack of physiological effects seen.

Nonetheless, there appears to be at least 240% more differentially expressed genes (DEGs) in CdSe/ZnS-treated cells than in Ag-treated (Figure 14). This is possibly due to CdSe/ZnS being internalized and trafficked to the nucleus, where it can interact with the biomolecules in the vicinity [122], implicated in particularly with transcription rates. For instance, Cd-QDs can interfere with transcription mechanisms (DNA/RNA polymerases) to alter normal gene expression. To support this claim, a previous publication revealed low levels of Cd^{2+} ions cause significant chromosomal damage in HFF-1 cells exposed to 7.5 nM QDs, while no physiological damage was observed [98]. Amongst the upregulated genes found in CdSe/ZnS- and AgNP-treated cells, I found many similarities in DEGs, such as an increase in rRNA transcription, ribosomal assembly and protein synthesis, tRNA modifications, and nuclear export. Some interesting differences found amongst the statistically upregulated genes between the two nanomaterials is that CdSe/ZnS-treated cells have a drastically higher number of DEGs

involved in amino acid metabolic processes. Amongst the downregulated genes found in each treatment of nanomaterial, I found similarities, such as a decrease in cellular ATP production, endocytosis, cell plasma membrane/wall integrity, and responses to oxidative stress [39]. I found a few notable differences amongst the downregulated genes in each treatment, the first being about 10 times more genes involved in responding to chemicals and many more genes that play a role in ubiquitin-mediated late endosome/multivesicular body trafficking/lysosomal degradation in CdSe/ZnS-treated cells.

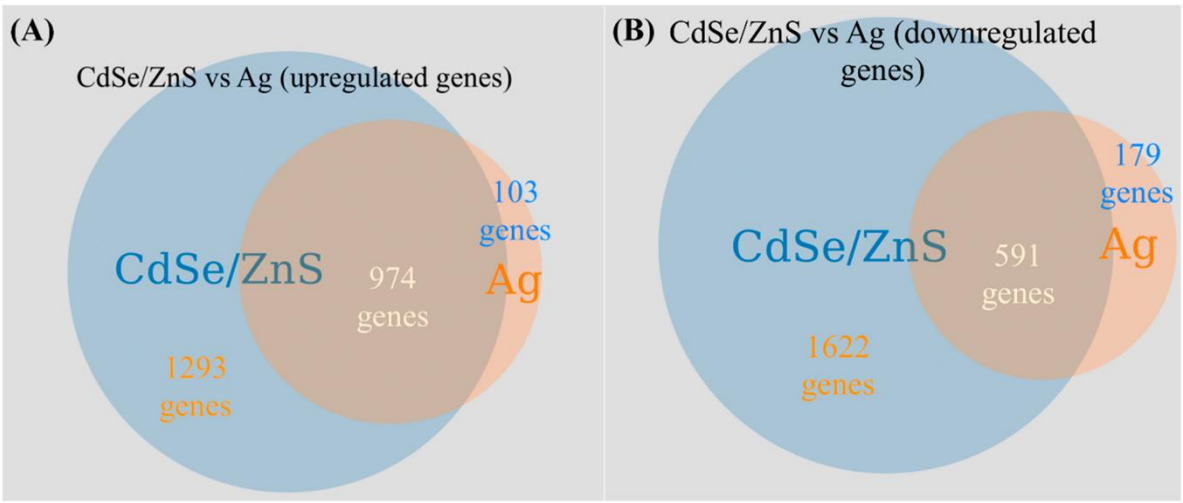

Figure 14. Gene expression Venn-diagram to visualize the shared and separate differentially expressed genes when exposed to CdSe/ZnS QDs and AgNPs. **(A)** All significant and upregulated genes found in CdSe/ZnS- and Ag-treated cells. The leftmost circle represents the number of genes exposed to CdSe/ZnS, the rightmost circle represents the genes exposed to AgNPs only, and the shared area of the two circles represents the quantity of shared differentially expressed genes in both treatments. **(B)** All significant and downregulated genes. The leftmost circle represents the genes exposed to CdSe/ZnS, the rightmost circle represents the genes exposed to AgNPs, and the middle area represents the same differentially expressed genes in both treatments.

In both Ag- and CdSe/ZnS-treated cells, no statistical change in the detectable ROS levels was detected. Ting Zhang et al. (2015) measured the levels of four oxidative stress markers, including hydroxyl radicals, in fibroblasts treated with CdSe and CdTe (2.2 nm) QDs,

lacking a ZnS shell, at 3.5, 7, and 14 µg/mL and found no difference in hydroxyl radical levels at 3.5 and 7 µg/mL, but indicated a statistical difference in ROS at 14 µg/mL [101]. Therefore, I surmised that CdSe/ZnS-QDs at 10 µg/mL and AgNPs at 5 µg/mL is not a sufficiently high enough concentration to statistically increase the generation of mitochondrial ROS or superoxide levels. Another possible explanation for not detecting a statistical change in mitochondrial ROS is because there are many possible types of ROS produced in the cell, and I selected to quantify only the superoxide for this study. The lack of ROS generation may also be attributed to the presence of the ZnS shell and slower internalization due to the larger diameter [19] of the tested CdSe/ZnS-QDs (4.1 nm).

A previous transcriptomic study on *Chlamydomonas reinhardtii* demonstrated that 20 nm AgNPs (1.5×10^5 mg/L) and 10 nm CdTe/CdS-QDs (2.0×10^4 mg/L) did not induce oxidative stress. The former induced significant damage to the cells' structural integrity, while green alga cells exposed to CdTe/CdS-QDs did not increase the expression of transcripts that encode proteasome subunits [104]. Consistently, I found several proteasome subunit genes (*RPN1/2/3/4/5/6/7/8/9/11/13/14* and *RPT2/3/4/5/6*) to be significantly downregulated in CdSe/ZnS-treated cells. This similar cellular response suggests that CdTe/CdS and CdSe/ZnS-QD exposure may induce similar transcriptional responses due to their similar composition. Additionally, AgNP-treated cells increased transcript levels that encode for proteins of the cell wall and flagella, suggesting AgNPs are more harmful to structures exposed to the external environment, whereas CdTe/CdS-treated cells downregulated more transcripts overall and resulted in less damage to external structures [104]. Similarly, the Zymolase experiments revealed CdSe/ZnS-QD exposure was less damaging to the cell wall and downregulated more transcripts in yeast than AgNP exposure.

It has long been thought that engineered nanoparticles could affect the integrity of the mechanism of DNA-damage repair pathways, which, in turn, can negatively impact the cellular homeostasis. The differentially expressed gene list contains genes that function in the yeast base excision repair (BER) pathways, including *APN2, NTG1, NTG2, RAD2, RAD4, RAD5, RAD6, RAD7,* and *RAD9* (data not shown). Ogg1 is also implicated in a BER pathway to excise 8-oxoG from the DNA backbone [123], and I found this gene to be highly upregulated. Further, genes implicated in a post-replication uracil excision repair, such as *DUT1, UNG1,* and *REV1* [124], were differentially expressed in the presence of CdSe/ZnS according to my list. Nucleotide excision repair (NER) pathway has the capacity to remove a large number of structurally unrelated helix-distorting lesions [123]. The following genes implicated in the yeast NER pathway were differentially expressed: *ABF1, RAD2, RAD3, RAD7, RAD16*, and *RAD26.* Taken together, my data provides evidence that CdSe/ZnS poses a threat to DNA repair pathways, and therefore, the precise action mechanism behind the threat awaits to be explored.

Upregulated mRNA Transcripts Implicated in Promoting Translation. I provided a model (Figure 15A,B) postulating potential physiological effects, induced by exposure to CdSe/ZnS-QDs. My model, therefore, depicted key differentially expressed genes and their corresponding cellular functions. Of these upregulated genes, the most noticeable groups of upregulated genes were for translation, including but not limited to, rRNA transcription, ribosome subunit assembly, ribosome exit, tRNA maturation, and translation machinery assembly in the cytoplasm. Given rRNA synthesis is a prerequisite for translation, my RNA-seq data was consistent in the genes, such as ECM16 [125] and RPA4 [126], required for rRNA synthesis; these genes were highly upregulated (Figure 15A). It is well known that rRNA molecules are associated with pre-ribosomal proteins in the nucleolus to form precursors of large

and small ribosomes, pre-large 66S subunit (LSU), and pre-small 40S subunit (SSU), respectively. My model only provided three genes (*FAF1*, *DBP8*, and *NSA2*) with at least 3-fold increases in their RNA transcripts, among many upregulated genes implicated in pre-ribosome assembly (Figure 15A). The Saccharomyces Genome Database presents the gene products of *FAF1* [127] and *DBP8* [128, 129] that are associated with the assembly of SSU, whereas *Nsa2* functions for LSU assembly [129]. In addition, the RNA-seq revealed that RNA transcripts coding for ribosomal proteins, including *RPS26B*, *RPS3*, and *RPL1B,* were increased by 40–100% (Figure 15A). The rise of these transcripts appears to be necessary to supply the demands for making functional ribosome precursors, such as SSU and LSU, which consist of rRNA and its binding partners, ribosomal proteins. After transportation to the cytoplasm with the aid of nucleoporins, such as Nup2 [130] and Pom152 [131], the SSU and LSU join together along with tRNAs to make a translation-competent supramolecular complex that manufactures proteins de novo to replace nonfunctional proteins that might have been damaged by exposure to ROS [132, 133]. In addition to increasing the rate of ribosomal production, I also noticed genes involved in tRNA maturation to be significantly increased to provide additional amino acid products required in translation. Finally, genes that aid in the initiation process of translation, including *FUN12* [134], are upregulated.

Downregulated mRNAs and Their Potential Impacts on the Cell Integrity. Based on the list of GO-terms generated with downregulated genes from the RNA-seq data, I illustrated the physiological effects or cellular processes induced by exposure to CdSe/ZnS-QDs (Figure 15B). I found that the exposed cells expressed decreased levels of RNA transcripts involved in oxidation-reduction processes, response to chemicals, pathways of endo/exocytosis, and various metabolic processes (Figure 10). Similar to the model for upregulated genes (Figure 15A), my

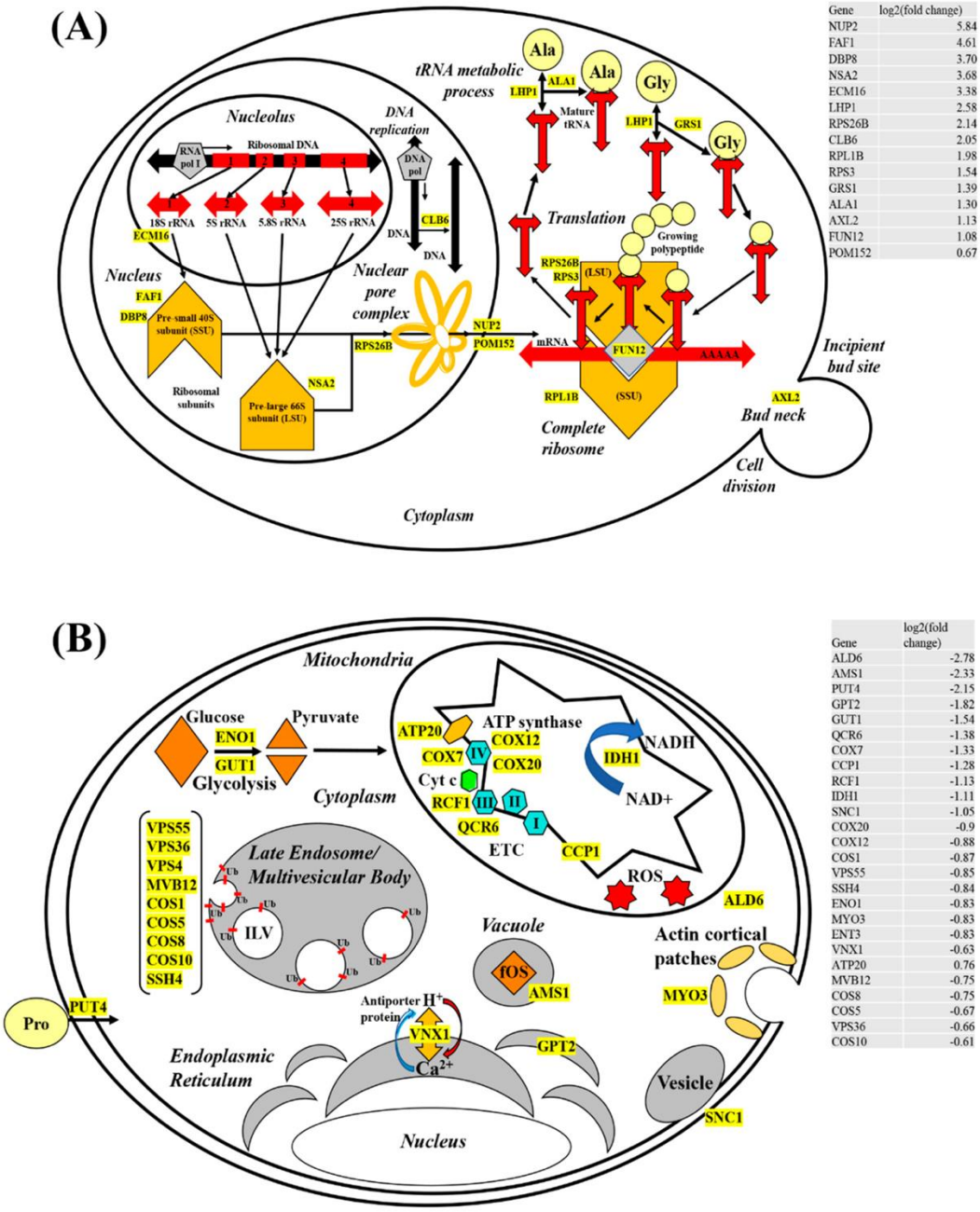

Figure 15. Schematic models of changes in cellular processes with CdSe/ZnS-QDs in yeast cells. Genes are strategically placed near representative illustrations they are thought to be involved in. **(A)** CdSe/ZnS leads to an increase in the expression of genes implicated in the pre-ribosomal assembly of small and large subunits and their nuclear export as well as maturing tRNA and complete ribosomes. **(B)** Several processes appear to be affected by exposure to CdSe/ZnS, including cell wall/membrane integrity, sugar import (see the main text), late endosome/multi-vesicular body function, and cellular respiration in the mitochondria.

model for downregulated genes highlighted only a few downregulated genes in the model that represent several more downregulated genes involved in the same cellular process. First, genes involved in endocytosis, including but not limited to *MYO3*, were downregulated. This indicates a potential defect in endocytosis with less number of copies of *Myo3* at the endocytic site, and therefore, it is of great interest in testing whether the endocytic process is hampered in the presence of Cd-QDs. Furthermore, it has been shown that CdSe/ZnS-QDs use endocytosis as the main route for their uptake, according to Liu et al. (2015) [19], but the question of whether they affect the process and rate of endocytosis, directly or indirectly, remains unknown. I found several downregulated genes that play a role in glycolysis. Among these genes, *ENO1* and *GUT1* code for a phosphopyruvate hydratase [135] and a glycerol kinase [136], respectively. Along with these genes, seven *HXT* genes (*HXT 2/17/5/4/9/8/13*) and five *SNF* (*SNF3/1/4/7/11*) genes coding for sugar transporter (SGD) were significantly downregulated based on the RNA-seq in response to Cd-QD exposure. It is highly likely that sugar transport genes and sugar-breaking enzyme genes mentioned above are simultaneously affected by the presence of Cd-QDs. However, I cannot exclude the possibility that *ENO1* and *GUT1* genes are downregulated as a consequence of low levels of sugars transported caused by the suboptimal activity of glucose transporters due to the presence of Cd-QDs.

Other mitochondrial genes (*ATP20, COX7, COX12, COX20, RCF1*, and *QCR6*) involved in respiration aid in ATP synthesis [137], electron transport complexes [138], and cytochrome c oxidase subunits [139, 140] were downregulated, suggesting energy production was significantly lessened. These genes code for transmembrane proteins residing at the inner membrane of mitochondria (Figure 15B), and their gene products play a major role in relaying electrons via reduction-oxidation cycles. Additionally, these proteins are aiding in transporting H^+ ions from

the matrix to the inner membrane space to create a proton gradient across the inner membrane. The energetic proton flow down the gradient facilitates ATP formation via the help of ATP20, a part of the ATP-synthase protein complex. Other metabolic genes, *CCP1* and *ALD6*, are required in the citric acid cycle (TCA cycle) and NAD+ regeneration, respectively [141]. Their highly-downregulated expression is suggestive of diminished levels of the electron carriers NADH, available for the electron transport chain (ETC), which may lead to the production of suboptimal amounts of ATP. Interestingly, mitochondrial genes involved in neutralizing ROS, such as *CCP* [141], are downregulated as well, thereby possibly contributing to increased ROS levels that result in cellular damage tied together. Downregulation of genes coding for mitochondrial ETC transmembrane proteins, TCA cycle proteins, and ROS neutralizing proteins might additively or synergistically aggravate mitochondrial functions, which is not a favorable environment to support many cellular processes that require ATP for their action mechanism. However, as depicted in the upregulation model (Figure 15A), I proposed an abnormally elevated translation process upon Cd-QD exposure. This does not seem to be consistent with the diminished level of ATP in cells with Cd-QDs. One possible explanation for this would be that the majority of available energy produced may be directed towards increasing translation. I conjectured that proteins in diverse cellular processes are damaged with the presence of Cd-QDs, making the cell prioritize the replenishment of the damaged proteins.

Late endosome/multivesicular body (MVB) genes (*VPS4/36/55, MVB12, COS1/5/8/10*, and *SHH4*) involved in ubiquitin (Ub)-dependent sorting of receptor proteins for vacuole degradation are significantly downregulated. Ub is a sorting tag that mediates the entry of worn-out receptors into intraluminal vesicles (ILVs) that is targeted to the lysosome or vacuole for degradation [142]. It is well understood how endosomes/MVBs play a role in the balance

between recycling and degrading proteins and lipids. This robust balancing act, consequently, contributes to diverse cellular processes, such as nutrient uptake, cell adhesion, cell migration, cytokinesis, cell polarity, and signal transduction [143]. In addition, *UBI4*, a gene that codes for ubiquitin [144], is also found to be downregulated by approximately 100%, according to my data. This suggests that receptor proteins destined for degradation in Cd-QDs exposed cells are not being turned over as efficiently as in healthy cells. With available energy in the cell more limited from mitochondrial damage, the cell likely compensates by downregulating regular processes, such as endosomal sorting and transport pathways. Modifying normal cell functions like the ones mentioned might allow the cells to conserve energy for processes of a higher priority, namely translation, for replacing proteins damaged by CdSe/ZnS-QD exposure. From my DEG analysis, I postulated that worn out and damaged receptor proteins accumulate due to late endosomal and proteasome downregulation. In addition, a previous study on the 20S proteasome subunit in maize revealed that the proteasome plays an important role in providing metal resistance in *Saccharomyces cerevisiae* [145]. These results suggest that the cell is choosing to redirect energy meant for degradation to higher priority processes, while simultaneously compromising its metal resistance. I observed no physiological effects, which suggests this possible energy prioritizing was not great enough to cause significant damage but was still detectable with high throughput sequencing technology.

Conclusion

The present work provided evidence that CdSe/ZnS-QDs exerted a mild cytotoxic effect on yeast when compared with AgNPs, but it was evident that Cd-QD-treated cells had more differentially expressed genes than AgNPs-treated cells. My working model behind the steep

upregulation in ribosomal biogenesis was most likely due to possible carboxylic acid stabilizing ligands interacting with cellular components or Cd-QD interactions with the damaged proteins as the stable QD particle or as free Cd^{2+} ions released from Cd-QDs. Whereas, a wide spectrum of routine cellular processes, including energy production and intracellular trafficking, appeared to be significantly impeded. We, therefore, proposed that the majority of available energy in the cell is directed to aid translation in order to replenish damaged proteins from Cd-QD exposure.

CHAPTER 4: COMPARING TRANSCRIPTOME PROFILES OF *SACCHAROMYCES CEREVISIAE* CELLS EXPOSED TO CADMIUM SELENIDE/ZINC SULFIDE AND INDIUM PHOSPHIDE/ZINC SULFIDE

Introduction

Quantum dots (QDs) are nano-sized semiconductor crystals well-known for their long-lasting fluorescence, photo-stability, and tunable optic properties [146-148]. The color of each QDs fluorescence is size-dependent, therefore, changing a QDs size will directly change its emission wavelength [148]. Soon after their development and introduction to the biological sciences, QDs proved to be powerful fluorescent probes [149, 150] that work better in applications that include nucleic acid detection, protein tracking, intracellular reporting, molecular imaging, drug delivery, and tumor diagnostics [147, 148, 151, 152]. Biological imaging with QDs is possible through modifying their surface by conjugating them with target-specific antibodies, peptides, or small molecules [147]. Despite their advantages, the use of QDs raises a lot of concern regarding their potential negative effects [146]. QD cytotoxicity has been investigated in many cell models including, but not limited to, yeast [22, 47], bronchial epithelial cells [153], macrophages, lymphocytes [107], and animal models such as mice [154], rats [155, 156], and non-human primates [156]. Some negative effects are, in part, due to their nano-size which enables them to adversely interact with organismal and microbial environments, including lung alveoli [157] and DNA within the nucleus of a cell [101, 146]. To combat these potential hazards, protective semiconductor shells have been developed that coat the toxic core of QDs. Zinc sulfide (ZnS) is a protective shell, encapsulating QDs, that can be synthesized onto the core of QDs (such as CdSe and InP, respectively) and have been shown to reduce cytotoxic effects

[146, 158]. Despite these attempts to improve their safety, concerns regarding exposure to QDs and QD-containing products persist [146, 159].

Several previous studies have revealed Cd- and Pb-based QDs to be toxic, causing significant cellular damage [146, 160], but cadmium selenide, cadmium telluride, and cadmium sulfide (CdSe, CdTe, and CdS, respectively) QDs are the most widely used [118]. Cadmium is a well-known carcinogen, that has been shown to damage the liver and kidneys, and the use of Cd-QDs in electronics has been banned by the European Union [161]. According to previous studies on Cd-QDs, heavy metal ions released from the surface of degrading QDs induce toxicity by indirectly inducing the generation of reactive oxygen species (ROS) [19, 160]. Due to these findings, there is still much debate over the risks of Cd-QD exposure and the continuation of their use in products and clinical research [162].

To overcome obstacles surrounding QD toxicity, a less toxic, Cd-free, QD could be a potential solution. A previous study provided evidence that InP/ZnS QDs are a less hazardous semiconductor nanocrystal compared to Cd-containing QDs [163, 164]. InP/ZnS QDs, similar to CdTe-QDs, can fluoresce, which has made them a practical alternative to Cd-QDs [118]. Studies conducted in vivo found an accumulation of indium from InP/ZnS QDs remained in major organs up to 84 days after injection in BALB/c mice, but histological analysis of the organism's blood did not reveal any discerning toxic effects [164]. A recent study revealed that InP/ZnS QDs are taken up into cells and high doses decreased cell viability and induced ROS generation and apoptosis [160].

Challenges regarding InP QDs, including their rapid oxidation and break down in biocompatible solutions, must be solved to reduce their cytotoxicity [118]. Similar to CdSe, InP QDs are coated with a ZnS-shell that improves stability and reduces toxicity [118]. Previous

studies have identified a potential drawback, by demonstrating the poor coordination strength between InP-cores and ZnS-shells, which makes it difficult for the core to be fully coated, resulting in holes that expose the InP-core. The addition of a second ZnS-shell to InP/ZnS QDs has been shown to improve coverage around InP-cores and reduce cytotoxicity [118]. Additionally, they revealed InP/ZnS QDs increased ROS levels, primarily superoxide, and InP/ZnS QDs with a second ZnS-shell reduced ROS levels, in the budding yeast [118].

Although InP-QDs has been suggested as a potential replacement for Cd-QDs due to their similar analogous bandgap characteristics to Cd-QDs [118], I attempted to better understand the potential mechanisms of toxicity of CdSe/ZnS and InP/ZnS QDs on the budding yeast, *Saccharomyces cerevisiae*. The present study implemented high throughput technologies (RNA-seq) to assess alterations in the transcriptomic profile of QD-treated yeast and examined the cytotoxic effects in response to CdSe/ZnS and InP/ZnS exposure. This study aims to measure toxicity by assessing each QDs effect on proliferation, ROS levels, and change in gene expression. Further, I investigated QD-mediated effects on cellular trafficking and found that CdSe/ZnS and InP/ZnS significantly alter Vps10-GFP trafficking. A detailed discussion on the potential toxic effects and their impacts on the cell caused by these quantum dots is provided in the discussion section.

Results

CdSe/ZnS QDs and InP/ZnS QDs Affect Normal Yeast Growth. To fully examine the effects of CdSe/ZnS QDs on yeast growth, I recorded the optical density of each sample (0, 10, 20, 50, and 100 μg/mL CdSe/ZnS) for 24 h (Figure 16). CdSe/ZnS QDs did not have a significant effect on yeast growth curves compared to the non-treated control, but higher

concentrations of CdSe/ZnS (20, 50, and 100 μg/mL) seemed to slightly stimulate growth as seen by the top 3 growth curves (red, orange, and green curves) in Figure 16A. InP/ZnS QDs significantly reduce yeast growth in a dose-dependent fashion (Figure 16B). Next, I graphed the final ODs of each sample at a steady-state on hour 24 (OD_{594} nm). I found CdSe/ZnS QDs had no significant effect on endpoints (Figure 16C) compared to the non-treated control. Once again, I show InP/ZnS QDs had a dose-dependent effect on growth. As concentrations increased, endpoints steadily decreased, and the highest concentration (100 μg/mL) was significantly reduced (Figure 16D). Furthermore, I calculated the doubling times of the yeast in each sample with the slope of the growth curve in the exponential phase (Figure 16E,F) and recorded the amount of time each sample remained in lag-phase (Figure 16G,H). Yeast treated with CdSe/ZnS QDs displayed no significant change in their endpoint OD (Figure 16C) or doubling times apart from yeast treated with 50 μg/mL CdSe/ZnS, which showed a significant increase in doubling time (Figure 16E). However, the amount of time spent in the lag-phase was significantly decreased in samples treated with 10, 50, and 100 μg/mL CdSe/ZnS (Figure 16G). The same components used to analyze the growth of yeast were investigated in samples treated with InP/ZnS QDs at concentrations of 0, 1, 10, 50, and 100 μg/mL. Interestingly, InP/ZnS QDs seemed to significantly decrease the endpoint OD at 100 μg/mL (Figure 16D) as well as significantly increase the doubling times of samples at concentrations of 1, 50, and 100 μg/mL (Figure 16F). Unlike CdSe/ZnS treated samples, yeast exposed to InP/ZnS QDs caused no significant difference in time spent in lag-phase when compared to the non-treated control (Figure 16H). Taking all the growth data obtained from CdSe/ZnS and InP/ZnS exposed yeast, a side-by-side comparison reveals each QD affects growth differently. CdSe/ZnS-treated samples significantly altered time spent in a lag phase when compared to the non-treated control and had

little to no effect on the endpoint ODs or doubling times. In contrast, InP/ZnS-treated samples significantly changed the endpoint ODs and doubling times and had no significant effect on time spent in lag-phase.

Due to recent advances in high-throughput sequencing technologies, we can now identify a very broad range of genes and cellular processes that change when exposed to certain materials. All CdSe/ZnS- and InP/ZnS-treated and non-treated samples underwent a total RNA extraction followed swiftly by an mRNA purification and cDNA conversion step. Each group, performed in triplicate, was sent to the Kansas Medical Genome Center where they sequenced the cDNA in each sample with an Illumina HiSeq 2500 sequencing system (Illumina®, San Diego, CA, USA) that created datasets of sequenced data of each sample replicate. All cDNA datasets were returned online and then uploaded to usegalaxy.org for computational data analysis. All three control and QD-treated replicates were concatenated resulting in one joined file of the three non-treated samples, one file of the three CdSe/ZnS-treated samples, and one file of the three InP/ZnS-treated samples. Next, each cDNA dataset was checked for quality (FastQC and FASTQ Quality Trimmer, respectively). After each dataset was cleaned up, they were mapped to the *S. cerevisiae* reference genome (S288C). A combined total of 81,205,179 reads were accepted from the three non-treated controls, a total of 79,562,512 and 82,520,772 accepted reads were accepted from the three Green CdSe/ZnS-treated samples and the three InP/ZnS-treated samples, respectively.

For CdSe/ZnS QD treated samples, 606 upregulated genes were identified and found to be implicated in transmembrane transport (13.6%), carboxylic acid metabolic processes (11.4%), amino acid metabolic processes (7.1%), cellular homeostasis (6.1%), cellular glucan metabolic processes (2.3%), and drug transmembrane export (0.8%), as depicted in Figure 17A. From the

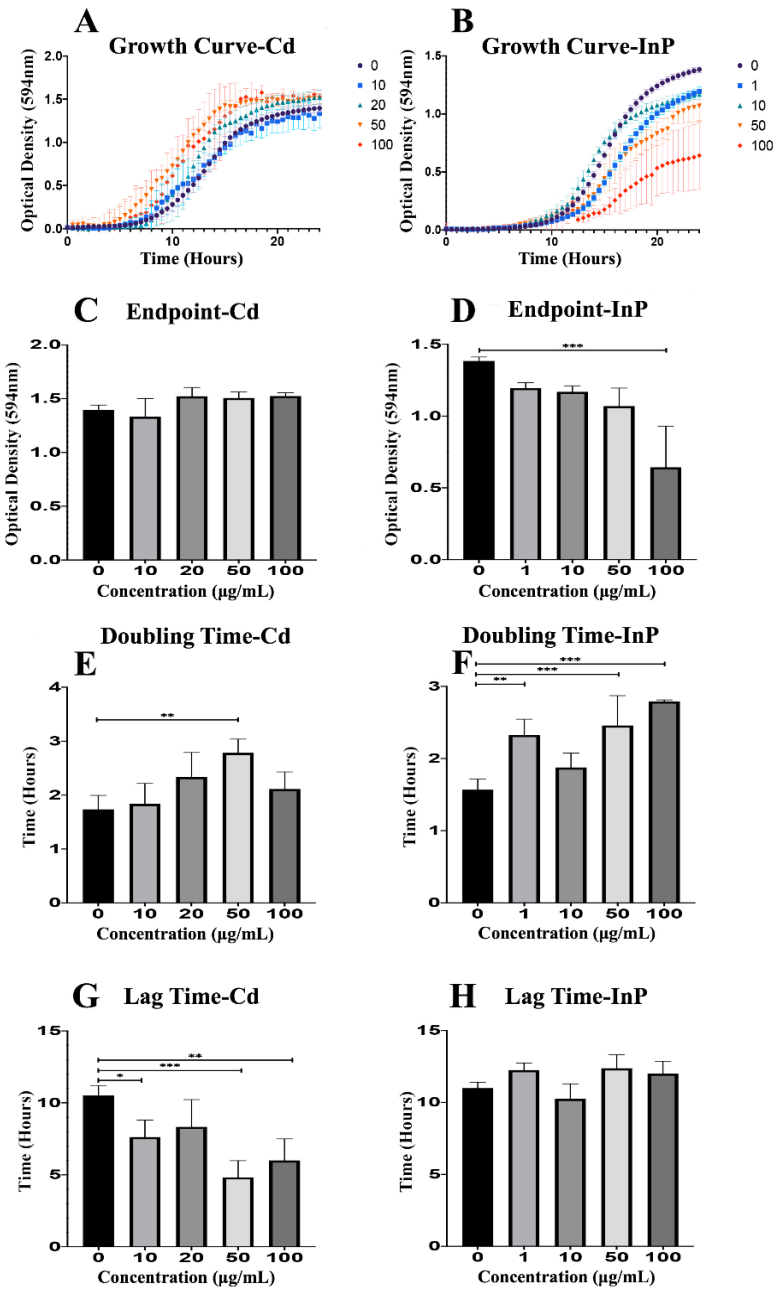

Figure 16. Growth assay to determine growth rates of CdSe/ZnS and InP/ZnS-treated yeast cells. **(A,B)** Quantification of cell optical densities over a 24-h period where the cells are treated with CdSe/ZnS and InP/ZnS QDs, respectively, at 30 °C while shaking. **(C,D)** Measurement of cell optical densities at 24 h of treatment with CdSe/ZnS and InP/ZnS QDs, respectively. The bar representing the average optical densities (ODs) (594 nm) of each concentration at the 24-h mark. **(E,F)** Doubling time takes place during the phase of exponential growth for the cells treated with CdSe/ZnS and InP/ZnS QDs, respectively, and was measured as the amount of time it takes for cells to double their ODs. **(G,H)** The mean lag time before the exponential growth phase. Significant statistical differences are represented with *($p < 0.05$), **($p < 0.01$), and ***($p < 0.001$).

GO terms listed above, 83, 69, and 37 upregulated genes were involved in transmembrane transport, carboxylic acid metabolism, and amino acid metabolism, respectively. Furthermore, 43, 14, and 5 upregulated genes were implicated in cellular homeostasis, cellular glucan metabolism, and drug transmembrane export, respectively (Figure 17A). From the pool of 2760 downregulated genes, many were involved in the macromolecule metabolic process (42.3%), component organization/biogenesis (36.9%), nitrogen compound metabolism (33.0%), protein metabolic processes (21.7%), and translation (8.6%). Among the downregulated GO terms listed above, 694, 612, 325, and 175 downregulated genes were found to be involved in metabolic processes, nitrogen compound metabolic processes, protein metabolic processes, and translation, respectively. Moreover, 152, 141, 103, 61, and 59 downregulated genes play a role in ncRNA processing, rRNA metabolic processes, ribosomal biogenesis, cell wall organization/biosynthesis, and external encapsulation structure organization, respectively. Lastly, 28, 22, and 17 downregulated genes were found to be implicated in large and small ribosomal assembly and rRNA export from the nucleus, respectively (Figure 17B).

In InP/ZnS-treated samples, 6488 genes were mapped to the genome and annotated, and of those genes, 2620 were found to be statistically increased or decreased compared to the non-treated controls. 1523 genes were found to be upregulated and 1097 genes downregulated. For Inp/ZnS QD treated samples, through analysis of GO terms, I identified several upregulated cellular processes including oxidation-reduction (11.8%), transmembrane transport (9.9%), drug metabolic process (6.1%), metal ion homeostasis (3.3%), electron transport chain (2.2%), cellular respiration (1.7%), glycogen metabolic process (1.2%), and NADP metabolic process (1.1%) (Figure 18A). From the GO-term analysis, I determined 180, 150, 93, and 51 upregulated genes are involved in oxidation-reduction, transmembrane transport, drug metabolic processes,

and metal ion homeostasis, respectively. Additionally, 34, 30, 18, and 16 upregulated genes were found to be involved in the electron transport chain, cellular respiration, glycogen metabolic processes, and NADP metabolic processes, respectively (Figure 18A). From all 1097 significantly downregulated genes, several were found to be involved in nitrogen compound metabolic processes (55.8%), cellular component organization/biogenesis (41.1%), protein metabolic processes (29.6%), translation (16.0%), ncRNA processing (13.9%), rRNA processing (11.9%), ribosome biogenesis (9.4%), cell wall organization/biogenesis (5.6%), external encapsulating structure organization (5.4%), ribosomal small and large subunit assembly (2% and 3.1%, respectively), and rRNA export from the nucleus (1.6%). GO analysis revealed that 612, 451, 325, and 175 downregulated genes play important roles in nitrogen compound metabolic processes, cellular component organization/biogenesis, protein metabolic processes, and translation, respectively. In addition, 152, 130, 103, 61, and 59 downregulated genes are involved in ncRNA processing, rRNA processing, ribosome biogenesis, cell wall organization/biogenesis, and external encapsulating structure organization, respectively. Lastly, 28, 22, and 17 downregulated genes were identified to play a role in the GO terms ribosomal small subunit assembly, ribosomal large subunit assembly, and rRNA export from the nucleus, respectively (Figure 18B).

RT-qPCR Validation of RNA-Seq Data. I then wanted to validate the fidelity of the RNA-seq results using RT-qPCR. With the Pfaffl method, I determined the fold-change of the downregulated genes (SPS100, YDL012C), upregulated genes (TIR1, HXK1), and housekeeping gene (ALG9) using RT-qPCR (Figure 19). The fold-change of CdSe/ZnS-treated SPS100 had an average fold-change of 0.72 and InP/ZnS-treated YDL012C had an average fold-change of 0.34 (Figure 19A&B). CdSe/ZnS-treated cells displayed an elevation of TIR1 mRNA level which had

A

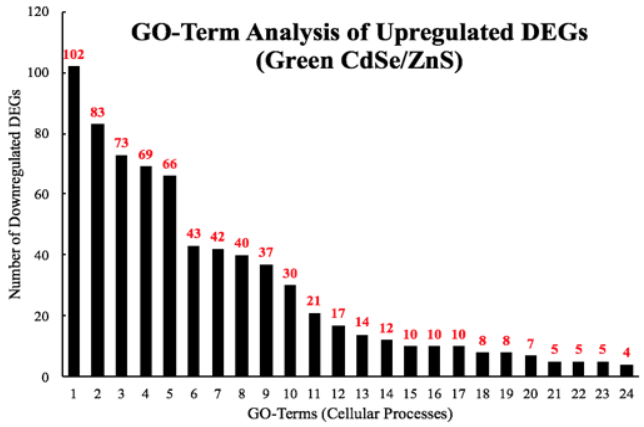

Key	GO-term
1	small molecule metabolic process
2	transmembrane transport
3	organic acid metabolic process
4	carboxylic acid metabolic process
5	oxidation-reduction process
6	cellular amino acid metabolic process
7	organic acid biosynthetic process
8	carbohydrate metabolic process
9	cellular homeostasis
10	monocarboxylic acid metabolic process
11	response to temperature stimulus
12	cellular polysaccharide metabolic process
13	cellular glucan metabolic process
14	cellular aldehyde metabolic process
15	secondary alcohol metabolic process
16	steroid biosynthetic process
17	sterol biosynthetic process
18	disaccharide metabolic process
19	oligosaccharide metabolic process
20	beta-glucan metabolic process
21	arginine biosynthetic process
22	drug transmembrane export
23	ornithine metabolic process
24	amine biosynthetic process

B

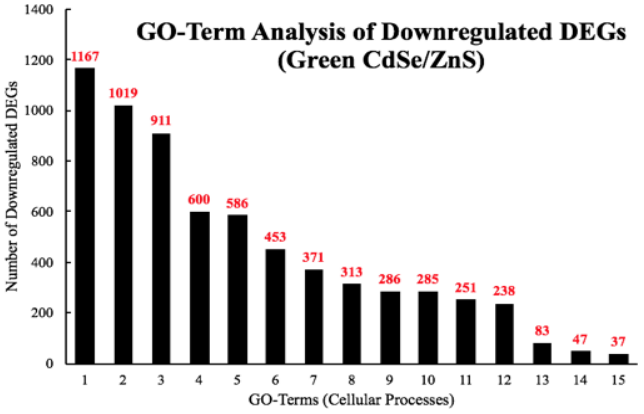

Key	GO-term
1	macromolecule metabolic process
2	cellular component organization/biogenesis
3	cellular nitrogen compound metabolic process
4	cellular protein metabolic process
5	nucleic acid metabolic process
6	RNA metabolic process
7	protein-containing complex subunit organization
8	protein-containing complex assembly
9	RNA processing
10	cellular amide metabolic process
11	peptide metabolic process
12	translation
13	mitochondrial translation
14	regulation of supramolecular fiber organization
15	transcription by RNA polymerase II

Figure 17. Bar graphs depicting the number of DEGs implicated in GO-terms from CdSe/ZnS and InP/ZnS-treated samples. The number of differentially expressed genes (DEGs) on each bar represents the number of an altered gene for the corresponding GO-term with *p*-values of 0.05 or below. The key with the corresponding GO-term. **(A)** The total number of upregulated DEGs implicated in the listed GO-terms in CdSe/ZnS-treated cells. **(B)** The total number of downregulated DEGs implicated in the listed GO-terms in CdSe/ZnS-treated cells.

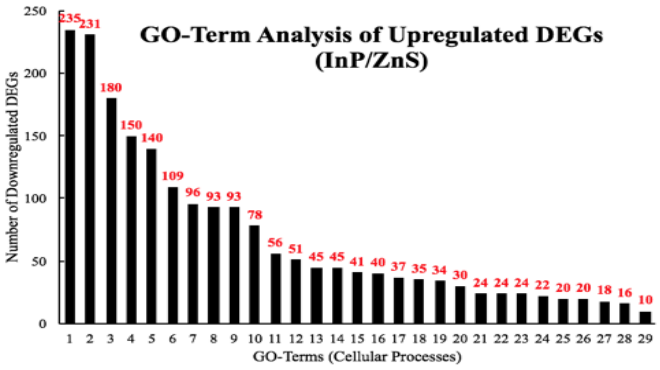

Key	GO-term
1	Phosphorus metabolic process
2	compound metabolic process
3	oxidation-reduction process
4	transmembrane transport
5	organophosphate metabolic process
6	carbohydrate metabolic process
7	cofactor metabolic process
8	drug metabolic process
9	nucleobase-containing small molecule metabolic process
10	generation of precursor metabolites and energy
11	energy derivation by oxidation of organic compounds
12	metal ion homeostasis
13	oxidoreduction coenzyme metabolic process
14	response to temperature stimulus
15	response to heat
16	pyridine-containing compound metabolic process
17	antibiotic metabolic process
18	nicotinamide nucleotide metabolic process
19	electron transport chain
20	cellular respiration
21	citrate metabolic process
22	response to inorganic substance
23	tricarboxylic acid cycle
24	oligosaccharide metabolic process
25	energy reserve metabolic process
26	disaccharide metabolic process
27	glycogen metabolic process
28	NADP metabolic process
29	trehalose metabolic process

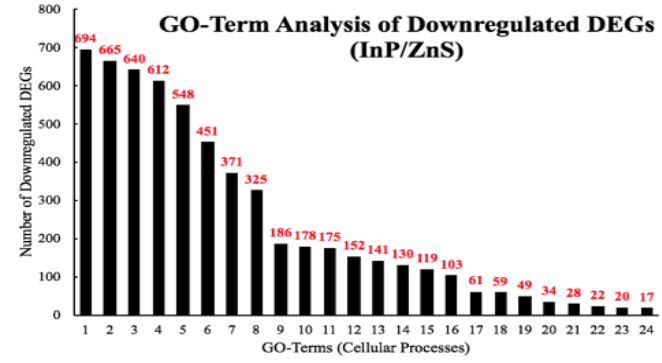

Key	GO-term
1	metabolic process
2	substance metabolic process
3	primary metabolic process
4	nitrogen compound metabolic process
5	macromolecule metabolic process
6	cellular component organization/biogenesis
7	biosynthetic process
8	protein metabolic process
9	cellular amide metabolic process
10	peptide metabolic process
11	translation
12	ncRNA processing
13	rRNA metabolic process
14	rRNA processing
15	ribonucleoprotein complex biogenesis
16	ribosome biogenesis
17	cell wall organization/biogenesis
18	external encapsulating structure organization
19	maturation of SSU-rRNA
20	ribosomal large subunit biogenesis
21	ribosomal large subunit assembly
22	ribosomal small subunit assembly
23	cell wall macromolecule metabolic process
24	rRNA export from nucleus

Figure 18. Bar graphs depicting the number of DEGs implicated in GO-terms from InP/ZnS-treated samples. The number of differentially expressed genes (DEGs) on each bar represents the number of an altered gene for the corresponding GO-term with *p*-values of 0.05 or below. The key with the corresponding GO-term. **(A)** The total number of upregulated DEGs implicated in the listed GO-terms in InP/ZnS-treated cells. **(B)** The total number of downregulated DEGs implicated in the listed GO-terms in InP/ZnS-treated cells.

an average fold-change of 1.29, and the HXK1 mRNA level in InP/ZnS-treated cells was increased more than 10 times when compared to that in non-treated cells (Figure 19A&B). Gene expression values below 1.0 are interpreted as downregulated and expression values greater than 1.0 are interpreted as upregulated genes compared to non-treated samples. Together, the RT-qPCR results clearly validated the RNA-seq results.

ROS Quantification in Response to CdSe/ZnS and InP/ZnS Exposure. It has long been believed that the cytotoxicity of QDs is, in part, due to their ability to cause oxidative stress in cells. Most studies will measure the levels of ROS to determine how much oxidative stress QDs are inflicting in certain cells and organisms. In my study, CdSe/ZnS and InP/ZnS QDs affected yeast differently according to the growth curves and gene expression data. I decided to measure ROS levels in CdSe/ZnS and InP/ZnS treated samples to determine if one is causing more oxidative stress than the other. Additionally, Table 4 depicts multiple genes implicated in antioxidant defenses [165] and shows the effect of Cd and InP QDs on each gene's expression to provide more insight on how they change oxidative stress response mechanisms in yeast. I quantified ROS levels (superoxide and peroxynitrite) in samples treated with CdSe/ZnS and InP/ZnS QDs at 10 and 100 µg/mL, respectively (Figure 20). The cells were cultured for six hours with the nanomaterials, then allowed to grow for 2 h with DHE (dihydroethidium) and DHR-123 (dihydrorhodamine-123) prior to measuring the oxidized DHE and DHR fluorescent byproducts, which indicate levels of superoxide and peroxynitrite, respectively (Figure 20). No significant changes in ROS levels were observed in yeast treated with 10 µg/mL CdSe/ZnS or InP/ZnS (Figure 20E,J). In cells dyed with DHE and treated with 100 µg/mL CdSe/ZnS, I observed a significant increase in superoxide levels (Figure 20C,E). In cells dyed with DHE and treated with 100 µg/mL InP/ZnS, I observed a significant decrease in superoxide levels (Figure

20D,E). In cells treated with DHR123, I observed a significant increase in peroxynitrite levels in those exposed to 100 µg/mL CdSe/ZnS QDs (Figure 20H,J) and a significant decrease in cells exposed to 100 µg/mL InP/ZnS QDs (Figure 20I,J). This suggests that both QDs have a unique effect on the generation of ROS in yeast and do not significantly affect ROS levels at concentrations lower than 10 µg/mL.

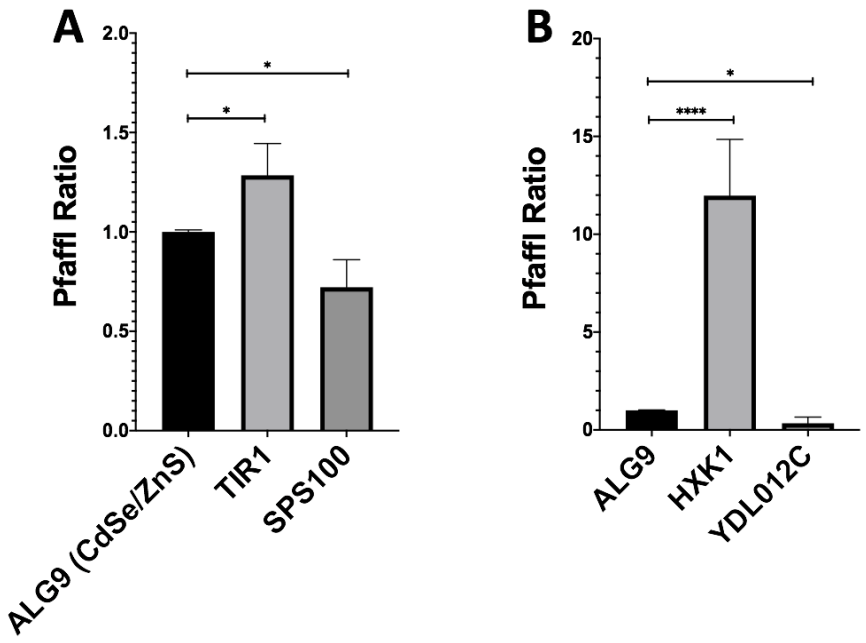

Figure 19. Gene expression ratios of ALG9 and one up- and downregulated gene from QD-treated samples determined by RT-qPCR. The reference gene ALG9 and other differentially expressed genes (from CdSe/ZnS and InP/ZnS-treated samples) were selected from the RNA-seq expression data and validated by determining their relative fold-change using the Pfaffl method. **(A)** Upregulated (TIR1) and downregulated (SPS100) genes with significantly altered gene expression levels Compared to ALG9 when treated with CdSe/ZnS. **(B)** Upregulated (HXK1) and downregulated (YDL012C) genes with significantly altered gene expression levels compared to ALG9 when treated with CdSe/ZnS. One asterisk (*) represents $p<0.05$, while 4 asterisks (****) represent $p<0.0001$.

DEGs Implicated in Cellular Trafficking. To better understand the mechanisms behind CdSe/ZnS and InP/ZnS toxicity, I investigated their effects on intracellular trafficking. Vps10-GFP was used to identify alterations in the intracellular trafficking of cargo between the

Table 4. DEGs Implicated in Antioxidant Defense

Yeast Antioxidant Genes	Function	Cd Up-Reg.	Cd Down-Reg.	InP Up-Reg.	InP Down-Reg.
Primary Antioxidant Defenses					
SOD1 (cytoplasmic superoxide dismutase)	Dis-mutation of superoxide radicals	x	*SOD1*	x	x
SOD2 (mitochondrial superoxide dismutase)		x	x	*SOD2*	x
CTT1 (cytoplasmic catalase T)	Decomposition of hydrogen peroxide	x	x	*CTT1*	x
GPX1–GPX3 (glutathione peroxidases)	Reduction of hydrogen peroxide, Reduction of alkyl hydro-peroxides	x	*GPX1*, *GPX2*	*GPX1*	*GPX2*
TRX2 (cytoplasmic thioredoxin)	Reduction of hydrogen peroxide and alkyl hydro-peroxides	x	*TRX2*	x	x

Table 4 Continued. DEGs Implicated in Antioxidant Defense

Secondary Antioxidant Defenses					
OGG1 (8-oxoguanine glycosylase/lyases)	Excision of oxidized DNA bases	x	*OGG1*	x	x

APN1 (AP endonuclease)	Cleavage of apurinic/apyrimidinic (AP) sites, Generation of 3′-hydroxyl groups at AP sites	x	*APN1*	*APN1*	x
GSH1 (glutathione)	Reduction of protein disulfides	*GSH1*	X	x	x
GRX2 (glutaredoxin)	Reduction of disulfides	x	x	*GRX2*	x
TRX2 (thioredoxin)	Reduction of protein disulfides, Reduction of oxidized glutathione	*TRX2*	x	x	x
GLR1 (glutathione reductase)	Reduction of oxidized glutathione	*GLR1*	x	*GLR1*	x
TRR2 (mitochondrial thioredoxin reductase)	Reduction of oxidized thioredoxin	x	x	*TRR2*	x
ZWF (glucose-6-phosphate dehydrogenase)	Reduction of NADP+ to NADPH	x	x	*ZWF1*	x

Table 4 Continued. DEGs Implicated in Antioxidant Defense

ZWF (glucose-6-phosphate dehydrogenase)	Reduction of NADP+ to NADPH	x	x	*ZWF1*	x
UBI4 (polyubiquitin)	Tagging oxidized proteins for degradation by the 26S proteasome	*UBI4*	x	*UBI4*	x

A table of genes implicated in antioxidant defense. It represents upregulated and downregulated genes in yeast exposed to CdSe/ZnS and InP/ZnS QDs. All genes incorporated in this table had *p*-values of 0.05 or below.

endosomes and Golgi. I hypothesized that CdSe/ZnS and InP/ZnS QDs would increase the number of Vps10-GFP puncta in yeast cells, more so in InP/ZnS QDs due to their more severe effects on growth. A previous study using cultured human cells revealed COOH-CdSe/ZnS QDs

were continuously taken up and accumulated in the endosomes. Additionally, they noted that the QDs were internalized at a fast rate and remained persistent up to six hours, which could possibly account for the greater number and disorder of Vps10-GFP puncta in the CdSe/ZnS-treated cells, but there are very few publications on the effects of QDs on intracellular trafficking.

In Table 5, I provided specific and in-depth information, such as the genes incorporated in intracellular trafficking complexes and whether those genes were upregulated or downregulated in samples exposed to CdSe/ZnS or InP/ZnS QDs. Due to the number of DEGs that were found to be involved in cellular trafficking complexes (Table 5), I decided to use confocal microscopy and yeast with GFP-tagged Vps10 (Vps10-GFP) to observe defects in trafficking. Defects in Vps10-GFP trafficking toward the trans-Golgi network were quantitated by comparing the number of Vps10-GFP puncta in QD-treated cells with untreated samples. Figure 21 revealed CdSe/ZnS QDs significantly increased the number of Vps10-GFP puncta after 6 h of incubation. In contrast, InP/ZnS QDs significantly decreased the number of Vps10-GFP puncta, resulting in fewer larger Vps10-GFP puncta compared to CdSe/ZnS.

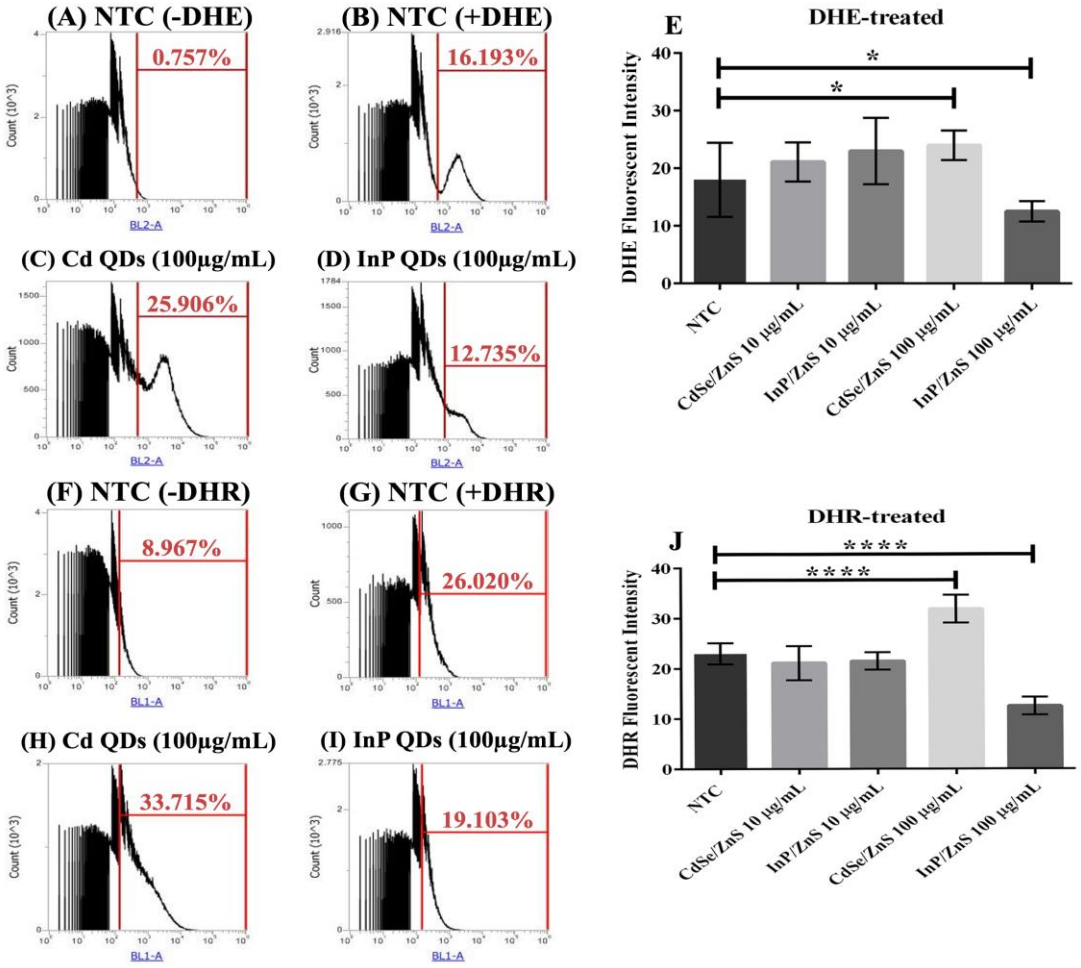

Figure 20. The Quantification of ROS levels in yeast treated with CdSe/ZnS and InP/ZnS QDs. Samples were treated with and incubated with dihydroethidium (DHE) or dihydrorhodamine (DHR) 2 h prior to measuring the oxidized DHE and DHR fluorescent byproducts, which was measured with flow cytometry, that allow us to observe changes in superoxide and peroxynitrite levels generated in each QD-treatment, respectively. **(A)** Non-treated sample without DHE. **(B)** Non-treated sample dyed with DHE. **(C)** DHE dyed sample treated with 100 µg/mL CdSe/ZnS. **(D)** DHE dyed sample treated with 100 µg/mL InP/ZnS. **(E)** Bar graph comparing % changes in superoxide levels. **(F)** Non-treated sample without DHR. **(G)** Non-treated sample dyed with DHR. **(H)** DHR dyed sample treated with 100 µg/mL CdSe/ZnS. **(I)** DHR dyed sample treated with 100 µg/mL InP/ZnS. **(J)** Bar graphs comparing % changes in peroxynitrite levels. One asterisk represent $p<0.05$ and four asterisk represent $p<0.0001$.

Table 5. Upregulated DEGs Implicated in Cellular Trafficking

Complex	CdSe/ZnS-Treated	InP/ZnS-Treated
Upregulated Genes		
SNARE	x	*NYV1, TLG2, SPO20, YPT7*
Retromer	x	x

Sorting Nexin	*SNX41*	*SNX4, SNX41*
GARP	x	*VPS52, VPS54*
Downregulated genes		
SNARE	*PEP12, VTI1, NYV1, YKT6, VAM3, VAM7, TLG1, TLG2, SSO1, SSO2, SEC9, SNC1, SNC2, SED5, GOS1, UFE1, USE1, SEC22, BOS1, BET1, VPS21*	*PEP12, VAM7, SSO1, SNC2, SED5*
Retromer	*VPS5, VPS17. VPS29, VPS35*	*VPS29*
Sorting Nexin	*SNX3, SNX4, MVP1*	x
GARP	*VPS51, VPS52, VPS53*	*VPS51*

A table that compares upregulated DEGs involved in cellular trafficking processes when exposed to green CdSe/ZnS and InP/ZnS QDs. The processes of interest include SNARE components, the Retromer, Sorting Nexin, and GARP complexes. All genes incorporated in this table had P-values of 0.05 or below.

Discussion

It has been well established that Cd-based QDs exhibit high levels of toxicity and their implementation in commercial and biomedical products has been an issue of concern. Recently, it has been suggested that Cd-based QDs could be replaced by less toxic InP-based QDs. Despite a large amount of research on Cd-QD toxicity, there have been few articles on the toxicity of

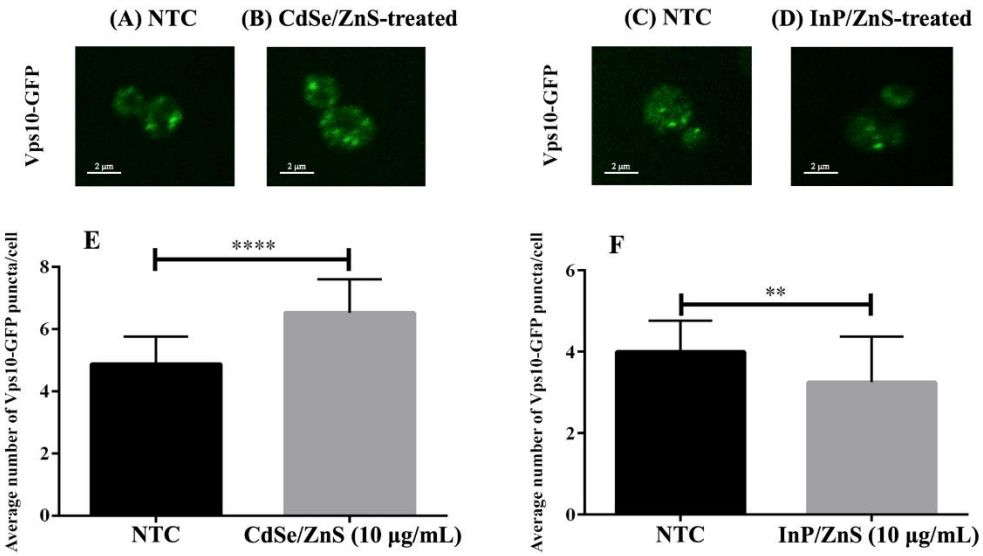

Figure 21. Cell images and bar graphs representing the number of Vps10-GFP puncta in CdSe/ZnS- and InP/ZnS-treated samples. **(A–D)** Representative images of wild type Vps10-GFP puncta in yeast. **(E)** Bar graph representing the average number of Vps10-GFP puncta per cell in CdSe/ZnS-treated samples. **(F)** Bar graph representing the average number of Vps10-GFP puncta per cell in InP/ZnS-treated samples. **(A, C)** Representative immunofluorescence image of a wild type Vps10-GFP cell from an NTC sample. **(B)** Representative immunofluorescence image of a cell from a sample treated with 10 µg/mL CdSe/ZnS. **(D)** Representative immunofluorescence image of a cell from a sample treated with 10 µg/mL InP/ZnS. Two asterisks represent $p < 0.01$ and four asterisks represent $p < 0.0001$.

InP-QDs and many researchers seemed to primarily focus on the effects QDs on growth and ROS levels. A comparison study on the toxicology of Cd- and InP-based QDs is important in determining if InP-QDs can safely replace Cd-QDs in future biological applications [163]. Regardless of which QD is more toxic, we cannot rule out the possibility that both QDs are significantly toxic, which could be possible through differences in their mechanisms of toxicity. My study investigated the cytotoxicity of CdSe/ZnS and InP/ZnS QDs on *S. cerevisiae*, and similar to previous studies, I conducted growth and ROS assays as well. Additionally, I conducted an in-depth genetic experiment (RNA-seq) to provide more specific information on cellular processes affected by analyzing changes in the quantity of mRNA transcripts in QD-treated cells. To my knowledge, the present work is the first to compare CdSe/ZnS and InP/ZnS

gene expression profiles and provide representative models of their cytotoxic effects. Interestingly, I identified many DEGs implicated in endocytosis and sorting pathways. Therefore, I attempted to visualize the effects of the QDs on intracellular trafficking by treating wild-type yeast expressing Vps10-GFP with the QDs and observing any changes with confocal microscopy. Together, I observed novel differences in the effects the QDs had on growth, ROS levels, and trafficking in *trans*-Golgi and transmembrane vesicle sorting pathways.

InP/ZnS QDs Inhibits Proliferation. Proliferation assays demonstrated a clear difference in effects between both QD-treatments, but InP/ZnS QDs appeared to have the greatest negative effect on growth. I showed that InP/ZnS QDs had the greatest effect on cellular growth at 100 μg/mL (Figure 16B), while CdSe/ZnS-treated cells displayed no significant difference in growth at the same concentration (Figure 16A). These results are not consistent with a study that tested the effects of double-capped CdSe/ZnS and InP/ZnS QDs, capped with mercaptopropionic acid, on proliferation. Using a colorimetric WST-8 proliferation assay, they showed CdSe/ZnS QDs significantly reduced viability in A549 (human lung carcinoma) and SH SY5Y (human neuroblastoma) cells at concentrations as low as 10 pM, and InP/ZnS QDs had no significant effect on viability at the same concentrations [163]. We cannot be sure if these inconsistent findings could be due to a difference in surface ligands, such as the difference between carboxylated shells and shells with mercaptopropionic acid ligands.

The MAPK pathway induces several cellular responses including proliferation, differentiation, development, inflammatory responses, and apoptosis in eukaryotic cells [166]. *MSG5*, a gene downregulated in InP/ZnS-treated samples, encodes a nuclear and cytoplasmic protein that inhibits the MAPK pathway through regulating MAPK nuclear export. One possible explanation for the reduction in proliferation with InP QDs (Figure 16B) could be due to an

MSG5-mediated immune response, triggering apoptosis. Apoptosis occurs normally in eukaryotic cells, for instance, in development, aging, and maintaining homeostasis in cell populations and is an important immune defense mechanism that occurs when cells become damaged by disease and noxious agents [167]. It is important to note that many conditions/stimuli can trigger apoptosis, and activation of apoptosis can differ between cell-types [167]. I first suspected that the greater impact on proliferation, in InP/ZnS-treated cells, was caused by a QD-mediated elevation in ROS, but after measuring ROS levels in QD-treated cells, my results suggested otherwise. A recent study that investigated the toxicity of the exact same InP/ZnS QDs on HeLa cells, found QD-treatments, at both 69 and 167 µg/mL, induced late apoptosis 4417% more than the non-treated controls [7]. This suggests that the observed reduction in proliferation by InP QDs might be primarily due to the activation of apoptosis pathways instead of increased ROS levels in InP/ZnS-treated cells.

CdSe/ZnS and InP/ZnS QDs Have Opposite Effects on ROS Generation. I found CdSe/ZnS QD treatments (100 µg/mL) significantly increased the levels of ROS, including superoxide and peroxynitrite, and InP/ZnS (100 µg/mL) statistically significantly decreased both ROS. Interestingly, a recent study that measured ROS levels in InP/ZnS-treated (69 and 167 µg/mL InP/ZnS) HeLa cervical cancer cells found InP/ZnS exposure to significantly decrease superoxide levels and significantly increase peroxynitrite levels. The decrease in superoxide levels they reported is consistent with my findings, but the increased peroxynitrite levels in their experiments contradict the effects of InP/ZnS on peroxynitrite levels in yeast. Interestingly, in a 2019 study, I investigated the effects of yellow CdSe/ZnS QDs on superoxide levels in yeast and found no significant change in ROS levels, but cells were treated with a much lower concentration (20 µg/mL) than in the current study (up to 100 µg/mL) [22]. Additionally, a study

on the cytotoxicity of InP/ZnS QDs used spin-trap electron paramagnetic resonance spectroscopy and reporter assays that revealed InP/ZnS considerably increased superoxide and hydroxyl radical levels in many cell types (NIH3T3 fibroblasts, KB cells, B16 murine melanoma cells, and MDA-MB-231 breast adenocarcinoma cells) [118]. These types of discretions in ROS production are not uncommon amongst different cell-types, including closely related, eukaryotic, microorganisms [7].

The RNA-seq analysis identified many mitochondrial genes, involved in ATPase activity, ETC, protein degradation, and mitochondrial translation, which were significantly downregulated in the presence of CdSe/ZnS QDs (Figure 22B). I conjecture that the significant decrease in metabolic activity, seen in CdSe/ZnS-treated samples, is directly associated with an increase in ROS levels. I observed considerably fewer downregulated mitochondrial genes in InP/ZnS-treated samples (Figure 22D) compared to CdSe/ZnS-treated samples (Figure 22B). On the other hand, the gene data revealed my InP/ZnS-treated cells significantly increased the expression of genes implicated in antioxidant defense activity, such as *SOD2, CTT1, GPX1, COQ3, APN1, GRX2, GLR1, TRR2, ZWF1,* and *UBI4* (Table 4). Additionally, I found an increase in the transcription of genes implicated in peroxisome structure and activity (*PEX3*, *PEX5*, *PEX7*, *PEX15*, *PEX17*, *PEX18*, *PEX19*, *PEX27*, *PEX29*, and *PEX32*), which are organelles that play a role in metabolism, signaling, and ROS detoxification. The different ROS levels and gene expression profiles of CdSe/ZnS and InP/ZnS-treated cells could be a consequence of their unique physiochemical characteristics that affect their uptake and trafficking [16]. However, results on QD toxicity can differ drastically due to different methods of synthesizing QDs, and it is not uncommon for QDs from one batch to affect organisms differently than the same QDs from a separate batch [118]. Future studies should characterize the

cellular uptake mechanisms used by each type of QD, the rate of their degradation, and their intracellular trafficking to better understand the associated cellular interactions and mechanisms of toxicity.

Comparing Gene Expression Profiles of Yeast Exposed to CdSe/ZnS and InP/ZnS QDs. I provide a model that depicts specific upregulated genes and potential physiological changes induced by exposure to CdSe/ZnS QDs (Figure 22A). Of the upregulated genes, the most serious seems to be those involved in transmembrane transport/cellular homeostasis, vacuole acidification, amino acid metabolic activity, protein folding (Table 6), and cellular trafficking (Table 5). In addition, several genes implicated in pre-RNA processing of ribosomal subunits (*SNR10*, *SNR17*, *SNR46*, *SNR49*, *SNR86*, and *NOP58*), protein folding (*KAR2* and *EUG1*), and amino acid metabolism (*ARG5*, *ARG6*, *ARO8*, *LYS1*, *LYS9*, *LEU1*, *LEU4*, and *LEU9*) were significantly upregulated. The upregulation of many genes implicated in protein production could be in response to a high level of nonfunctional proteins that might have been damaged by significantly increased superoxide levels [132, 133] resulting from CdSe/ZnS exposure or CdSe/ZnS-protein interactions within the cells. I also noticed two upregulated genes, *YDR5* and *YDR15*, which are both ATP-binding cassette (ABC) transporters implicated in yeast's drug efflux [168, 169]. It is generally believed that these ABC transporters play an important role in cellular detoxification and their upregulation suggests that yeast cells are interpreting the presence of CdSe/ZnS QDs as a xenobiotic attack [168]. The upregulation of genes involved in cellular detoxification could explain why CdSe/ZnS had no significant effect on cellular growth (Figure 16A). However, we still do not fully understand the mechanisms involved in shortening the lag phase of samples exposed to CdSe/ZnS (Figure 16G).

The expression of genes implicated in endocytosis (*ARP2*, *ARP3*, *GTS1*, *CLC1*, *BBC1*, *BZZ1*, *SCD5*, *MYO3*, and *MYO5*) and the ETC function (*COX5A*, *COX5B*, *COX6*, *COX7*, *COX8*, *COX9*, *COX10*, *COX11*, *COX12*, *COX14*, and *COX17*) was significantly lowered in CdSe/ZnS-treated samples (Figure 22B) [31,34,35]. Additionally, genes implicated in proteasome assembly (*ECM29* and *PBA1*) were downregulated, suggesting an unbalanced protein degradation and production under unfavorable conditions or unbalanced ROS levels with these QDs. This idea is consistent with the prior finding where the function of 26S proteasomes was crippled by the oxidative stress caused by H2O2 [170]. Interestingly, I found the expression of genes implicated in *trans*-Golgi network trafficking (*SNX3*, *SNX4*, *MVP1*, *Vps21*, *Vps51*, *Vps52*, and *Vps53* implicated in transport between the endosome and Golgi) was downregulated in CdSe/ZnS-treated cells and after further testing, I observed a defect in trafficking through an increased number of Vps10-GFP puncta (Table 7) [16].

I also created a detailed model of the potential effects induced by InP/ZnS QDs (Figure 22C). InP/ZnS exposure upregulates approximately 3 times as many genes compared to CdSe/ZnS-treated samples (Figure 23A). Significantly upregulated processes in InP/ZnS-treated samples include endocytosis, peroxisome assembly, proteasome assembly/activity, the Cvt pathway, the ETC, and oxide reduction metabolic processes (Table 6). Interestingly, I found the downregulation of ETC genes to be unique to CdSe/ZnS-treated cells. An opposite effect on ETC was observed in InP/ZnS-treated samples where ETC genes were significantly upregulated, including *AIM31*, *COX4*, *COX5B*, *COX6*, *COX7*, *COX9*, *COX12*, *COX13*, and *COX15* (Figure 22C). I also found many genes associated with endocytosis to be downregulated in CdSe/ZnS-treated samples, but significantly up- and downregulated in InP/ZnS-treated samples. Upregulated endocytosis genes included *LSB6*, *SDB17*, *YAP1801*, *CHC1*, and *ACT1*, while

downregulated endocytosis genes consisted of MYO3, *MYO5*, *ENT1*, *ARK1*, and *VRP1* (Table 8). Interestingly, after gene expression analysis, I found proteasome assembly to be a downregulated process in CdSe/ZnS-treated samples (*PBA1* and *ECM29*) and upregulated in InP/ZnS-treated samples (*ECM29*, *CDC34, CDC53*, *HRT3*, and *DIA2*).

InP/ZnS significantly downregulates approximately half the number of genes when compared to the number of downregulated genes from CdSe/ZnS-treated cells (Figure 23B). DEGs that are depicted in Figure 21D are significantly downregulated processes including endocytosis, rRNA processing, translation, the Cvt pathway, actin and microtubule growth, vesicle fusion, and protein targeting to the plasma membrane, and *trans*-Golgi network trafficking (Table 9). A gene encoding a microtubule plus-end tracking protein, *BIK1*, was downregulated in InP/ZnS-treated samples. These proteins are known to play roles in key cellular processes including cell motility, intracellular trafficking, and pathways that align the mitotic spindle with the division axis of the cell, making them crucial in cell division [171]. Another important player implicated in cell division is a gene encoding a capping protein, *CAP2*. In samples exposed to InP/ZnS, *CAP2* was significantly downregulated. In yeast, single actin monomers are used to synthesize actin cables involved in polarized growth, and in yeast lacking *CAP1* or *CAP2* have low levels of free actin due to excessive F-actin assembly in cortical patches, which is detrimental to the assembly on actin cables [172]. These genes, downregulated in InP/ZnS-treated samples, might contribute to InP/ZnS QDs' negative impact on proliferation compared to CdSe/ZnS QDs. Additionally, I found noticeably fewer DEGs involved in endocytosis, SNAREs, and the Retromer when treated with InP/ZnS (Table 5), which suggests different uptake and trafficking mechanisms are at work compared to CdSe/ZnS-treated samples.

Effects of CdSe/ZnS and InP/ZnS QDs on the Intracellular Trafficking of Vps10-GFP. Cargo trafficking in yeast is primarily done by a complex endosomal system that sorts lipids, proteins, and a variety of cargo. The system begins when cargo is endocytosed and trafficked to the early endosome where it is sorted and either sent to the lysosome for degradation or targeted to the Golgi or plasma membrane through a retrograde or recycling pathway. Endosome-to-Golgi retrograde and Endosome-to-plasma membrane recycling pathways orchestrate the re-use of sorting receptors and are important in creating the lysosome and determines what is sent to compose the plasma membrane. These pathways are responsible for many cellular functions including homeostasis and quality control of lipids and proteins. Negatively impacting the endosomal sorting pathways have been linked to many diseases including, but not limited to, cancer, Parkinson's disease, and Alzheimer's [173].

Vps10 is an integral sorting receptor protein that plays a role in the sorting of newly synthesized carboxypeptidase A at the *trans*-Golgi and that shuttles back and forth between the *trans*-Golgi and the endosome [173]. I treated yeast containing Vps10-GFP with the QDs and observed alterations in the phenotypes compared to non-treated cells via confocal microscopy. [16]. I found significant differences in the number of puncta in QD-treated cells. CdSe/ZnS QDs significantly increased the number of puncta and InP/ZnS QDs significantly decreased the number in yeast. [16], both of the QDs have the same carboxylic acid ligands on their surface. Additionally, each QD possesses identical ZnS shells that surround their respective cores (CdSe and InP). This suggests that differences in Vps10-GFP phenotypes are due to their different physiochemical effects of CdSe and InP-cores. It is important to note that understanding the cellular mechanisms that are coordinated by their different physiochemical properties is essential in evaluating QD toxicity and is still poorly understood.

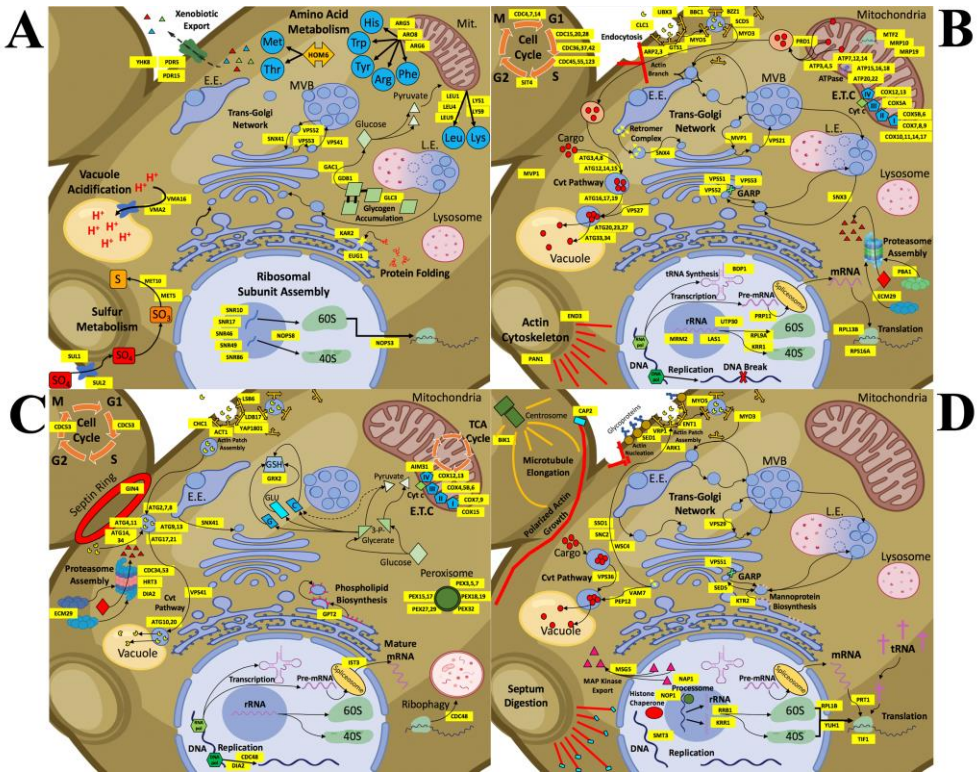

Figure 22. Detailed schematic models representing changes in cellular processes with CdSe/ZnS QDs or InP/ZnS QDs in the budding yeast. **(A)** CdSe/ZnS QD exposure causes an increase in the expression of genes involved in cellular processes such as transmembrane transport/cellular homeostasis, vacuole acidification, amino acid metabolic activity, protein folding, and trafficking within the *trans*-Golgi network. **(B)** Decreased expression in many genes treated with CdSe/ZnS has revealed many important downregulated processes involved in endocytosis, the Cvt pathway, rRNA processing, proteasome assembly, metabolic activity, cell cycle regulation, and trafficking within the *trans*-Golgi network. **(C)** Yeast exposed to InP/ZnS QDs has upregulated many genes required for processes like endocytosis, peroxisome assembly, proteasome assembly and activity, the Cvt pathway, the ETC, and oxido-reduction metabolic processes. **(D)** Several more processes are downregulated when exposed to InP/ZnS QDs including endocytosis, rRNA processing, translation, the Cvt pathway, actin and microtubule growth, vesicle fusion, and protein targeting to the plasma membrane, and some *trans*-Golgi network trafficking.

Comparing the Biological Effects of CdSe/ZnS with Known Biological Effects of Cd in *Saccharomyces cerevisiae.* Many types of metals and metalloids are widespread in nature and can accumulate to high concentrations locally. These metals are not QDs but greatly affect biological systems. Organisms have dealt with metals and evolved proteins that require metals for catalytic functions and maintaining the correct structure [174]. On the other hand, some

metals such as Cd interact and inhibit enzymes that disrupt normal cellular processes and contribute to their toxicity, however, relatively little is known about their molecular mechanisms of toxicity.

Table 6. CdSe/ZnS Induced DEGs Implicated in Upregulated Cellular Processes.

Upregulated GO-Terms (CdSe/ZnS)	Genes in Figure 22A
Transmembrane transport/cellular homeostasis	*YHK8, PDR5,* and *PDR15*
Vacuole acidification	*VMA2* and *VMA16*
Amino acid metabolic activity	*ARG5, ARO8, ARG6, LEU1, LEU4, LEU9, and LYS1/9*
Protein folding	*KAR2* and *EUG1*
Trafficking within the *trans*-Golgi network	*VPS41 and SNX41*

A table listing the GO-terms and genes in Figure 22A. It represents the multiple upregulated cellular processes and genes in yeast exposed to 10 μg/mL CdSe/ZnS QDs. All genes incorporated in this table exhibited expression levels significantly higher than expression levels of NTC samples.

Using transcriptomic experiments and bioinformatics analysis, common metal-responsive (CMR) genes have been identified. The transcriptome changes made when exposed to most metals were analyzed and similar changes in gene regulation were observed, and make up the

Table 7. CdSe/ZnS Induced DEGs Implicated in Downregulated Cellular Processes.

Downregulated GO-Terms (CdSe/ZnS)-Downregulated)	Genes in Figure 22B
Endocytosis	*MYO3, MYO5, CLC1, ARP2, ARP3, BZZ1, SCD5, BBC1,* and *GTS1*
The Cvt pathway	*ATG3, ATG4, ATG8, ATG12, ATG14, ATG15, ATG16, ATG17, ATG19, ATG20, ATG23, ATG27, ATG33, and ATG34*
rRNA processing	*MRM2, LAS1, UTP30, RPL9A, and KRR1*
Proteasome assembly	*PBA1* and *ECM29*
Metabolic activity	*ATP3, ATP4, ATP5, ATP7, ATP12, ATP14, ATP15, ATP16, ATP18, ATP20, ATP22, MRP10, MRP19, and MTF2*
Cell cycle regulation	*CDC4, CDC7, CDC14, CDC15, CDC20, CDC28, CDC36, CDC37, CDC42, CDC45, CDC55, CDC123, and SIT4*
Cellular trafficking	*SNX3, SNX4, MVP1, VPS21, VPS51, VPS52, and VPS53*

A table listing the GO-terms and genes in Figure 22B. It represents the multiple downregulated cellular processes and genes in yeast exposed to 10 μg/mL CdSe/ZnS QDs. All genes incorporated in this table exhibited expression levels significantly lower than expression levels of NTC samples.

CMR genes [174]. CMR genes were enriched with GO-terms of biological processes including metal ion transport/homeostasis, ROS detoxification, carbohydrate metabolism, fatty acid metabolism, and RNA polymerase II transcription [174]. The GO-term analysis of genes differentially expressed by CdSe/ZnS QDs were not enriched with similar GO-terms, which suggests that their transcriptomic profile is not similar to that of yeast exposed to Cd.

Interestingly, the transcriptomic profile of cells treated with InP/ZnS had many similar GO-terms to the CMR genes, which could suggest InP/ZnS QDs affect yeast very similarly to toxic metals and metalloids.

Table 8. InP/ZnS Induced DEGs Implicated in Upregulated Cellular Processes.

Upregulated GO-Terms (InP/ZnS)	Genes in Figure 22C
Endocytosis	*LSB6, SDB17, YAP1801, CHC1, and ACT1*
Peroxisome assembly	*PEX3, PEX5, PEX7, PEX15, PEX17, PEX18, PEX19, PEX27, PEX29, and PEX32*
Proteasome assembly and activity	*ECM29, CDC34/53, HRT3, and DIA2*
The Cvt pathway	*ATG2, ATG4, ATG7, ATG8, ATG9, ATG10, ATG11, ATG13, ATG14, ATG17, ATG20, ATG21, ATG34, and VPS41*
ETC	*AIM31 and COX4, COX5B, COX6, COX7, COX9, COX12, COX13, and COX15*
Oxido-reduction metabolic processes	*GRX2*

A table listing the GO-terms and genes in Figure 22C. It represents the multiple upregulated cellular processes and genes in yeast exposed to 100 μg/mL InP/ZnS QDs. All genes incorporated in this table exhibited expression levels significantly higher than expression levels of NTC samples.

Cd metals specifically inhibit proteins that protect cells from oxidative stress including glutathione and thioredoxins. When these enzymes are inhibited it results in an increase of ROS levels due to a decrease in functional antioxidant genes [174]. The RNA-seq data revealed that the CdSe/ZnS-treated group significantly downregulated two out of three thioredoxins (TRX1

and TRX2). Alternatively, the InP/ZnS-treated group did not significantly change the expression of any thioredoxin. These results suggest that CdSe/ZnS QDs and Cd metal have different mechanisms of toxicity on yeast.

Table 9. InP/ZnS Induced DEGs Implicated in Downregulated Cellular Processes.

Downregulated GO-Terms (InP/ZnS)	**Genes in Figure 22D**
Endocytosis	*MYO3, MYO5, ENT1, ARK1, and VRP1*
rRNA processing	*RRB1, KRR1, RPL1B, and YUH1*
Translation	*PRT1 and TIF1*
The Cvt pathway	*VPS36*
Actin and microtubule growth	*CAP2 and BIK1, respectively*
Vesicle fusion and protein targeting to the plasma membrane	*SSO1, SNC2, and WSC4, respectively*
Cellular trafficking	*SED5, VAM7, PEP12, VPS29, and VPS51*

A table listing the GO-terms and genes in Figure 22D. It represents the multiple downregulated cellular processes and genes in yeast exposed to 100 µg/mL InP/ZnS QDs. All genes incorporated in this table exhibited expression levels significantly lower than expression levels of NTC samples.

Conclusion

In the present study, I provided evidence that CdSe/ZnS and InP/ZnS QDs have a mild cytotoxic effect on yeast. In comparison, each QD appeared to exert unique cytotoxic effects in a variety of tests. CdSe/ZnS QDs differentially regulated gene expression in a greater number of genes, including all up and downregulated genes, than InP/ZnS QDs. Notably, InP/ZnS QDs upregulated hundreds of more genes than CdSe/ZnS QDs. Interestingly, with another cytotoxic experiment, I observed InP/ZnS QDs had a greater and dose-dependent effect on proliferation whereas I observed no significant change in CdSe/ZnS-treated samples. As depicted in my working models, I showed a significant downregulation in mitochondrial/ETC function and genes implicated in *trans*-Golgi network trafficking in the presence of CdSe/ZnS QDs more so than in InP/ZnS-treated samples. Additionally, the confocal microscopy analysis revealed

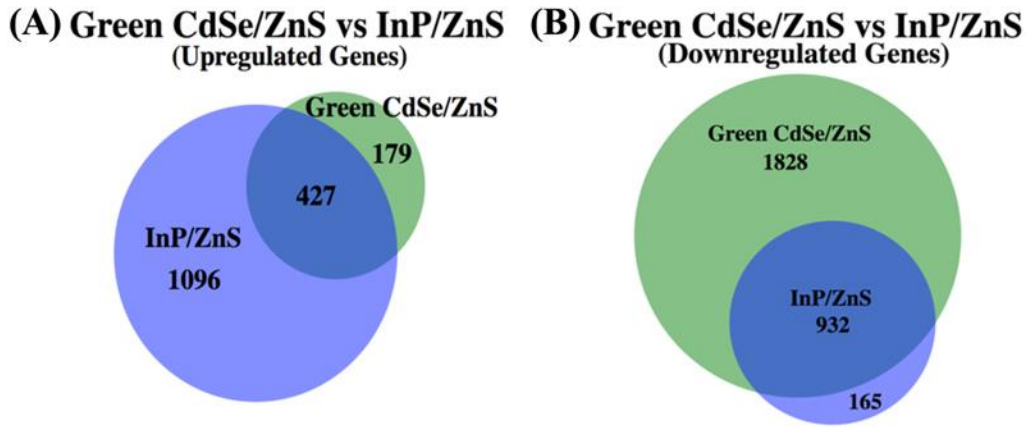

Figure 23. A proportionately accurate Venn-diagram that represents the number of up- and downregulated genes whose expression has been significantly changed when exposed to CdSe/ZnS QDs or InP/ZnS QDs. The overlapped segments of each Venn-diagram represent genes that are differentially expressed when exposed to CdSe/ZnS and InP/ZnS QDs. The portions of the Venn-diagram that do not overlap are up- or downregulated genes that become differentially expressed only when exposed to CdSe/ZnS QDs or InP/ZnS QDs. (**A**) Every gene whose expression was significantly increased when compared to the normal gene expression in yeast cells when exposed to CdSe/ZnS or InP/ZnS QDs. (**B**) Every gene whose expression was significantly decreased when exposed to CdSe/ZnS or InP/ZnS QDs.

changes in Vps10-GFP trafficking in both QDs. It is generally believed that QDs, such as CdSe/ZnS and InP/ZnS, are trafficked and processed differently due to their individual physio-chemical properties. Based on my results, each QD induced dissimilar cytotoxic effects in the experiments on the budding yeast. Currently, we understand little about the physiochemical effects, and the mechanisms behind QD toxicity must be solved before they can be used in the life sciences or medicine. It is essential, to our health and the environment, that the toxicity of all QDs used, industrially or commercially, are thoroughly tested and understood in diverse cell types and organismal models. The next steps in studying QD toxicity should include proteomic analysis to identify novel protein interactions and better understand the effects on how their physiochemical properties coordinate their toxicity.

REFERENCES

1. Stark, R.; Grzelak, M.; Hadfield, J. RNA sequencing: the teenage years. *Nat Rev Genet* **2019**, 20, 631-656.

2. Libralato, G.; Galdiero, E.; Falanga, A.; Carotenuto, R.; De Alteriis, E.; Guida, M. Toxicity Effects of Functionalized Quantum Dots, Gold and Polystyrene Nanoparticles on Target Aquatic Biological Models: A Review. *Molecules* **2017**, 22.

3. Buglak, A.A.; Zherdev, A.V.; Dzantiev, B.B. Nano-(Q)SAR for Cytotoxicity Prediction of Engineered Nanomaterials. *Molecules* **2019**, 24.

4. Hsieh, S.F.; Bello, D.; Schmidt, D.F.; Pal, A.K.; Stella, A.; Isaacs, J.A.; Rogers, E.J. Mapping the biological oxidative damage of engineered nanomaterials. *Small* **2013**, 9, 1853-1865.

5. Baig, S.; Xu, J.; Wu, P.; Chen, B.; Wang, M. Formation of visible single-mode light sources using quantum dots. *Proceedings of SPIE* **2008**.

6. Hens, B.; Smothers, J.; Rizvanovic, H.; Patel, R.; Wu, Q.; Kim, K. The Future of Anticancer Drugs: A Cytotoxicity Assessment Study of CdSe/ZnS Quantum Dots. *Nanotheranostics* **2020**, 19, 20.

7. Davenport, V.; Horstmann, C.; Patel, R.; Wu, Q.; Kim, K. An assessment of InP/ZnS as potential anti-cancer therapy: Quantum dot treatment induces stress on HeLa cells **2020**.

8. Woodman, S.; Short, J.C.; Mcdermott, H.; Linan, A.; Bartlett, K.; Gadila, S.K.; Schmelzle, K.; Wanekaya, A.; Kim, K. Carbon Nanomaterials Alter Global Gene Expression Profiles. *J Nanosci Nanotechnol* **2016**, 16, 5207-5217.

9. Snyder-Talkington, B.N.; Dong, C.; Singh, S.; Raese, R.; Qian, Y.; Porter, D.W.; Wolfarth, M.G.; Guo, N.L. Multi-Walled Carbon Nanotube-Induced Gene Expression Biomarkers for Medical and Occupational Surveillance. *Int J Mol Sci* **2019**, 20.

10. Chang, S.; Zhao, X.; Li, S.; Liao, T.; Long, J.; Yu, Z.; Cao, Y. Cytotoxicity, cytokine release and ER stress-autophagy gene expression in endothelial cells and alveolar-

endothelial co-culture exposed to pristine and carboxylated multi-walled carbon nanotubes. *Ecotoxicol Environ Saf* **2018**, 161, 569-577.

11. Sukhanova, A.; Bozrova, S.; Sokolov, P.; Berestovoy, M.; Karaulov, A.; Nabiev, I. Dependence of Nanoparticle Toxicity on Their Physical and Chemical Properties. *Nanoscale Res Lett* **2018**, 13, 44.

12. Hardman, R. A toxicologic review of quantum dots: toxicity depends on physicochemical and environmental factors. *Environ Health Perspect* **2006**, 114, 165-172.

13. Rajendiran, K.; Zhao, Z.; Pei, D.S.; Fu, A. Antimicrobial Activity and Mechanism of Functionalized Quantum Dots. *Polymers (Basel)* **2019**, 11.

14. Monras, J.P.; Collao, B.; Molina-Quiroz, R.C.; Pradenas, G.A.; Saona, L.A.; Duran-Toro, V.; Ordenes-Aenishanslins, N.; Venegas, F.A.; Loyola, D.E.; Bravo, D.; Calderon, P.F.; Calderon, I.L.; Vasquez, C.C.; Chasteen, T.G.; Lopez, D.A.; Perez-Donoso, J.M. Microarray analysis of the Escherichia coli response to CdTe-GSH Quantum Dots: understanding the bacterial toxicity of semiconductor nanoparticles. *BMC Genomics* **2014**, 15, 1099.

15. Hossen, S.; Hossain, M.K.; Basher, M.K.; Mia, M.N.H.; Rahman, M.T.; Uddin, M.J. Smart nanocarrier-based drug delivery systems for cancer therapy and toxicity studies: A review. *J Adv Res* **2019**, 15, 1-18.

16. Manshian, B.B.; Martens, T.F.; Kantner, K.; Braeckmans, K.; De Smedt, S.C.; Demeester, J.; Jenkins, G.J.S.; Parak, W.J.; Pelaz, B.; Doak, S.H.; Himmelreich, U.; Soenen, S.J. The role of intracellular trafficking of CdSe/ZnS QDs on their consequent toxicity profile. *J Nanobiotechnology* **2017**, 15, 45.

17. Breus, V.V.; Pietuch, A.; Tarantola, M.; Basche, T.; Janshoff, A. The effect of surface charge on nonspecific uptake and cytotoxicity of CdSe/ZnS core/shell quantum dots. *Beilstein J Nanotechnol* **2015**, 6, 281-292.

18. Fan, J.; Shao, M.; Lai, L.; Liu, Y.; Xie, Z. Inhibition of autophagy contributes to the toxicity of cadmium telluride quantum dots in Saccharomyces cerevisiae. *Int J Nanomedicine* **2016**, 11, 3371-3383.

19. Liu, J.; Hu, R.; Liu, J.; Zhang, B.; Wang, Y.; Liu, X.; Law, W.C.; Liu, L.; Ye, L.; Yong, K.T. Cytotoxicity assessment of functionalized CdSe, CdTe and InP quantum dots in two human cancer cell models. *Mater Sci Eng C Mater Biol Appl* **2015**, 57, 222-231.

20. Yang, Y.; Zhu, H.; Colvin, V.L.; Alvarez, P.J. Cellular and transcriptional response of Pseudomonas stutzeri to quantum dots under aerobic and denitrifying conditions. *Environ Sci Technol* **2011**, 45, 4988-4994.

21. Yang, Y.; Mathieu, J.M.; Chattopadhyay, S.; Miller, J.T.; Wu, T.; Shibata, T.; Guo, W.; Alvarez, P.J. Defense mechanisms of Pseudomonas aeruginosa PAO1 against quantum dots and their released heavy metals. *ACS Nano* **2012**, 6, 6091-6098.

22. Horstmann, C.; Kim, D.S.; Campbell, C.; Kim, K. Transcriptome Profile Alteration with Cadmium Selenide/Zinc Sulfide Quantum Dots in Saccharomyces cerevisiae. *Biomolecules* **2019**, 9.

23. Hosiner, D.; Gerber, S.; Lichtenberg-Frate, H.; Glaser, W.; Schuller, C.; Klipp, E. Impact of acute metal stress in Saccharomyces cerevisiae. *PLoS One* **2014**, 9, e83330.

24. Marmiroli, M.; Pagano, L.; Pasquali, F.; Zappettini, A.; Tosato, V.; Bruschi, C.V.; Marmiroli, N. A genome-wide nanotoxicology screen of Saccharomyces cerevisiae mutants reveals the basis for cadmium sulphide quantum dot tolerance and sensitivity. *Nanotoxicology* **2016**, 10, 84-93.

25. Pasquali, F.; Agrimonti, C.; Pagano, L.; Zappettini, A.; Villani, M.; Marmiroli, M.; White, J.C.; Marmiroli, N. Nucleo-mitochondrial interaction of yeast in response to cadmium sulfide quantum dot exposure. *J Hazard Mater* **2017**, 324, 744-752.

26. Majumdara, S.; Maa, C.; Villanie, M.; Zuverza-Menaa, N.; Paganod, L.; Huangb, Y.; Zappettinie, A.; Kellerb, A.A.; Marmirolid, N.; Dhankherf, O.P.; White, J.C. Surface coating determines the response of soybean plants to cadmium sulfide quantum dots. *Elsevier* **2019**, 14.

27. Simon, D.F.; Domingos, R.F.; Hauser, C.; Hutchins, C.M.; Zerges, W.; Wilkinson, K.J. Transcriptome sequencing (RNA-seq) analysis of the effects of metal nanoparticle exposure on the transcriptome of Chlamydomonas reinhardtii. *Appl Environ Microbiol* **2013**, 79, 4774-4785.

28. Dua, P.; Jeong, S.; Lee, S.-E.; Hong, S.W.; Kim, S.; Lee, D.-K. Evaluation of Toxicity and Gene Expression Changes Triggered by Quantum Dots. *Bulletin of the Korean Chemical Society* **2010**, 31, 6.

29. Zhang, T.; Stilwell, J.L.; Gerion, D.; Ding, L.; Elboudwarej, O.; Cooke, P.A.; Gray, J.W.; Alivisatos, A.P.; Chen, F.F. Cellular effect of high doses of silica-coated quantum dot profiled with high throughput gene expression analysis and high content cellomics measurements. *Nano Lett* **2006**, 6, 800-808.

30. Mitchell, H.D.; Markillie, L.M.; Chrisler, W.B.; Gaffrey, M.J.; Hu, D.; Szymanski, C.J.; Xie, Y.; Melby, E.S.; Dohnalkova, A.; Taylor, R.C.; Grate, E.K.; Cooley, S.K.; Mcdermott, J.E.; Heredia-Langner, A.; Orr, G. Cells Respond to Distinct Nanoparticle Properties with Multiple Strategies As Revealed by Single-Cell RNA-Seq. *ACS Nano* **2016**, 10, 10173-10185.

31. Loiseau, A.; Asila, V.; Boitel-Aullen, G.; Lam, M.; Salmain, M.; Boujday, S. Silver-Based Plasmonic Nanoparticles for and Their Use in Biosensing. *Biosensors (Basel)* **2019**, 9.

32. Liao, C.; Li, Y.; Tjong, S.C. Bactericidal and Cytotoxic Properties of Silver Nanoparticles. *Int J Mol Sci* **2019**, 20.

33. Zhang, X.F.; Liu, Z.G.; Shen, W.; Gurunathan, S. Silver Nanoparticles: Synthesis, Characterization, Properties, Applications, and Therapeutic Approaches. *Int J Mol Sci* **2016**, 17.

34. Prabhu, S.; Poulose, E.K. Silver nanoparticles: mechanism of antimicrobial action, synthesis, medical applications, and toxicity effects. *International Nano Letters* **2012**.

35. Lee, S.H.; Jun, B.H. Silver Nanoparticles: Synthesis and Application for Nanomedicine. *Int J Mol Sci* **2019**, 20.

36. Siddiqi, K.S.; Husen, A.; Rao, R.a.K. A review on biosynthesis of silver nanoparticles and their biocidal properties. *J Nanobiotechnology* **2018**, 16, 14.

37. Kalinska, A.; Jaworski, S.; Wierzbicki, M.; Golebiewski, M. Silver and Copper Nanoparticles-An Alternative in Future Mastitis Treatment and Prevention? *Int J Mol Sci* **2019**, 20.

38. Ashmore, D.; Chaudhari, A.; Barlow, B.; Barlow, B.; Harper, T.; Vig, K.; Miller, M.; Singh, S.; Nelson, E.; Pillai, S. Evaluation of E. coli inhibition by plain and polymer-coated silver nanoparticles. *Rev Inst Med Trop Sao Paulo* **2018**, 60, e18.

39. Wang, J.; Li, J.; Guo, G.; Wang, Q.; Tang, J.; Zhao, Y.; Qin, H.; Wahafu, T.; Shen, H.; Liu, X.; Zhang, X. Silver-nanoparticles-modified biomaterial surface resistant to staphylococcus: new insight into the antimicrobial action of silver. *Sci Rep* **2016**, 6, 32699.

40. Liu, Y.; Wu, N.; Dong, J.; Gao, Y.; Zhang, X.; Mu, C.; Shao, N.; Yang, G. Hfq is a global regulator that controls the pathogenicity of Staphylococcus aureus. *PLoS One* **2010**, 5.

41. Tian, H.; Liao, Q.; Liu, M.; Hou, J.; Zhang, Y.; Liu, J. Antibacterial activity of silver nanoparticles target sara through srna-teg49, a key mediator of hfq, in staphylococcus aureus. *Int J Clin Exp Med* **2015**, 8, 5794-5799.

42. Deabes, M.M.; Khalil, W.K.B.; Attallah, A.G.; El-Desouky, T.A.; Naguib, K.M. Impact of Silver Nanoparticles on Gene Expression in Aspergillus Flavus Producer Aflatoxin B1. *Open Access Maced J Med Sci* **2018**, 6, 600-605.

43. Yabe, K.; Nakajima, H. Enzyme reactions and genes in aflatoxin biosynthesis. *Appl Microbiol Biotechnol* **2004**, 64, 745-755.

44. Mishra, S.; Singh, H.B. Silver nanoparticles mediated altered gene expression of melanin biosynthesis genes in Bipolaris sorokiniana. *Microbiol Res* **2015**, 172, 16-18.

45. Lee, A.R.; Lee, S.J.; Lee, M.; Nam, M.; Lee, S.; Choi, J.; Lee, H.J.; Kim, D.U.; Hoe, K.L. Editor's Highlight: A Genome-wide Screening of Target Genes Against Silver Nanoparticles in Fission Yeast. *Toxicol Sci* **2018**, 161, 171-185.

46. Sillapawattana, P.; Gruhlke, M.C.; Schaffer, A. Effect of silver nanoparticles on the standard soil arthropod Folsomia candida (Collembola) and the eukaryote model organism Saccharomyces cerevisiae. *Environ Sci Eur* **2016**, 28, 27.

47. Horstmann, C.; Campbell, C.; Kim, D.S.; Kim, K. Transcriptome profile with 20 nm silver nanoparticles in yeast. *FEMS Yeast Res* **2019**, 19.

48. Gurunathan, S.; Qasim, M.; Park, C.; Yoo, H.; Choi, D.Y.; Song, H.; Park, C.; Kim, J.H.; Hong, K. Cytotoxicity and Transcriptomic Analysis of Silver Nanoparticles in Mouse Embryonic Fibroblast Cells. *Int J Mol Sci* **2018**, 19.

49. Huang, C.L.; Hsiao, I.L.; Lin, H.C.; Wang, C.F.; Huang, Y.J.; Chuang, C.Y. Silver nanoparticles affect on gene expression of inflammatory and neurodegenerative responses in mouse brain neural cells. *Environ Res* **2015**, 136, 253-263.

50. Yuan, Y.G.; Zhang, S.; Hwang, J.Y.; Kong, I.K. Silver Nanoparticles Potentiates Cytotoxicity and Apoptotic Potential of Camptothecin in Human Cervical Cancer Cells. *Oxid Med Cell Longev* **2018**, 2018, 6121328.

51. Gliga, A.R.; Di Bucchianico, S.; Lindvall, J.; Fadeel, B.; Karlsson, H.L. RNA-sequencing reveals long-term effects of silver nanoparticles on human lung cells. *Sci Rep* **2018**, 8, 6668.

52. Nallanthighal, S.; Heiserman, J.P.; Cheon, D.J. The Role of the Extracellular Matrix in Cancer Stemness. *Front Cell Dev Biol* **2019**, 7, 86.

53. Nel, A.; Xia, T.; Madler, L.; Li, N. Toxic potential of materials at the nanolevel. *Science* **2006**, 311, 622-627.

54. Damoiseaux, R.; George, S.; Li, M.; Pokhrel, S.; Ji, Z.; France, B.; Xia, T.; Suarez, E.; Rallo, R.; Madler, L.; Cohen, Y.; Hoek, E.M.; Nel, A. No time to lose--high throughput screening to assess nanomaterial safety. *Nanoscale* **2011**, 3, 1345-1360.

55. Colvin, V.L. The potential environmental impact of engineered nanomaterials. *Nat Biotechnol* **2003**, 21, 1166-1170.

56. Kwolek-Mirek, M.; Zadrag-Tecza, R. Comparison of methods used for assessing the viability and vitality of yeast cells. *FEMS Yeast Res* **2014**, 14, 1068-1079.

57. Riley, R.S.; Day, E.S. Gold nanoparticle-mediated photothermal therapy: applications and opportunities for multimodal cancer treatment. *Wiley Interdiscip Rev Nanomed Nanobiotechnol* **2017**, 9.

58. Connor, E.E.; Mwamuka, J.; Gole, A.; Murphy, C.J.; Wyatt, M.D. Gold nanoparticles are taken up by human cells but do not cause acute cytotoxicity. *Small* **2005**, 1, 325-327.

59. Patra, H.K.; Banerjee, S.; Chaudhuri, U.; Lahiri, P.; Dasgupta, A.K. Cell selective response to gold nanoparticles. *Nanomedicine* **2007**, 3, 111-119.

60. Goodman, C.M.; Mccusker, C.D.; Yilmaz, T.; Rotello, V.M. Toxicity of gold nanoparticles functionalized with cationic and anionic side chains. *Bioconjug Chem* **2004**, 15, 897-900.

61. Ge, L.; Li, Q.; Wang, M.; Ouyang, J.; Li, X.; Xing, M.M. Nanosilver particles in medical applications: synthesis, performance, and toxicity. *Int J Nanomedicine* **2014**, 9, 2399-2407.

62. Kim, J.S.; Kuk, E.; Yu, K.N.; Kim, J.H.; Park, S.J.; Lee, H.J.; Kim, S.H.; Park, Y.K.; Park, Y.H.; Hwang, C.Y.; Kim, Y.K.; Lee, Y.S.; Jeong, D.H.; Cho, M.H. Antimicrobial effects of silver nanoparticles. *Nanomedicine* **2007**, 3, 95-101.

63. Sun, D.; Zhang, W.; Mou, Z.; Chen, Y.; Guo, F.; Yang, E.; Wang, W. Transcriptome Analysis Reveals Silver Nanoparticle-Decorated Quercetin Antibacterial Molecular Mechanism. *ACS Appl Mater Interfaces* **2017**, 9, 10047-10060.

64. Nadworny, P.L.; Wang, J.; Tredget, E.E.; Burrell, R.E. Anti-inflammatory activity of nanocrystalline silver in a porcine contact dermatitis model. *Nanomedicine* **2008**, 4, 241-251.

65. Ray, P.C.; Yu, H.; Fu, P.P. Toxicity and environmental risks of nanomaterials: challenges and future needs. *J Environ Sci Health C Environ Carcinog Ecotoxicol Rev* **2009**, 27, 1-35.

66. Sondi, I.; Salopek-Sondi, B. Silver nanoparticles as antimicrobial agent: a case study on E. coli as a model for Gram-negative bacteria. *J Colloid Interface Sci* **2004**, 275, 177-182.

67. Kim, K.J.; Sung, W.S.; Suh, B.K.; Moon, S.K.; Choi, J.S.; Kim, J.G.; Lee, D.G. Antifungal activity and mode of action of silver nano-particles on Candida albicans. *Biometals* **2009**, 22, 235-242.

68. Madhavan, P.; Hong, P.Y.; Sougrat, R.; Nunes, S.P. Silver-enhanced block copolymer membranes with biocidal activity. *ACS Appl Mater Interfaces* **2014**, 6, 18497-18501.

69. Garcia-Saucedo, C.; Field, J.A.; Otero-Gonzalez, L.; Sierra-Alvarez, R. Low toxicity of HfO2, SiO2, Al2O3 and CeO2 nanoparticles to the yeast, Saccharomyces cerevisiae. *J Hazard Mater* **2011**, 192, 1572-1579.

70. Nogueira, D.R.; Mitjans, M.; Rolim, C.M.; Vinardell, M.P. Mechanisms Underlying Cytotoxicity Induced by Engineered Nanomaterials: A Review of In Vitro Studies. *Nanomaterials (Basel)* **2014**, 4, 454-484.

71. Boenigk, J.; Beisser, D.; Zimmermann, S.; Bock, C.; Jakobi, J.; Grabner, D.; Grobetamann, L.; Rahmann, S.; Barcikowski, S.; Sures, B. Effects of silver nitrate and silver nanoparticles on a planktonic community: general trends after short-term exposure. *PLoS One* **2014**, 9, e95340.

72. Orsini, L.; Gilbert, D.; Podicheti, R.; Jansen, M.; Brown, J.B.; Solari, O.S.; Spanier, K.I.; Colbourne, J.K.; Rusch, D.B.; Decaestecker, E.; Asselman, J.; De Schamphelaere, K.A.; Ebert, D.; Haag, C.R.; Kvist, J.; Laforsch, C.; Petrusek, A.; Beckerman, A.P.; Little, T.J.; Chaturvedi, A.; Pfrender, M.E.; De Meester, L.; Frilander, M.J. Daphnia magna transcriptome by RNA-Seq across 12 environmental stressors. *Sci Data* **2017**, 4, 170006.

73. Hwang, I.S.; Lee, J.; Hwang, J.H.; Kim, K.J.; Lee, D.G. Silver nanoparticles induce apoptotic cell death in Candida albicans through the increase of hydroxyl radicals. *FEBS J* **2012**, 279, 1327-1338.

74. Vazquez-Munoz, R.; Avalos-Borja, M.; Castro-Longoria, E. Ultrastructural analysis of Candida albicans when exposed to silver nanoparticles. *PLoS One* **2014**, 9, e108876.

75. Ivask, A.; Kurvet, I.; Kasemets, K.; Blinova, I.; Aruoja, V.; Suppi, S.; Vija, H.; Kakinen, A.; Titma, T.; Heinlaan, M.; Visnapuu, M.; Koller, D.; Kisand, V.; Kahru, A. Size-dependent toxicity of silver nanoparticles to bacteria, yeast, algae, crustaceans and mammalian cells in vitro. *PLoS One* **2014**, 9, e102108.

76. Kiani-Esfahani, A.; Tavalaee, M.; Deemeh, M.R.; Hamiditabar, M.; Nasr-Esfahani, M.H. DHR123: an alternative probe for assessment of ROS in human spermatozoa. *Syst Biol Reprod Med* **2012**, 58, 168-174.

77. Nazarewicz, R.R.; Bikineyeva, A.; Dikalov, S.I. Rapid and specific measurements of superoxide using fluorescence spectroscopy. *J Biomol Screen* **2013**, 18, 498-503.

78. Jones, A.M.; Garg, S.; He, D.; Pham, A.N.; Waite, T.D. Superoxide-mediated formation and charging of silver nanoparticles. *Environ Sci Technol* **2011**, 45, 1428-1434.

79. Kaveh, R.; Li, Y.S.; Ranjbar, S.; Tehrani, R.; Brueck, C.L.; Van Aken, B. Changes in Arabidopsis thaliana gene expression in response to silver nanoparticles and silver ions. *Environ Sci Technol* **2013**, 47, 10637-10644.

80. Zheng, S.; Lan, P.; Liu, X.; Ye, K. Interaction between ribosome assembly factors Krr1 and Faf1 is essential for formation of small ribosomal subunit in yeast. *J Biol Chem* **2014**.

81. Phipps, K.R.; Charette, J.; Baserga, S.J. The small subunit processome in ribosome biogenesis-progress and prospects. *Wiley Interdiscip Rev RNA* **2011**, 2, 1-21.

82. Woolford, J.L., Jr.; Baserga, S.J. Ribosome biogenesis in the yeast Saccharomyces cerevisiae. *Genetics* **2013**, 195, 643-681.

83. Klueh, U.; Wagner, V.; Kelly, S.; Johnson, A.; Bryers, J.D. Efficacy of silver-coated fabric to prevent bacterial colonization and subsequent device-based biofilm formation. *J Biomed Mater Res* **2000**, 53, 621-631.

84. Rai, M.K.; Deshmukh, S.D.; Ingle, A.P.; Gade, A.K. Silver nanoparticles: the powerful nanoweapon against multidrug-resistant bacteria. *J Appl Microbiol* **2012**, 112, 841-852.

85. Morones, J.R.; Elechiguerra, J.L.; Camacho, A.; Holt, K.; Kouri, J.B.; Ramirez, J.T.; Yacaman, M.J. The bactericidal effect of silver nanoparticles. *Nanotechnology* **2005**, 16, 2346-2353.

86. Jung, W.K.; Koo, H.C.; Kim, K.W.; Shin, S.; Kim, S.H.; Park, Y.H. Antibacterial activity and mechanism of action of the silver ion in Staphylococcus aureus and Escherichia coli. *Appl Environ Microbiol* **2008**, 74, 2171-2178.

87. Ghosh, S.; Patil, S.; Ahire, M.; Kitture, R.; Kale, S.; Pardesi, K.; Cameotra, S.S.; Bellare, J.; Dhavale, D.D.; Jabgunde, A.; Chopade, B.A. Synthesis of silver nanoparticles using Dioscorea bulbifera tuber extract and evaluation of its synergistic potential in combination with antimicrobial agents. *Int J Nanomedicine* **2012**, 7, 483-496.

88. Abbaszadegan, A.; Nabavizadeh, M.; Gholami, A.; Aleyasin, Z.S.; Dorostkar, S.; Saliminasab, M.; Ghasemi, Y.; Hemmateenejad, B.; Sharghi, H. Positively charged imidazolium-based ionic liquid-protected silver nanoparticles: a promising disinfectant in root canal treatment. *Int Endod J* **2015**, 48, 790-800.

89. Lara, H.H.; Romero-Urbina, D.G.; Pierce, C.; Lopez-Ribot, J.L.; Arellano-Jimenez, M.J.; Jose-Yacaman, M. Effect of silver nanoparticles on Candida albicans biofilms: an ultrastructural study. *J Nanobiotechnology* **2015**, 13, 91.

90. Lesage, G.; Bussey, H. Cell wall assembly in Saccharomyces cerevisiae. *Microbiol Mol Biol Rev* **2006**, 70, 317-343.

91. Catala, M.; Aksouh, L.; Abou Elela, S. RNA-dependent regulation of the cell wall stress response. *Nucleic Acids Res* **2012**, 40, 7507-7517.

92. Hsin, Y.-H.; Chen, C.-F.; Huang, S.; Shih, T.-S.; Lai, P.-S.; Chueh, P.J. The apoptotic effect of nanosilver is mediated by a ROS- and JNK-dependent mechanism involving the mitochondrial pathway in NIH3T3 cells. *Toxicol Lett* **2008**.

93. Asharani, P.V.; Low Kah Mun, G.; Hande, M.P.; Valiyaveettil, S. Cytotoxicity and genotoxicity of silver nanoparticles in human cells. *ACS Nano* **2009**, 3, 279-290.

94. Bressan, E.; Ferroni, L.; Gardin, C.; Rigo, C.; Stocchero, M.; Vindigni, V.; Cairns, W.; Zavan, B. Silver nanoparticles and mitochondrial interaction. *Int J Dent* **2013**, 2013, 312747.

95. Galvan Marquez, I.; Ghiyasvand, M.; Massarsky, A.; Babu, M.; Samanfar, B.; Omidi, K.; Moon, T.W.; Smith, M.L.; Golshani, A. Zinc oxide and silver nanoparticles toxicity in the baker's yeast, Saccharomyces cerevisiae. *PLoS One* **2018**, 13, e0193111.

96. Kolarov, J.; Kolarova, N.; Nelson, N. A third ADP/ATP translocator gene in yeast. *J Biol Chem* **1990**, 265, 12711-12716.

97. Giraud, M.F.; Velours, J. The absence of the mitochondrial ATP synthase delta subunit promotes a slow growth phenotype of rho- yeast cells by a lack of assembly of the catalytic sector F1. *Eur J Biochem* **1997**, 245, 813-818.

98. Manshian, B.B.; Soenen, S.J.; Al-Ali, A.; Brown, A.; Hondow, N.; Wills, J.; Jenkins, G.J.; Doak, S.H. Cell type-dependent changes in CdSe/ZnS quantum dot uptake and toxic endpoints. *Toxicol Sci* **2015**, 144, 246-258.

99. Chinen, A.B.; Guan, C.M.; Ferrer, J.R.; Barnaby, S.N.; Merkel, T.J.; Mirkin, C.A. Nanoparticle Probes for the Detection of Cancer Biomarkers, Cells, and Tissues by Fluorescence. *Chem Rev* **2015**, 115, 10530-10574.

100. Liu, Q.; Li, H.; Xia, Q.; Liu, Y.; Xiao, K. Role of surface charge in determining the biological effects of CdSe/ZnS quantum dots. *Int J Nanomedicine* **2015**, 10, 7073-7088.

101. Zhang, T.; Wang, Y.; Kong, L.; Xue, Y.; Tang, M. Threshold Dose of Three Types of Quantum Dots (QDs) Induces Oxidative Stress Triggers DNA Damage and Apoptosis in Mouse Fibroblast L929 Cells. *Int J Environ Res Public Health* **2015**, 12, 13435-13454.

102. Kuo, T.R.; Lee, C.F.; Lin, S.J.; Dong, C.Y.; Chen, C.C.; Tan, H.Y. Studies of intracorneal distribution and cytotoxicity of quantum dots: risk assessment of eye exposure. *Chem Res Toxicol* **2011**, 24, 253-261.

103. Tang, M.; Li, Z.; Chen, L.; Xing, T.; Hu, Y.; Yang, B.; Ruan, D.Y.; Sun, F.; Wang, M. The effect of quantum dots on synaptic transmission and plasticity in the hippocampal dentate gyrus area of anesthetized rats. *Biomaterials* **2009**, 30, 4948-4955.

104. Tang, M.; Wang, M.; Xing, T.; Zeng, J.; Wang, H.; Ruan, D.Y. Mechanisms of unmodified CdSe quantum dot-induced elevation of cytoplasmic calcium levels in primary cultures of rat hippocampal neurons. *Biomaterials* **2008**, 29, 4383-4391.

105. Arslan, Z.; Ates, M.; Mcduffy, W.; Agachan, M.S.; Farah, I.O.; Yu, W.W.; Bednar, A.J. Probing metabolic stability of CdSe nanoparticles: alkaline extraction of free cadmium from liver and kidney samples of rats exposed to CdSe nanoparticles. *J Hazard Mater* **2011**, 192, 192-199.

106. Aaron, J.S.; Greene, A.C.; Kotula, P.G.; Bachand, G.D.; Timlin, J.A. Advanced optical imaging reveals the dependence of particle geometry on interactions between CdSe quantum dots and immune cells. *Small* **2011**, 7, 334-341.

107. Wang, X.; Tian, J.; Yong, K.T.; Zhu, X.; Lin, M.C.; Jiang, W.; Li, J.; Huang, Q.; Lin, G. Immunotoxicity assessment of CdSe/ZnS quantum dots in macrophages, lymphocytes and BALB/c mice. *J Nanobiotechnology* **2016**, 14, 10.

108. Pathakoti, K.; Hwang, H.M.; Xu, H.; Aguilar, Z.P.; Wang, A. In vitro cytotoxicity of CdSe/ZnS quantum dots with different surface coatings to human keratinocytes HaCaT cells. *J Environ Sci (China)* **2013**, 25, 163-171.

109. Romoser, A.; Ritter, D.; Majitha, R.; Meissner, K.E.; Mcshane, M.; Sayes, C.M. Mitigation of quantum dot cytotoxicity by microencapsulation. *PLoS One* **2011**, 6, e22079.

110. Derfus, A.M.; Chan, W.C.W.; Bhatia, S.N. Probing the Cytotoxicity Of Semiconductor Quantum Dots. *Nano Lett* **2004**, 4, 11-18.

111. Kirchner, C.; Liedl, T.; Kudera, S.; Pellegrino, T.; Munoz Javier, A.; Gaub, H.E.; Stolzle, S.; Fertig, N.; Parak, W.J. Cytotoxicity of colloidal CdSe and CdSe/ZnS nanoparticles. *Nano Lett* **2005**, 5, 331-338.

112. Wang, Y.; Wang, X.; Wang, C.; Peng, F.; Wang, R.; Xiao, X.; Zeng, J.; Kang, H.; Fan, X.; Sha, L.; Zhang, H.; Zhou, Y. Transcriptomic Profiles Reveal the Interactions of Cd/Zn in Dwarf Polish Wheat (Triticum polonicum L.) Roots. *Front Physiol* **2017**, 8, 168.

113. Winnik, F.M.; Maysinger, D. Quantum dot cytotoxicity and ways to reduce it. *Acc Chem Res* **2013**, 46, 672-680.

114. Han, X.; Lai, L.; Tian, F.; Jiang, F.L.; Xiao, Q.; Li, Y.; Yu, Q.; Li, D.; Wang, J.; Zhang, Q.; Zhu, B.; Li, R.; Liu, Y. Toxicity of CdTe quantum dots on yeast Saccharomyces cerevisiae. *Small* **2012**, 8, 2680-2689.

115. Atha, D.H.; Nagy, A.; Steinbruck, A.; Dennis, A.M.; Hollingsworth, J.A.; Dua, V.; Iyer, R.; Nelson, B.C. Quantifying engineered nanomaterial toxicity: comparison of common cytotoxicity and gene expression measurements. *J Nanobiotechnology* **2017**, 15, 79.

116. Xu, G.; Lin, G.; Lin, S.; Wu, N.; Deng, Y.; Feng, G.; Chen, Q.; Qu, J.; Chen, D.; Chen, S.; Niu, H.; Mei, S.; Yong, K.T.; Wang, X. The Reproductive Toxicity of CdSe/ZnS Quantum Dots on the in vivo Ovarian Function and in vitro Fertilization. *Sci Rep* **2016**, 6, 37677.

117. Huang, X.; Li, Y.; Pan, J.; Li, M.; Lai, Y.; Gao, J.; Li, X. RNA-Seq identifies redox balance related gene expression alterations under acute cadmium exposure in yeast. *Environ Microbiol Rep* **2016**, 8, 1038-1047.

118. Chibli, H.; Carlini, L.; Park, S.; Dimitrijevic, N.M.; Nadeau, J.L. Cytotoxicity of InP/ZnS quantum dots related to reactive oxygen species generation. *Nanoscale* **2011**, 3, 2552-2559.

119. Kunstman, P.; Coulon, J.; Kolmykov, O.; Moussa, H.; Balan, L.; Medjahdi, G.; Lulek, J.; Schneidera, R. One step synthesis of bright luminescent core/shell CdTexS1−x/ZnS quantum dots emitting from the visible to the near infrared. *J. Lumin* **2018**.

120. Casal, M.; Paiva, S.; Queiros, O.; Soares-Silva, I. Transport of carboxylic acids in yeasts. *FEMS Microbiol Rev* **2008**, 32, 974-994.

121. Geisler-Lee, J.; Wang, Q.; Yao, Y.; Zhang, W.; Geisler, M.; Li, K.; Huang, Y.; Chen, Y.; Kolmakov, A.; Ma, X. Phytotoxicity, accumulation and transport of silver nanoparticles by Arabidopsis thaliana. *Nanotoxicology* **2013**, 7, 323-337.

122. Filali, S.; Geloen, A.; Lysenko, V.; Pirot, F.; Miossec, P. Live-stream characterization of cadmium-induced cell death using visible CdTe-QDs. *Sci Rep* **2018**, 8, 12614.

123. Boiteux, S.; Jinks-Robertson, S. DNA repair mechanisms and the bypass of DNA damage in Saccharomyces cerevisiae. *Genetics* **2013**, 193, 1025-1064.

124. Lawrence, C.W. Cellular functions of DNA polymerase zeta and Rev1 protein. *Adv Protein Chem* **2004**, 69, 167-203.

125. Dragon, F.; Gallagher, J.E.; Compagnone-Post, P.A.; Mitchell, B.M.; Porwancher, K.A.; Wehner, K.A.; Wormsley, S.; Settlage, R.E.; Shabanowitz, J.; Osheim, Y.; Beyer, A.L.; Hunt, D.F.; Baserga, S.J. A large nucleolar U3 ribonucleoprotein required for 18S ribosomal RNA biogenesis. *Nature* **2002**, 417, 967-970.

126. Peyroche, G.; Milkereit, P.; Bischler, N.; Tschochner, H.; Schultz, P.; Sentenac, A.; Carles, C.; Riva, M. The recruitment of RNA polymerase I on rDNA is mediated by the interaction of the A43 subunit with Rrn3. *EMBO J* **2000**, 19, 5473-5482.

127. Shirai, C.; Takai, T.; Nariai, M.; Horigome, C.; Mizuta, K. Ebp2p, the yeast homolog of Epstein-Barr virus nuclear antigen 1-binding protein 2, interacts with factors of both the 60 S and the 40 s ribosomal subunit assembly. *J Biol Chem* **2004**, 279, 25353-25358.

128. Fromont-Racine, M.; Senger, B.; Saveanu, C.; Fasiolo, F. Ribosome assembly in eukaryotes. *Gene* **2003**, 313, 17-42.

129. Harnpicharnchai, P.; Jakovljevic, J.; Horsey, E.; Miles, T.; Roman, J.; Rout, M.; Meagher, D.; Imai, B.; Guo, Y.; Brame, C.J.; Shabanowitz, J.; Hunt, D.F.; Woolford, J.L., Jr. Composition and functional characterization of yeast 66S ribosome assembly intermediates. *Mol Cell* **2001**, 8, 505-515.

130. Hood, J.K.; Casolari, J.M.; Silver, P.A. Nup2p is located on the nuclear side of the nuclear pore complex and coordinates Srp1p/importin-alpha export. *J. Cell Sci.* **2000**.

131. Wozniak, R.W.; Blobel, G.; Rout, M.P. POM152 is an integral protein of the pore membrane domain of the yeast nuclear envelope. *J. Cell Boil.* **1994**.

132. Belyy, A.; Levanova, N.; Tabakova, I.; Rospert, S.; Belyi, Y. Ribosomal Protein Rps26 Influences 80S Ribosome Assembly in Saccharomyces cerevisiae. *mSphere* **2016**, 1.

133. Venema, J.; Tollervey, D. Ribosome synthesis in Saccharomyces cerevisiae. *Annu Rev Genet* **1999**, 33, 261-311.

134. Choi, S.K.; Lee, J.H.; Zoll, W.L.; Merrick, W.C.; Dever, T.E. Promotion of met-tRNAiMet binding to ribosomes by yIF2, a bacterial IF2 homolog in yeast. *Science* **1998**, 280, 1757-1760.

135. Tkach, J.M.; Yimit, A.; Lee, A.Y.; Riffle, M.; Costanzo, M.; Jaschob, D.; Hendry, J.A.; Ou, J.; Moffat, J.; Boone, C.; Davis, T.N.; Nislow, C.; Brown, G.W. Dissecting DNA damage response pathways by analysing protein localization and abundance changes during DNA replication stress. *Nat Cell Biol* **2012**, 14, 966-976.

136. Grauslund, M.; Lopes, J.M.; Rønnow, B. Expression of GUT1, which encodes glycerol kinase in Saccharomyces cerevisiae, is controlled by the positive regulators Adr1p, Ino2p and Ino4p and the negative regulator Opi1p in a carbon source-dependent fashion. *Nucleic Acids Res.* **1999**.

137. Reinders, J.; Wagner, K.; Zahedi, R.P.; Stojanovski, D.; Eyrich, B.; Van Der Laan, M.; Rehling, P.; Sickmann, A.; Pfanner, N.; Meisinger, C. Profiling phosphoproteins of yeast mitochondria reveals a role of phosphorylation in assembly of the ATP synthase. *Mol Cell Proteomics* **2007**, 6, 1896-1906.

138. Herrmann, J.M.; Funes, S. Biogenesis of cytochrome oxidase—Sophisticated assembly lines in the mitochondrial inner membrane. *Gene* **2005**.

139. Strogolova, V.; Furness, A.; Robb-Mcgrath, M.; Garlich, J.; Stuart, R.A. Members of the Hypoxia-Induced Gene 1 Protein Family, Are Critical Components of the Mitochondrial Cytochrome bc1-Cytochrome c Oxidase Supercomplex. *Mol. Cell. Boil.* **2012**.

140. M.Yang; B.L.Trumpower. Deletion of QCR6, the gene encoding subunit six of the mitochondrial cytochrome bc1 complex, blocks maturation of cytochrome c1, and causes temperature-sensitive petite growth in Saccharomyces cerevisiae. *J. Boil. Chem.* **1994**.

141. Charizanis, C.; Juhnke, H.; Krems, B.; Entian, K.D. The mitochondrial cytochrome c peroxidase Ccp1 of Saccharomyces cerevisiae is involved in conveying an oxidative stress signal to the transcription factor Pos9 (Skn7). *Mol Gen Genet* **1999**, 262, 437-447.

142. Macdonald, C.; ; Buchkovich, N.J.; ; Stringer, D.K.; ; Emr, S.D.; ; Piper, R.C. Cargo ubiquitination is essential for multivesicular body intralumenal vesicle formation. *EMBO Rep.* **2012**.

143. Grant, B.D.; Donaldson, J.G. Pathways and mechanisms of endocytic recycling. *Nat Rev Mol Cell Biol* **2009**, 10, 597-608.

144. Finley, D.; Özkaynak, E.; Varshavsky, A. The yeast polyubiquitin gene is essential for resistance to high temperatures, starvation, and other stresses. *Cell* **1987**.

145. Forzani, C.; Lobreaux, S.; Mari, S.; Briat, J.F.; Lebrun, M. Metal resistance in yeast mediated by the expression of a maize 20S proteasome alpha subunit. *Gene* **2002**, 293, 199-204.

146. Ayupova, D.; Dobhal, G.; Laufersky, G.; Nann, T.; Goreham, R.V. An In Vitro Investigation of Cytotoxic Effects of InP/Zns Quantum Dots with Different Surface Chemistries. *Nanomaterials (Basel)* **2019**, 9.

147. Rosenthal, S.J.; Chang, J.C.; Kovtun, O.; Mcbride, J.R.; Tomlinson, I.D. Biocompatible quantum dots for biological applications. *Chem Biol* **2011**, 18, 10-24.

148. Ellis, M.A.; Grandinetti, G.; Fichter, K.M. Synthesis of Cd-free InP/ZnS Quantum Dots Suitable for Biomedical Applications. *J Vis Exp* **2016**, e53684.

149. Bruchez, M., Jr.; Moronne, M.; Gin, P.; Weiss, S.; Alivisatos, A.P. Semiconductor nanocrystals as fluorescent biological labels. *Science* **1998**, 281, 2013-2016.

150. Chan, W.C.; Nie, S. Quantum dot bioconjugates for ultrasensitive nonisotopic detection. *Science* **1998**, 281, 2016-2018.

151. Ankireddy, S.R.; Kim, J. Dopamine-functionalized InP/ZnS quantum dots as fluorescence probes for the detection of adenosine in microfluidic chip. *Int J Nanomedicine* **2015**, 10 Spec Iss, 121-128.

152. Gao, J.; Chen, K.; Luong, R.; Bouley, D.M.; Mao, H.; Qiao, T.; Gambhir, S.S.; Cheng, Z. A novel clinically translatable fluorescent nanoparticle for targeted molecular imaging of tumors in living subjects. *Nano Lett* **2012**, 12, 281-286.

153. Zheng, W.; Xu, Y.M.; Wu, D.D.; Yao, Y.; Liang, Z.L.; Tan, H.W.; Lau, A.T.Y. Acute and chronic cadmium telluride quantum dots-exposed human bronchial epithelial cells: The effects of particle sizes on their cytotoxicity and carcinogenicity. *Biochem Biophys Res Commun* **2018**, 495, 899-903.

154. Liu, J.; Yang, C.; Liu, J.; Hu, R.; Hu, Y.; Chen, H.; Law, W.C.; Swihart, M.T.; Ye, L.; Wang, K.; Yong, K.T. Effects of Cd-based Quantum Dot Exposure on the Reproduction and Offspring of Kunming Mice over Multiple Generations. *Nanotheranostics* **2017**, 1, 23-37.

155. Ma-Hock, L.; Brill, S.; Wohlleben, W.; Farias, P.M.; Chaves, C.R.; Tenorio, D.P.; Fontes, A.; Santos, B.S.; Landsiedel, R.; Strauss, V.; Treumann, S.; Ravenzwaay, B. Short term inhalation toxicity of a liquid aerosol of CdS/Cd(OH)(2) core shell quantum dots in male Wistar rats. *Toxicol Lett* **2012**, 208, 115-124.

156. Ye, L.; Yong, K.T.; Liu, L.; Roy, I.; Hu, R.; Zhu, J.; Cai, H.; Law, W.C.; Liu, J.; Wang, K.; Liu, J.; Liu, Y.; Hu, Y.; Zhang, X.; Swihart, M.T.; Prasad, P.N. A pilot study in non-human primates shows no adverse response to intravenous injection of quantum dots. *Nat Nanotechnol* **2012**, 7, 453-458.

157. Lu, X.; Zhu, T.; Chen, C.; Liu, Y. Right or left: the role of nanoparticles in pulmonary diseases. *Int J Mol Sci* **2014**, 15, 17577-17600.

158. Su, Y.; He, Y.; Lu, H.; Sai, L.; Li, Q.; Li, W.; Wang, L.; Shen, P.; Huang, Q.; Fan, C. The cytotoxicity of cadmium based, aqueous phase - synthesized, quantum dots and its modulation by surface coating. *Biomaterials* **2009**, 30, 19-25.

159. Oh, E.; Liu, R.; Nel, A.; Gemill, K.B.; Bilal, M.; Cohen, Y.; Medintz, I.L. Meta-analysis of cellular toxicity for cadmium-containing quantum dots. *Nat Nanotechnol* **2016**, 11, 479-486.

160. Chen, T.; Li, L.; Xu, G.; Wang, X.; Wang, J.; Chen, Y.; Jiang, W.; Yang, Z.; Lin, G. Cytotoxicity of InP/ZnS Quantum Dots With Different Surface Functional Groups Toward Two Lung-Derived Cell Lines. *Front Pharmacol* **2018**, 9, 763.

161. Hussain, S.; Won, N.; Nam, J.; Bang, J.; Chung, H.; Kim, S. One-pot fabrication of high-quality InP/ZnS (core/shell) quantum dots and their application to cellular imaging. *Chemphyschem* **2009**, 10, 1466-1470.

162. Mo, D.; Hu, L.; Zeng, G.; Chen, G.; Wan, J.; Yu, Z.; Huang, Z.; He, K.; Zhang, C.; Cheng, M. Cadmium-containing quantum dots: properties, applications, and toxicity. *Appl Microbiol Biotechnol* **2017**, 101, 2713-2733.

163. Brunetti, V.; Chibli, H.; Fiammengo, R.; Galeone, A.; Malvindi, M.A.; Vecchio, G.; Cingolani, R.; Nadeau, J.L.; Pompa, P.P. InP/ZnS as a safer alternative to CdSe/ZnS core/shell quantum dots: in vitro and in vivo toxicity assessment. *Nanoscale* **2013**, 5, 307-317.

164. Lin, G.; Ouyang, Q.; Hu, R.; Ding, Z.; Tian, J.; Yin, F.; Xu, G.; Chen, Q.; Wang, X.; Yong, K.T. In vivo toxicity assessment of non-cadmium quantum dots in BALB/c mice. *Nanomedicine* **2015**, 11, 341-350.

165. Moradas-Ferreira, P.; Costa, V. Adaptive response of the yeast Saccharomyces cerevisiae to reactive oxygen species: defences, damage and death. *Redox Rep* **2000**, 5, 277-285.

166. Zhang, W.; Liu, H.T. MAPK signal pathways in the regulation of cell proliferation in mammalian cells. *Cell Res* **2002**, 12, 9-18.

167. Elmore, S. Apoptosis: a review of programmed cell death. *Toxicol Pathol* **2007**, 35, 495-516.

168. Mamnun, Y.M.; Schuller, C.; Kuchler, K. Expression regulation of the yeast PDR5 ATP-binding cassette (ABC) transporter suggests a role in cellular detoxification during the exponential growth phase. *FEBS Lett* **2004**, 559, 111-117.

169. Wolfger, H.; Mamnun, Y.M.; Kuchler, K. The yeast Pdr15p ATP-binding cassette (ABC) protein is a general stress response factor implicated in cellular detoxification. *J Biol Chem* **2004**, 279, 11593-11599.

170. Wang, X.; Yen, J.; Kaiser, P.; Huang, L. Regulation of the 26S proteasome complex during oxidative stress. *Sci Signal* **2010**, 3, ra88.

171. Stangier, M.M.; Kumar, A.; Chen, X.; Farcas, A.M.; Barral, Y.; Steinmetz, M.O. Structure-Function Relationship of the Bik1-Bim1 Complex. *Structure* **2018**, 26, 607-618 e604.

172. Shin, M.; Van Leeuwen, J.; Boone, C.; Bretscher, A. Yeast Aim21/Tda2 both regulates free actin by reducing barbed end assembly and forms a complex with Cap1/Cap2 to balance actin assembly between patches and cables. *Mol Biol Cell* **2018**, 29, 923-936.

173. Ma, M.; Burd, C.G. Retrograde trafficking and plasma membrane recycling pathways of the budding yeast Saccharomyces cerevisiae. *Traffic* **2020**, 21, 45-59.

174. Wysocki, R.; Tamas, M.J. How Saccharomyces cerevisiae copes with toxic metals and metalloids. *FEMS Microbiol Rev* **2010**, 34, 925-951.